Advances in the Development of Novel Cobalt Fischer–Tropsch Catalysts for Synthesis of Long-Chain Hydrocarbons and Clean Fuels

Andrei Y. Khodakov,*,† Wei Chu,†,‡ and Pascal Fongarland†

Unité de Catalyse et de Chimie du Solide, UMR 8181 CNRS, USTL-ENSCL-ECLille, Bat C3, Cité scientifique, 59655 Villeneuve d'Ascq, France and Department of Chemical Engineering, Sichuan University, Chengdu 610065, China

Received July 28, 2006

Contents

* To whom correspondence should be addressed. Phone: + 33 3 20 33 54 37. Fax: + 33 3 20 43 65 61. E-mail: andrei.khodakov@univ-lille1.fr.
† Unité de Catalyse et de Chimie du Solide.
‡ Sichuan University.

10.1021/cr050972v CCC: $65.00
Published on Web 05/09/2007

Andrei Y. Khodakov graduated from the Moscow State University in 1987 and received his Ph.D. degree in 1991 from the Institute of Organic Chemistry of the Russian Academy of Sciences (supervisor Professor V.B. Kazanskii) and habilitation à diriger des recherches in 2002 from the University of Sciences and Technologies of Lille. Between 1992 and 1999 he acquired experience in several top academic and industrial institutions: the University of California at Berkeley and Lawrence Berkeley National Laboratory in the United States, the Institut Français du Pétrole, Ecole Nationale Supérieure de Chimie de Paris (ENSCP), and Laboratoire pour l'Utilisation de Rayonnement Electromagnétique (LURE) in France, and the University of Edinburgh and University of Manchester Institute of Science and Technology (UMIST) in the United Kingdom. Since 1999 he has been appointed to a research position of the Centre National de la Recherche Scientifique (CNRS, France). Currently, he is the leader of the Fischer–Tropsch research group in the Unité de Catalyse et de Chimie du Solide, UMR 8181 CNRS. His research interests cover heterogeneous catalysis, catalysts design, catalyst characterization, in situ and operando techniques, and kinetics of catalytic reactions.

Wei Chu was born in 1965 in Jiangsu, China. He graduated from Nanjing University in 1984, obtained his Ph.D. degree in 1991 (ULP, Strasbourg, France) under the supervision of Professor A. Kiennemann, and then carried out postdoctoral work at the State Key Laboratory of Catalysis in Dalian (SKLC, DICP, CAS). In 1995 he was promoted to Senior Research Professor at the Chengdu Institute of Organic Chemistry (CIOC, Chinese Academy of Sciences). In 2001 he moved to Sichuan University as a Full Professor. Since 1998, he has been invited as a visiting professor to many high-ranked universities (Montpellier University in France; Hokkaido University in Japan; TUM in Munich, Germany; USTL in Lille, France). His scientific contributions have been awarded numerous prizes including the New Century Excellent Talent award (NCET-05-783) by the Chinese Ministry of Education and the 2004 Prize for Advances in Sciences and Technologies of the Sichuan Province. He has been nominated as a Leading Scientist of the Sichuan Province of China in 2003 and a Leading Scientist of Sichuan University for the National 985 Project of China in 2005. He has been a scientific committee member of the Chinese Young Scientist Catalysis Conferences since 1996 and is currently an Editorial Board member of the journal *Natural Gas Chemical Industry*. He has published more than 100 papers in peer-reviewed journals, edited a book *Catalyst Engineering*, and obtained seven patents. His research interests are in the area of heterogeneous catalysis, environmental catalysis, Fischer–Tropsch synthesis, C1 chemistry, energy materials, porphyrins and fine chemicals, plasma, and nanomaterials.

1. Introduction

In this section we discuss the challenges in catalyst design for Fischer−Tropsch synthesis.

1.1. Brief Historical Perspective

The first experiments on catalytic hydrogenation of carbon monoxide were carried out at the beginning of 20th century. In 1902, Sabatier and Senderens synthesized methane from a mixture of CO or CO_2 with hydrogen; the reaction was performed on cobalt or nickel catalysts at temperatures of 473−453 K and under atmospheric pressure. In 1922, Hans Fischer and Franz Tropsch proposed the Synthol process,[1] which gave, under high pressure (>100 bar), a mixture of aliphatic oxygenated compounds via reaction of carbon monoxide with hydrogen over alkalized iron chips at 673 K. This product was transformed after heating under pressure into "Synthine", a mixture of hydrocarbons.

Important progress in the development of Fischer−Tropsch (abbreviated further in the text as FT) synthesis was made in 1923. It was found that more and more heavy hydrocarbons could be produced[2] when the Synthol process was conducted at lower pressure (∼7 bar). Heavy hydrocarbons were the main products of carbon monoxide hydrogenation on Fe/ZnO and Co/Cr_2O_3 contacts. In 1926, Hans Fischer and Franz Tropsch published their first reports[3] about hydrocarbon synthesis.

After 1927 under the supervision of Roelen, the problems of chemical engineering had been tackled. A series of fixed bed and circulating bed reactors was developed. These reactors had already a presentiment of the later industrial processes. In 1934, the FT process was licensed by Ruhrchemie and reached industrial maturity in 2 years. In April 1936,

Pascal Fongarland obtained his Ph.D. degree in 2003 at the University of Lyon 1. His studies were carried out at the Laboratoire de Génie des Procédés Catalytiques (Villeurbanne, France) and addressed hydrodesulfurization kinetics. During that period he spent 16 months at the Chemical Reaction Engineering Laboratory (Saint-Louis, MO), where he was involved in research on circulating fluidized bed reactors. After receiving his Ph.D. degree he was recruited as a postdoctoral fellow in the Unité de Catalyse et Chimie du Solide (CNRS, Lille, France) and performed kinetic investigations of Fischer–Tropsch synthesis in slurry stirred tank reactor. In 2005 he was appointed as an Assistant Professor of Chemical Engineering of the Ecole Centrale de Lille. His research interests are related to experimental studies and modeling of multiphase reactors and kinetics of complex catalytic reactions such as Fischer–Tropsch synthesis and hydrotreatment of petroleum feedstocks.

Table 1. Comparison of Cobalt and Iron FT Catalysts

parameter	cobalt catalysts	iron catalyst
cost	more expensive	less expensive
lifetime	resistant to deactivation	less resistant to deactivation (coking, carbon deposit, iron carbide)
activity at low conversion	comparable	
productivity at high conversion	higher; less significant effect of water on the rate of carbon monoxide conversion	lower; strong negative effect of water on the rate of carbon monoxide conversion
maximal chain growth probability	0.94	0.95
water gas shift reaction $CO + H_2O \rightarrow CO_2 + H_2$	not very significant; more noticeable at high conversions	significant
maximal sulfur content	<0.1 ppm	<0.2 ppm
flexibility (temperature and pressure)	less flexible; significant influence of temperature and pressure "on hydrocarbon selectivity	flexible; methane selectivity is relatively low even at 613 K
H_2/CO ratio	~2	0.5−2.5
attrition résistance	good	not very resistant

the first large-scale FT plant operated in Braunkohle-Benzin. In 1938, Germany had a capacity of 660 000 tons of primary products per year. After World War II, ARGE (Arbeitsgemeinschaft Ruhrchemie und Lurgi) developed a large-scale process with a fixed bed FT reactor. At the same period, Kellog proposed a technology based on circulating catalyst bed. Both the ARGE and Kellog processes were realized by Sasol in South Africa. The Sasol One plant was built in Sasolburg in 1955. In 1969, the Natref crude oil refinery was commissioned. In 1980 and 1982, Sasol Two and Sasol Three, respectively, began production in Secunda.[4] Major accomplishments of Sasol in the design of catalysts, reactors, and processes for FT synthesis have been summarized in a recently published monograph.[5]

In the 1980s, expensive investments in the FT research and development programs picked up again in major petroleum companies. The global resurgence of interest in FT synthesis has been primarily driven by the problems of utilization of stranded gas, diversification of sources of fossil fuels, and environmental concerns. Synthetic liquid fuels generally have a very low content of sulfur and aromatic compounds compared to gasoline or diesel from crude oil. FT synthesis has been considered as a part of gas to liquids (GTL) technology, which converts natural and associated gases to more valuable middle distillates and lubricants.

The abundant reserves of natural gas in many parts of the world have made it attractive to commission new plants based on FT technology. In 1993, the Shell Bintulu 12 500 barrels per day (bpd) plant came into operation. In June 2006, the Sasol Oryx 34 000 bpd plant was inaugurated. SasolChevron is currently building its Escarvos GTL plant in Nigeria. Shell and Exxon signed the agreement on building 140 000 and 150 000 bpd GTL-FT plants in Qatar. Thus, after several decades of research and development, FT technology has finally come to the stage of full-scale industry and worldwide commercialization. The history of catalyst design for FT synthesis has been recently reviewed by Bartholomew.[6] More information on the early history of FT synthesis and historical patents is available at www.fischer-tropsch.org.

1.2. Catalysts for Fischer–Tropsch Synthesis

All group VIII metals have noticeable activity in the hydrogenation of carbon monoxide to hydrocarbons

$$n\mathrm{CO} + 2n\mathrm{H_2} \rightarrow \mathrm{C}_n\mathrm{H}_{2n} + n\mathrm{H_2O}$$

$$n\mathrm{CO} + (2n+1)\,\mathrm{H_2} \rightarrow \mathrm{C}_n\mathrm{H}_{2n+2} + n\mathrm{H_2O}$$

Ruthenium followed by iron, nickel, and cobalt are the most active metals for the hydrogenation of carbon monoxide. Vannice[7] et al. showed that the molecular average weight of hydrocarbons produced by FT synthesis decreased in the following sequence: Ru > Fe > Co > Rh > Ni > Ir > Pt > Pd. Thus, only ruthenium, iron, cobalt, and nickel have catalytic characteristics which allow considering them for commercial production. Nickel catalysts under practical conditions produce too much methane. Ruthenium is too expensive; moreover, its worldwide reserves are insufficient for large-scale industry.

Cobalt and iron are the metals which were proposed by Fischer and Tropsch as the first catalysts for syngas conversion. Both cobalt and iron catalysts have been used in the industry for hydrocarbon synthesis. A brief comparison of cobalt and iron catalysts is given in Table 1. Cobalt catalysts are more expensive, but they are more resistant to deactivation. Although the activity at low conversion of two metals is comparable, the productivity at higher conversion is more significant with cobalt catalysts. Water generated by FT synthesis slows the reaction rate on iron to a greater extent than on cobalt catalysts. At relatively low temperatures (473−523 K), chain growth probabilities of about 0.94 have been reported[8−10] for cobalt-based catalysts and about 0.95 for iron catalysts. The water−gas shift reaction is more significant on iron than on cobalt catalysts

$$\mathrm{CO} + \mathrm{H_2O} \rightarrow \mathrm{CO_2} + \mathrm{H_2}$$

Iron catalysts usually produce more olefins. Both iron and cobalt catalysts are very sensitive to sulfur, which could readily contaminate them. For iron-based catalysts, the syngas should not contain more than 0.2 ppm of sulfur. For Co catalysts, the amount of sulfur in the feed should be much less than 0.1 ppm.[9−11] Cobalt catalysts supported on oxide supports are generally more resistant to attrition than iron coprecipitated counterparts; they are more suitable for use in slurry-type reactors. Iron catalysts produce hydrocarbons and oxygenated compounds under different pressures, H_2/CO ratios, and temperatures (up to 613 K). Cobalt catalysts operate at a very narrow range of temperatures and pressures; an increase in temperature leads to a spectacular increase in methane selectivity. Iron catalysts seem to be more appropriate for conversion of biomass-derived syngas to hydrocarbons than cobalt systems because they can operate at lower H_2/CO ratios.

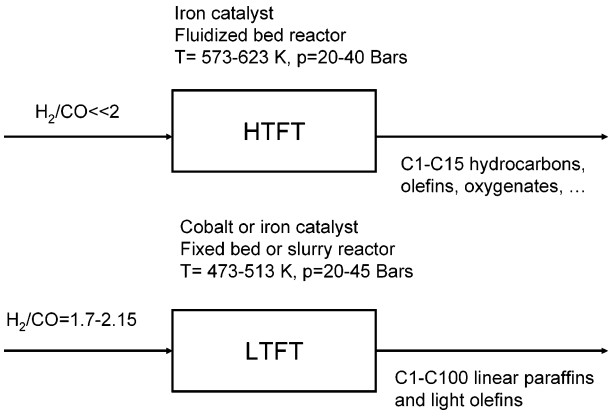

Figure 1. High- and low-temperature FT processes.

Currently, there are two FT operating modes:[11−13] high- and low-temperature FT processes (Figure 1). In the high-temperature FT (573−623 K, HTFT) process[14] syngas reacts in a fluidized bed reactor in the presence of iron-based catalyst to yield hydrocarbons in the C1−C15 hydrocarbon range. This process is primarily used to produce liquid fuels, although a number of valuable chemicals, e.g., α-olefins, can be extracted from the crude synthetic oil. Oxygenates in the aqueous stream are separated and purified to produce alcohols, acetic acid, and ketones including acetone, methyl ethyl ketone, and methyl isobutyl ketone.

Both iron and cobalt (Fe, Co) catalysts can be used in the low-temperature FT (473−513 K, LTFT) process[8,10] (Figure 1) for synthesis of linear long-chain hydrocarbon waxes and paraffins. High-quality sulfur-free diesel fuels are produced in this process. Most of the FT technologies developed in last two decades are based on the LTFT process. These new LTFT processes have involved syngas with a high H_2/CO ratio, which is generated by vaporeforming, autothermal reforming, or partial oxidation using natural gas as a feedstock.

Because of their stability, higher per pass conversion,[8] and high hydrocarbon productivity, cobalt catalysts represent the optimal choice for synthesis of long-chain hydrocarbons in the LTFT process.

1.3. Active Sites in Cobalt Catalysts

Information about the nature of the active sites is crucial for the design of cobalt FT catalysts. There is currently a consensus in the literature that FT synthesis proceeds on cobalt metal particles. The attribution of catalyst FT activity to cobalt metal phases has been built on a series of experimental findings. First, it was found that unsupported metallic cobalt and cobalt monocrystals were active[15] in FT synthesis. Secondly, cobalt metallic phases were always detected in the active FT catalyst before, during, and even after FT synthesis. Thirdly, Iglesia[16−19] et al. showed (Figure 2) that for large cobalt metal particles the reaction rate is proportional to the number of cobalt surface sites. Figure 2 suggests that turnover rates do not depend on cobalt dispersion for series of the catalytic supports. FT synthesis is therefore a structure-insensitive reaction.[20]

The statement about invariance of FT turnover frequency on cobalt particle sizes is probably valid only for larger cobalt particles; several exceptions might be expected[21] when cobalt particles are getting smaller or when they contain[22] different cobalt metal phases.

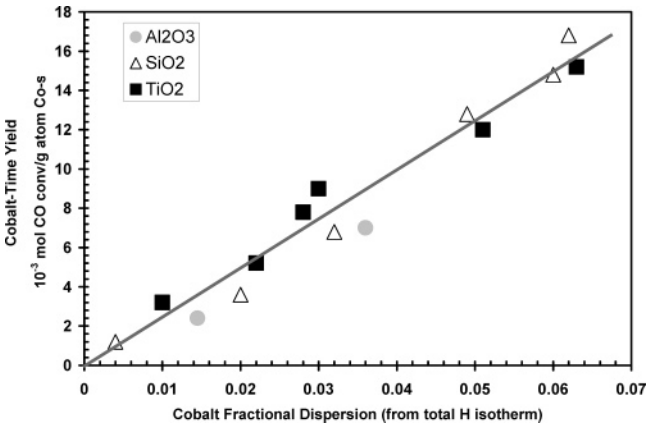

Figure 2. Cobalt time yield for a variety of cobalt alumina-, silica-, titania-supported catalysts. FT synthesis at 473 K, 2 MPa, $H_2/CO = 2$, 50−60% conversion (reproduced from ref 16, Copyright 2004, with kind permission from Springer Science and Business Media).

FT reaction rates and hydrocarbon selectivities on cobalt-supported catalysts could significantly evolve during the reaction. A dependence of carbon monoxide conversion and methane selectivity on time on stream, which is frequently observed[23] in a slurry reactor with cobalt alumina-supported catalysts, is shown in Figure 3. The decrease in the number

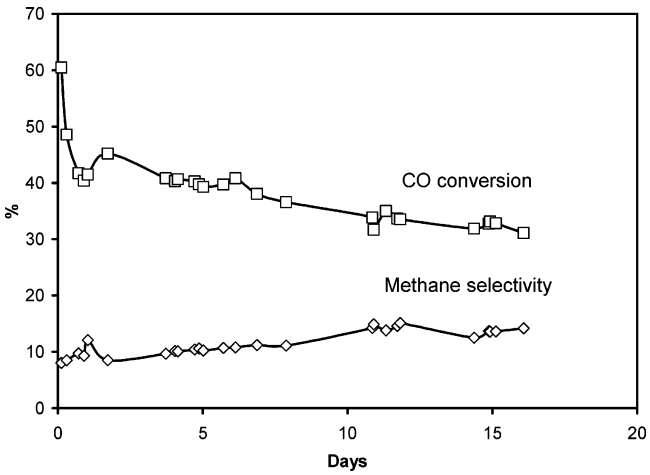

Figure 3. Evolution of carbon monoxide conversion and methane selectivity over Co/Al_2O_3 catalyst in slurry reactor ($T = 493$ K, 2 MPa, inlet $H_2/CO = 2.2$, data obtained in our laboratory).

of cobalt active sites (catalyst deactivation) could be one of the reasons responsible for the evolution of catalyst performance. In addition to active cobalt metallic phases, a working FT catalyst could contain several other cobalt species: cobalt carbide, cobalt oxides, cobalt support mixed compounds, etc. These species are probably not directly involved in FT synthesis. Cobalt carbide formation seems to be related[24] to a deactivation process. Oxidized cobalt species (Co_3O_4, CoO, etc.) do not catalyze FT synthesis either. Oxidation of cobalt metallic species during the reaction leads to catalyst deactivation[8,17,19] and reduces FT reaction rates. At the same time, cobalt oxidized species could probably affect the rate of several side and secondary reactions, such as water−gas shift, olefin isomerization, reinsertion, and hydrogenolysis.

1.4. Synergy between Catalyst and Catalytic Reactor

Commercial reactors for FT synthesis involve different technologies. Circulating bed and fluidized bed reactors are

used for the high-temperature FT processes (HTFT), which lead to gaseous products, while multitubular fixed bed and slurry reactors are dedicated to the low-temperature FT processes (LTFT), which manufacture liquid middle distillate fractions and hydrocarbon waxes.[14,25−28]

Several important issues have to be taken into consideration while choosing the reactor for FT synthesis. In addition to intrinsic chemical kinetics, the yield of hydrocarbons in the commercial reactor is affected by several other phenomena: interphase and intraphase mass transfer, heat transfer (FT synthesis is highly exothermic), and hydrodynamics of the flows. The mechanical stability of the catalyst is also an important issue, especially in fluidized bed and slurry bubble column reactors. The highest hydrocarbon yields can only be obtained when all phenomena are understood, controlled, and optimized. The optimal industrial reactor should use the catalyst at its maximum capacities for syngas conversion and should attain maximal hydrocarbons selectivities.

The process efficiency therefore depends on both the catalyst and catalytic reactor. This suggests that the FT reactor should be adapted to a specific catalyst. The design of novel catalysts should take into consideration the constraints imposed by the reactor.

1.5. Goals of This Review

Most of the recent reviews about FT synthesis have focused on either development of the reactors and processes for FT synthesis[8,11,14,29−35] or kinetic and mechanistic aspects of this reaction.[16,17,19,36−39] Very few reviews have specifically addressed recent developments in the design and characterization of cobalt catalysts.

The goal of the present review is to discuss different approaches to the FT catalyst design elaborated over the last 10−15 years. The catalyst design involves catalyst synthesis, catalyst activation, characterization of catalysts and their active phases, and evaluation of catalytic performance. The review contains four main sections. Section 2 tackles synthesis of cobalt FT catalysts. Section 3 focuses on comparative analysis of in-situ, ex-situ, and operando catalyst characterization techniques. Section 4 reviews the strategies for initial evaluation of FT catalyst performance.

2. Synthesis of Cobalt Fischer−Tropsch Catalysts

The catalytic performance of FT catalysts strongly depends on the methods of catalyst preparation. Preparation of cobalt-supported catalysts involves several important steps: choice of appropriate catalyst support, choice of method of deposition of the active phase, catalyst promotion, and oxidative and reductive treatments.

The goal of active phase deposition is to spread cobalt onto porous support and provide the precursors of cobalt metal clusters. Properties of the catalysts, number of cobalt metal sites, their characteristics, and localization on the support could be controlled by promotion with noble metals and oxides. The effect of promotion on the structure of cobalt catalysts has been also recently reviewed by Morales and Weckhuysen.[40]

The catalytic performance of FT catalysts is usually strongly affected by different oxidizing and reducing pretreatments. The catalytic support could also influence the performance of FT catalysts.

2.1. Types of Cobalt Catalysts and Methods of Deposition of Active Phase

2.1.1. Impregnations

Cobalt-supported catalysts for FT synthesis are very often prepared by impregnation. Impregnation is a method of cobalt deposition on porous support in which a dry support is contacted with a solution containing dissolved cobalt precursors.[41] In this section we discuss impregnation techniques which involve solutions of cobalt salts and cobalt carbonyls.

2.1.1.1. Impregnation Using Solutions of Cobalt Salts. Incipient wetness impregnation is the most common method to prepare cobalt-supported catalysts. In the incipient impregnation method a solution of cobalt salt, typically cobalt nitrate, is contacted with a dry porous support. After being contacted, the solution is aspired by the capillary forces inside the pores of the support. The incipient wetness occurs when all pores of the support are filled with the liquid and there is no excess moisture over and above the liquid required to fill the pores. Although at the first sight the practical execution of incipient wetness impregnation is simple, the fundamental phenomena underlying impregnation and drying are extremely complex. Reproducible synthesis of cobalt catalyst requires careful control of all impregnation parameters: temperature and time of support drying, rate of addition of impregnating solution, temperature and time of drying, etc. An experimental set up used in our laboratory for incipient wetness impregnation is shown in Figure 4.

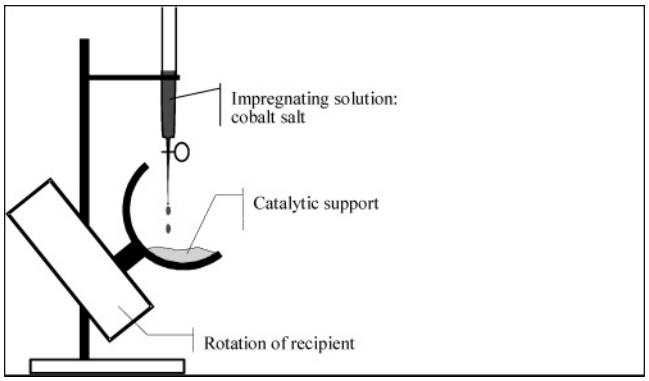

Figure 4. Scheme of experimental set up for incipient wetness impregnation. The solution is added dropwise during rotational motion of the recipient.

The initial repartition of cobalt on the support depends to a larger extent on the type and concentration of hydroxyl groups on the surface and pH of impregnating solution.[42] At the stage immediately after impregnation, the interaction between the metal precursor and the support is relatively weak, thereby allowing redistribution of the active phase over the support body during drying and calcination.

The distribution of Co^{2+} ions on the support after impregnation is affected by electrostatic interactions. Porous oxides such as alumina, silica, and titania have different points of zero charge (PZC).[43] At pH below the PZC, the surfaces of the corresponding oxides are charged positively; at pH higher than the PZC, the surface of the support is charged negatively. If the impregnating solution has a pH below the point of zero charge, repulsion between the surface of the support and Co^{2+} atoms results in nonhomogeneous repartition of cobalt ions. At pH higher than the point of zero charge, Co^{2+} cations are distributed much more homo-

Table 2. Effect of Cobalt Source on the Activity and Selectivity of Cobalt Alumina-Supported Catalysts[a]

cobalt source	*T*, K	bulk activity, mol/h/kg	specific activity, mol CO/mol Co/min	selectivity, %						
				C_1	C_{2-4}	C_{5-11}	C_{12-18}	C_{19-23}	C_{24+}	C_{5-23}
$Co_2(CO)_8$	513	35.3	0.29	7.9	13.7	37.0	23.4	8.9	9.1	69.3
	533	38.5	0.32	10.4	15.0	44.5	25.8	2.0	2.3	72.3
$Co(NO_3)_2$	513	15.8	0.09	10.9	6.5	12.9	19.8	21.9	28.0	54.6
	533	29.9	0.21	16.5	11.1	26.5	23.8	10.6	11.5	60.9

[a] $P = 2.07$ MPa, $CO/H_2 = 1$, and SV = 2 nL/h per g of catalysts; original data in ref 62.

genously. Further increase in pH could lead to dissolution of the support in the impregnating solution.

Dissolution of silica at pH higher than 7 was previously observed by Ming[44] et al. Alumina can dissolve in acid solutions at pH lower than 1. After dissolution, aluminum ions in the presence of cobalt ions, could form hydrotalcite-like structures, e.g., $Co_6Al_2CO_3(OH)_{16}\cdot 4H_2O$. These amorphous hydrotalcite-like structures are then physically adsorbed and loosely bonded to the original alumina surface.[45] The pH of the impregnating solution could also affect the sizes of cobalt oxide particles. A correlation between the particle size of cobalt oxide and the pH of the impregnating solution of cobalt nitrate was observed in the catalysts supported by titania.[46]

The concentration, distribution, and nature of hydroxyl groups of the support also play an important role in the genesis of the dispersion of supported metal. The concentration of these hydroxyl groups can be controlled by pretreatment of the support with organic compounds and tetraethylorthosilicate. Zhang[47] et al. found that pretreatment of silica with acetic acid, 1-propanol, and 1-butanol prior to impregnation resulted in higher cobalt dispersion and better activity in the FT reaction. It was found that pretreatment by organic solvent modified the surface properties of silica, enhancing simultaneously cobalt dispersion and reducibility. Pretreatment[48] of alumina with ammonia, ammonium nitrate, acetic acid, and ethanol prior to impregnation also affects the texture, acidity of the support, and catalytic performance of the final catalysts. The number of acid sites decreased in the ammonia- and ammonium-nitrate-treated aluminas, while in the acetic-acid-treated alumina, the concentration of acid sites increased. Higher carbon monoxide conversion and C5+ selectivity were observed on less acid ammonia and ammonium-nitrate-treated catalysts. Initial pretreatment of alumina and titania by TEOS was reported to reduce formation of inactive mixed oxide species.[49]

Slurry (wet) impregnation represents another technique of introduction of cobalt phase to the catalyst supports. Slurry impregnation entails use of an amount of impregnating liquid in excess of what can be accommodated by the total pore volume of selected porous support.[50] The support is usually added to the impregnating solution heated at 333−363 K to yield a slurry.[51] The slurry is stirred continuously during impregnation. After removal of the excess liquid phase, the catalyst is dried at subatmospheric pressure or in flow of air. The initial drying at subatmospheric water is essential to inhibit diffusion of active component to the outer surface of catalyst grains.

2.1.1.2. Impregnation with Cobalt Carbonyl Solutions. Impregnation is one of the simple techniques for immobilizing transition-metal carbonyls on porous oxides. Metal carbonyl impregnating methods have been described by Bailey and Langer.[52] A significant amount of the literature about impregnation with cobalt carbonyls was published[53−55] in the 1980s. It is generally expected that impregnation with cobalt carbonyl produces cobalt catalysts with high metal dispersion. In many cases cobalt metal particles could be obtained at low temperature without use of a reductive atmosphere. Note that reduction is indispensable for obtaining cobalt metal particles in the catalysts prepared via impregnation and decomposition of cobalt salts. After initial physical adsorption, the carbonyls react with surface sites, e.g., surface oxygen sites, hydroxyl groups. A wide range of surface species were identified[56−58] when cobalt carbonyls were gradually losing CO ligands and form, for example, $Co_2(CO)_6L$ or $Co_6(CO)_{16-n}L_n$ species, where L denotes a surface site. Decomposition of metal carbonyl also occurs[59] at FT reaction conditions even in the presence of syngas. During thermal decomposition, the supported metal complex can be also oxidized to cobalt oxides via a reaction with surface hydroxyl groups of the support.

Both monometallic and bimetallic carbonyls have been used for catalyst preparation. $Co_2(CO)_8$ and $Co_4(CO)_{12}$ are the most important cobalt carbonyl precursors. A comparative study of impregnation with $Co_2(CO)_8$ and $Co_4(CO)_{12}$ was performed by Niemelä[60] et al. It was found that $Co_2(CO)_8$ transformed to $Co_4(CO)_{12}$ on silica support during catalyst drying. Nevertheless, the supported catalysts derived from these two precursors exhibited distinct characteristics and reactivity. $Co_2(CO)_8$-derived catalyst had a lower extent of reduction but higher cobalt dispersion than that prepared from $Co_4(CO)_{12}$. Cobalt carbonyl catalysts exhibited[61] a more rapid deactivation during carbon monoxide hydrogenation than a conventional one prepared from cobalt nitrate.

Cobalt catalysts with 3−4 wt % Co content were prepared by Withers[62] et al. using zirconium *n*-propoxide and dicobalt octacarbonyl. Dry SiO_2 was impregnated with a hexane solution of zirconium *n*-propoxide and $Co_2(CO)_8$ dissolved in a mixture of hexane and toluene. The bulk activity of the carbonyl catalysts in the slurry reactor (Table 2) was more than twice that of the catalysts prepared using conventional impregnation with cobalt nitrate, while the specific activity was even more than 3 times higher. Johnson[63] et al. also found a higher catalytic activity of cobalt catalysts supported on alumina prepared from decomposition of tetracobalt dodecacarbonyl than that of conventional cobalt catalysts, while their selectivities were very similar. Lee[64] et al. prepared cobalt-containing zeolite catalysts using ion exchange, carbonyl complex impregnation, and water impregnation. Though exhibiting lower FT reaction rates, the catalysts prepared using carbonyl impregnation had enhanced selectivity to higher hydrocarbons.

Impregnation with carbonyls could also lead to bimetallic catalysts. Bimetallic particles were obtained[65] on alumina using co-adsorption of dicobalt octacarbonyl and diruthenium hexacarbonyl tetrachloride complexes from pentane solutions. Small Co/Ru superparamagnetic and ferromagnetic nanoparticles were prepared[66] using impregnation of MCM-41 silica with a dark red saturated tetrahydrofuran solution of $[NEt_4][Co_3Ru(CO)_{12}]$. Bimetallic Co/Rh particles were

synthesized[67−69] in silica by co-impregnation using monometallic $Co_2(CO)_8$, $Co_4(CO)_{12}$, $Rh_4(CO)_{12}$, and $[Rh(CO)_2Cl]_2$ and bimetallic Co/Rh carbonyls.[70] Mixed Fe/Co catalysts supported by Al_2O_3 and TiO_2 were prepared by Khomenko[71] and Duvenhage.[72] Ten percent Co/TiO_2 and $CoFe/TiO_2$ catalysts were made by impregnation from a solution of $Co_2(CO)_8$, $[C_pFe(CO)_2]_2$, and dimer $C_p(CO)_2FeCo(CO)_4$ in dry oxygen-free tetrahydrofuran.

2.1.2. Co-Precipitation Method

The co-precipitation method has been commonly used for preparation of iron FT catalysts, while for cobalt-supported catalysts very few papers have been published. The precipitation method to prepare cobalt-based catalysts has been employed by the research group in Novosibirsk. Khassin[73−76] et al. prepared cobalt−alumina catalysts using either co-precipitation of Co^{2+} and Al^{3+} ions or Co^{2+} ion precipitation onto freshly prepared Mg−Al or Zn−Al hydrotalcite.[75] It has been shown that, at moderate temperatures, hydrotalcite decomposition yields cobalt oxide phase supported by a highly defective inverted spinel-like structure. Co−Al-precipitated catalysts exhibited low reducibility. Promotion of Co−Al catalysts with Mg^{2+} or Zn^{2+} increased the extent of Co reduction up to 100%. A highly dispersed Co^0 phase was present in all reduced co-precipitated catalysts.

Zirconia-supported cobalt catalysts were prepared by Chen[77] et al. using co- precipitation of mixed cobalt nitrate and zirconyl chloride with sodium carbonate. In the catalysts, the bulk Co/Zr ratio varied from 20 to 80 mol %. No Co_3O_4 clusters were detected by FTIR and EXAFS at low cobalt loadings. This is probably indicative of formation of mixed Co−Zr barely reducible compounds. For catalysts containing higher cobalt contents, the FT reaction rates increased with the increase in Co/Zr bulk ratio (Figure 5).

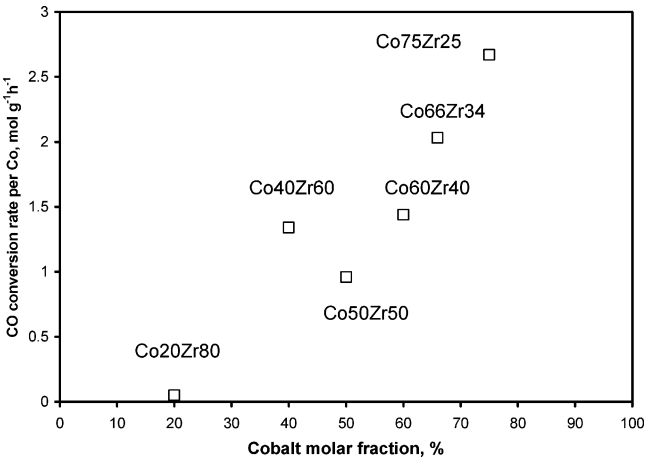

Figure 5. Rate of carbon monoxide conversion over Co−Zr-precipitated catalysts (T = 473 K, 1500 h^{-1}, 2MPa, H_2/CO = 2; plotted from original data in ref 77).

2.1.3. Deposition–Precipitation Method

The deposition−precipitation method is based on precipitation combined with deposition from a liquid medium.[78] The method combines all the advantages of the precipitation method related to control of the size and size distribution of precipitated particles but diminishes the risk of formation of bulk mixed compounds of support and active phase.[79,80] With this technique a solvated metal precursor is deposited exclusively onto the surface of a suspended support by slow and homogeneous introduction of a precipitating agent, generally hydroxyl ions, in such a way as to avoid nucleation of a solid precursor compound in the bulk solution. The most important issue in this method is to prevent precipitation far from the support surface. Generally, hydrolysis of urea at 323−373 K is used to achieve a slow and homogeneous increase in pH.[81,82] The process consists of two steps: (1) precipitation from the bulk solution both in support pores and over support and (2) interaction of the precipitate with the support surface. A fine and homogeneous phase can be obtained by involving surface OH groups of the support in the precipitation process. In the deposition process, adsorption of the metal ions onto the support coincides with nucleation and growth of a surface compound. The support surface acts as a nucleating agent.

The deposition−precipitation technique has been developed for preparation of highly loaded and highly dispersed oxide-supported metal catalysts.[83−85] In the case of catalysts supported on SiO_2 structures, the deposition−precipitation method was studied by Geus[86−88] and then extensively explored by Burattin[79,80,83,84] et al. This method allows obtaining catalysts with high metal loading and dispersion. This method has been previously applied to Ni/SiO_2, Ni/Hβ-zeolite,[89,90] and Ni/SBA-15[91] catalysts.

The deposition−precipitation method has been also extended to carbon-supported catalysts. Carbon nanofibers (CNFs) have been used as templates for manipulating the properties of Ni catalyst particles.[92−94] De Jong[95,96] et al. applied this method for synthesis of Co/CNF catalysts and was successful in obtaining high cobalt dispersion.

A new deposition−precipitation method has been recently proposed by Lok.[97−99] This method is based on slow decomposition of aqueous cobalt amine carbonate complexes at 333−383 K. The pH is homogeneously decreasing from moderately basic to neutral values by controlled evaporation of ammonia from an ammonia/carbonate buffer solution. Cobalt amine carbonate solution may be prepared by dissolving basic cobalt carbonate in an aqueous solution of ammonium carbonate containing ammonium hydroxide. The method leads to a uniform distribution of very small Co crystallites of 3−5 nm. The cobalt metal surface area measured by hydrogen chemisorption can attain 50−100 m^2/g per gram of cobalt. Due to the high dispersion and Co loadings, high activity in FT synthesis has been reported.

2.1.4. Sol–Gel Method

Sol−gel is another technique to prepare catalysts for FT synthesis.[100−103] The sol−gel process also allows mastering and adjusting the surface area, porosity, and particle size of prepared catalysts.[104,105,108] Although the sol−gel method has been known as one of the easiest ways to obtain uniform structure, the microscopic feature strongly depends on the preparation method. A typical sol−gel procedure was employed by Okabe[100,106] et al. The required amount of $Co(NO_3)_2 \cdot 6H_2O$ was dissolved in ethylene glycol. Tetraethyl orthosilicate was added to the solution, and the mixture was heated under vigorous stirring to form a homogeneous solution. Pore size modifiers, such as *N*,*N*-dimethylformamide, formamide, and polyethylene glycol (average molecular weight = 2000), were added to the solution at that stage. Distilled water and ethanol were then added to the solution dropwise at room temperature, resulting in a homogeneous clear sol. The sol was slowly hydrolyzed by heating at a temperature higher than 353 K for more than 40 h to form a glassy transparent gel. The gel was dried and calcined in

nitrogen and air flow at 823 K for 15 h and then reduced in hydrogen flow at 773 K for 15 h. After reduction, transmission electron microscopy displayed a uniform distribution of Co metal particles of 3−5 nm diameter. XPS depth profile analysis of the sol−gel catalysts indicated that the Co concentration was uniform in three dimensions. The sol−gel method proved to be more suitable for uniform preparation of highly loaded catalysts (about 60 wt %) than impregnation. While CO conversion was low over the sol−gel catalyst without a promoter, addition of a trace amount of noble metal drastically improved cobalt reducibility and catalytic activity. Moggi[107] et al. reported a similar sol−gel procedure. Cobalt nitrate hexahydrate was dissolved in dry tetrahydrofuran, then tetraethyl orthosilicate and water were added, and the homogeneous sol was transferred in a vessel suitable for evaporation of the solvent. The obtained gel was then dried in vacuum at room temperature.[107] In such a catalyst, most of the cobalt particles were occluded in SiO_2 matrix and cobalt reduction was very difficult. As expected, a very low catalytic activity was observed in carbon monoxide hydrogenation. Ernst and Kiennemann[108] et al. studied the FT activity and selectivity of Co/SiO_2 prepared by a pseudo sol−gel technique in acidic and basic media. It was found that the FT reaction rate increased with the specific surface area. High hydrocarbon selectivity was favored in the case of silica-dispersed cobalt catalyst with a pore diameter less than 4 nm.

The sol−gel preparation method could be coupled with drying at supercritical conditions. Eyring et al.[109] reported preparation of three cobalt catalysts supported by aerogel with cobalt loading varying from 2% to 10%. Transmission electron micrographs showed the presence of discrete cobalt metal particles of 50−70 nm for 2% and 6% loadings. The 10% Co catalyst exhibited long needles of cobalt.

2.1.5. Eggshell Catalysts

In recent years, many studies have been concerned with control of the metal profile in support particles.[110−113] A review of this research area was given by Gavriilidis[114] et al. The choice of the optimal catalyst profile in the support is determined by the required activity, selectivity, and other characteristics of the chemical reaction (kinetics, mass transfer).

Eggshell catalysts are advantageous in the case of fast reactions with strong diffusion restrictions because the active component is concentrated close to the external pellet surface. Eggshell catalysts have been proposed to overcome difficulties due to diffusion limitations in catalyst pellets in fixed bed FT reactors. It was suggested[115] that smaller than 0.2 mm pellets were required to avoid mass-transport restrictions. Such small catalyst particles would lead to a very significant pressure drop in large commercial fixed bed reactors. Eggshell catalyst pellets of 2 mm diameter introduce design flexibility by decoupling the characteristic diffusion distance in catalyst pellets from pressure drop and other reactor constraints.

There are several methods to prepare eggshell catalysts. Most of these methods are based on controlled catalyst impregnation and drying. These methods involve several parameters: metal concentration in the impregnating solution, solution viscosity, support condition (dry or wet), impregnation time, and drying procedure. These parameters affect the eggshell thickness, metal distribution, metal morphology, and metal crystallite size.

Eggshell catalysts can be produced during drying depending on the relative strength of adsorption, diffusion, and convection. During drying, the liquid solution is transported by capillary flow and diffusion[116−120] and the precursor may be redistributed by adsorption/desorption phenomena.[116,117] Solvent with higher viscosity[121] could prevent migration of the active phase and lead to a more uniform distribution of cobalt atoms inside the catalyst grains. The approach based on solutions of chelated metal complexes with high viscosity was further developed in work by de Jong and co-workers.[122] A desired metal profile can be obtained also by impregnation of a single component or successive or competitive impregnation of two or more components, called multicomponent impregnation.[114,117,123]

Earlier studies of the distribution of the active phase in the catalyst grains have predominately addressed Pt-based catalysts. Maatman[124] showed that for platinum deposition from chloroplatinic acid on an alumina support, co-impregnation can control the distribution of the active phase in a pellet. A nonuniform distribution of active component occurs when the support (alumina) acts like a chromatographic column separating the solution and active phase.

Since then, co-impregnation techniques have been widely used to prepare nonuniformly distributed cobalt catalysts. Peluso et al.[125] and Galarraga[126] et al. demonstrated that the preparation conditions of CoZr eggshell SiO_2 catalysts for FT synthesis influenced the production of middle distillates, particularly the C_{10}–C_{20} hydrocarbon fraction. On this basis it was established that an optimum eggshell catalyst should have 10 wt % Co deposited in the half radius of a 1.81 mm diameter particle. This eggshell catalyst displayed encouraging CO conversion and selectivity, yielding 65 wt % hydrocarbons in the diesel range. Mathematic modeling demonstrated that wet impregnation using low metal concentration solutions improved metal dispersion by producing a more progressive eggshell profile than incipient wetness impregnation.[127]

Zhuang[128] et al. showed that eggshell catalysts with a sharp boundary could be prepared by covering the inside of the pellet with a defined amount of *n*-undecane prior to the impregnation procedure. In this technique the aqueous solution (either the impregnation solution or the leaching solution) is prevented from entering the core of the catalyst pellet since the pore volume in the center of the catalyst pellet is filled with the hydrophobic organic solvent. A partial coverage of silica pellets with a hydrocarbon, *n*-undecane, protects that part of the pellet, yielding an eggshell catalyst.

Iglesia[129] et al. proposed an alternative route to synthesize eggshell catalysts by controlling the rate of diffusion of molten cobalt salt into the support. The eggshell cobalt catalysts were prepared by placing SiO_2 spheres into molten cobalt nitrate (melting point 373 K). Molten cobalt nitrate was poured uniformly over SiO_2 spheres. For melt impregnation, the shell thickness was less than 0.2 mm for contact times less than 30 s (Figure 6).

2.1.6. Monolithic Catalysts

One of the largest advantages of monolithic catalysts is a low pressure drop in a large-scale reactor because of thin catalyst layers with a tunable thickness.[130,131] Thin catalyst layers also eliminate effects of diffusion limitations. Heat generated by FT reaction can be removed in monolithic catalysts by recycling liquid through the channels of the monolith and an external heat exchanger. Tailoring the layer

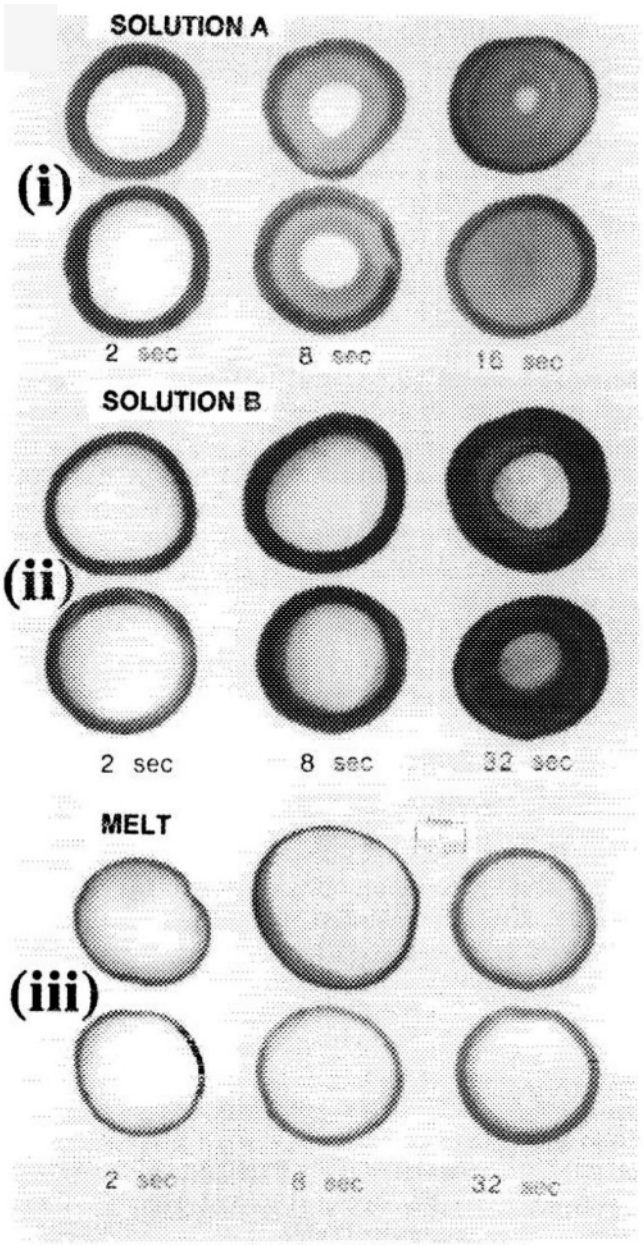

Figure 6. Optical micrographs of eggshell Co/SiO_2 catalysts prepared using (i) controlled immersion in aqueous cobalt nitrate solution, (ii) aqueous cobalt nitrate solution viscosified with hydroxyethyl cellulose, and (iii) cobalt nitrate melt. Contact time, 1−30 s; melt at 353 K (reproduced from ref 129, Copyright 1995, with permission from Elsevier).

thickness allows design of monolithic catalysts with optimal activity and selectivity[132] in FT synthesis. No wax−catalyst separation is necessary in monolithic reactors.

Two research groups have been working in the area of monolithic catalysts for FT reaction. Three types of monolith are generally used: cordierite γ-Al_2O_3 and steel monoliths (i.e., steel sheets).[133−136,138] These monolithic catalysts consist of long parallel channels separated by thin walls[136] (Figure 7). The walls can be either made of cordierite on which a high surface area catalyst support can be wash coated or a suitable catalyst support such as alumina and silica. The wash-coating procedure is described in detail by Nijhuis et al.[137] Different coating thicknesses could be achieved by repeating the coating process. Cobalt active phase in monolith catalysts is deposited by either aqueous co-impregnation[133] or homogeneous deposition[138] precipitation from an aqueous

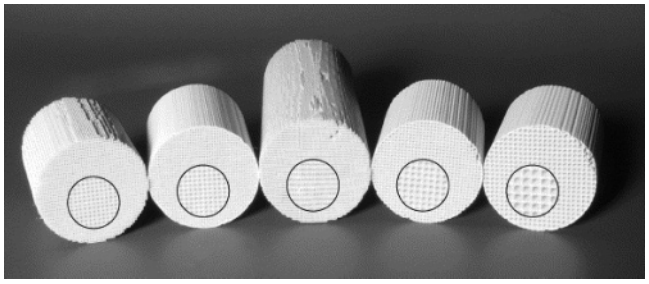

Figure 7. Photo of several monolithic catalyst structures (reproduced from ref 136, Copyright 2003, with permission from Elsevier).

solution of cobalt nitrate and urea. An overall cobalt loading of 10−20 wt % can be obtained.

Carbon monoxide conversions between 7% and 50% were attained with cordierite-based catalysts.[138] Normal α-olefins and paraffins are major FT products[138] over cordierite monolithic catalysts. The olefins and paraffins follow ASF distribution with chain growth probabilities between 0.77 and 0.93 depending on the reaction conditions. Carbon monoxide conversion was only slightly affected by wash-coat thicknesses, while the selectivity to methane increased with layer thickness. Monoliths with a wash-coat layer thicker than about 50 μm suffer from diffusion limitations, accompanied by the expected decrease in the apparent activation energy.[133,139,140]

2.1.7. Colloidal, Microemulsion, and Solvated Metal Atom Dispersion Methods

2.1.7.1. Colloidal Method. Colloidal synthesis has been widely used[141] as an efficient route to control metal particle size and shape, crystallinity, and crystal structure. Metal colloids displayed remarkable catalytic performance in a wide range of reactions. Stabilization of colloidal systems is a crucial issue in the synthesis of metal colloids and colloid-based supported catalysts. Although colloids encapsulated in polymer matrix are very stable, it is not economical and convenient to recover them from the polymer by conventional methods. In addition, metal sites in a colloidal particle, which is included in polymer, could be inaccessible for reacting molecules.

Thus, research has primarily focused on immobilization of surfactant-stabilized colloids on catalytic supports.[142−146] The surfactant-stabilized colloids usually tend to agglomerate even under very mild conditions. Thus, during synthesis of the colloids the presence of surfactant is essential to disperse and stabilize nanoparticles in the solvent.[147−151] The colloidal metallic systems could be stabilized using different surfactants such as organic thiols, carboxylates, poly(acrylic acid), oleic acid, phosphonates, and trioctylphosphine.[152]

Several methodological approaches have been developed to prepare metallic heterogeneous catalysts from colloidal systems: polyol method, ethylene glycol method, modified coordination capture method, pseudo-colloidal method, etc.

In the polyol process[153] boiling alcohol is used as both a reductant and a solvent. In a typical synthesis 1,2-dodecanediol is added into hydrated cobalt acetate solution dissolved in diphenyl ether containing oleic acid and trioctylphosphine. Nanoparticles could be isolated by size using selective precipitation. The cobalt particle size is controlled by changing the relative concentrations of both precursor and stabilizer.

The ethylene glycol method is based on complexation of colloidal metal particles by carboxylic species produced via oxidation of ethylene glycol. This method has been described by Qiu[154] et al. for synthesis of cobalt nanoparticles supported by carbon nanofibers. The typical procedure is presented below. To obtain a colloidal suspension of cobalt, the pH of the cobalt nitrate solution was adjusted to 13 using 2.5 M NaOH in ethylene glycol. The suspension was refluxed at 453 K for 3 h to ensure complete reduction of cobalt. During refluxing, ethylene glycol is reducing cobalt species and oxidized to glycolic and oxalic acids. After cooling to room temperature, the pH was decreased using HCl solution. A pH lower than 7 was essential for deposition of cobalt particles on carbon nanofibers.

The coordination capture method has been proposed by Liu[155,156] et al. The method involves capture of colloidal metal particles onto the surface of functionalized silica by ligand coordination.[157,158] The coordination capture method, however, suffers from the need for a series of complicated steps to prepare the functionalized support. Strong coordination ligands (e.g., mercapto group) are required. These ligands could be disastrous for the catalytic properties of metal catalysts.

Using a pseudo-colloid method, Wang[159−161] et al. prepared cobalt nanoparticles supported by faujasite zeolites. Cobalt particles with a maximum size distribution of 1−2 nm, which are probably located inside the supercages of faujasite zeolite, were obtained using a higher concentration of $NaBH_4$ aqueous solution (10 M), while formation of cobalt particles larger than 20 nm was observed when lower temperatures of Co^{2+}−faujaiste zeolites pretreatments and lower concentrations of $NaBH_4$ (0.1 and 0.5 M) were used. The smaller cobalt nanoparticles, which were located inside the supercages of faujasite zeolite, exhibit CO conversions in FT synthesis higher than the larger cobalt particles outside the supercages.

In our recent research work[162] alumina-supported nanosized cobalt catalysts were prepared using the colloid method from a slurry of alumina and cobalt chloride solution using reduction with sodium borohydride. The unsupported cobalt catalyst was almost inactive in FT synthesis. The alumina-supported cobalt catalysts prepared using reduction with sodium borohydride exhibited relatively high carbon monoxide hydrogenation rates with a considerable methane selectivity.

2.1.7.2. Microemulsion Method. A considerable number of reports have recently addressed the microemulsion method for preparation of metal-supported catalysts. The microemulsion method was recently reviewed by Capek.[163] The method usually involves microemulsion stabilizer. A stabilizer (emulsifier) is a molecule that possesses both polar and nonpolar moieties. In diluted water (or oil) solution, emulsifier dissolves; it is present in the form of monomer. When the concentration of emulsifier exceeds the critical micelle concentration, the molecules of emulsifier associate spontaneously to form aggregates−micelles. Formation of oil-in-water (o/w) or water-in-oil (w/o) reverse micelles could be driven by hydrophobic or hydrophilic interactions of the hydrophobic tail or hydrophilic polar group, respectively. Because microemulsions typically have droplet diameters much smaller than the wavelength of visible light, they can be characterized visually by formation of an optically transparent single phase. A particle size in the range of 5−50 nm depends on the size of microemulsion droplets and can be controlled by adjusting the water to surfactant ratio or concentration of reagents. These small microemulsion droplets can be viewed as nanoreactors.[164,165] The metal particles produced by this method usually have a spherical shape. Modification of the synthesis procedure, however, could result in rods[166] or rings.[167]

Below is a brief description of the typical microemulsion procedure. The method consists of preparing two microemulsions (Figure 8): the first microemulsion contains metal salt encapsulated in the droplets, and the second microemulsion represents reducing agent ($NaBH_4$, N_2H_4, etc.) located inside the droplets. Then two microemulsions are mixed together. The metal salt inside the micelles is reducing to metallic particles by the reducing agent; the rate of the reduction is controlled by the intermicelle exchange rate.[168]

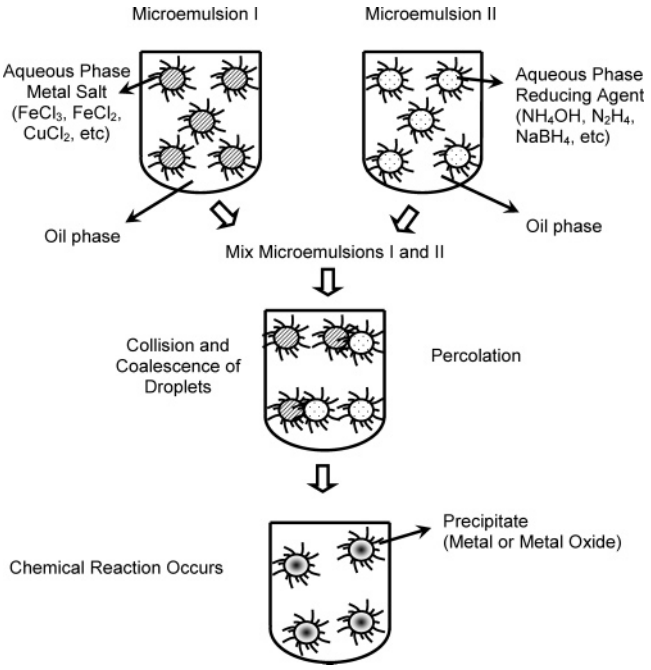

Figure 8. Principal stages of metal nanoparticle preparation using the microemulsion approach (reproduced from ref 163, Copyright 2004, with permission from Elsevier).

The example of making cobalt metallic nanoparticles has been given by Chen.[169] Cobalt fine particles were prepared using a H_2O/sodium di-2-ethyl hexysolfosuccinate (AOT)/isooctane ternary system. The cobalt-containing microemulsion was prepared by mixing AOT in isooctane with an aqueous solution of cobalt chloride. The reducing microemulsion was obtained by mixing AOT in isooctane with an aqueous solution of $NaBH_4$. Both emulsions were transparent. Then they were mixed; the color of the product turned from light pink to black in a few seconds. The size of the produced cobalt metal particles was lower than 3 nm.

Despite a great deal of promise, very few studies have focused on the preparation of cobalt-supported catalysts for FT synthesis from microemulsion systems. Most of the literature has primarily addressed Pd, Rh, Fe, and Ru catalysts.

2.1.7.3. Solvated Metal Atom Dispersion Method. The solvated metal atom dispersion (SMAD) method was proposed in the 1980s by Klabunde et al. The method employs free metal atoms (vapor), which are solvated in an organic solvent at low temperatures.[170] The support is impregnated with this solution. The deposited metal clusters maintain their

reduction state, and thus, they could be used without any reduction for catalytic reactions. The typical catalyst preparation procedure is described in ref 171. The SMAD apparatus possessed four water-cooled copper electrodes, two $W-Al_2O_3$ metal vaporization crucibles, and two separate power supplies. Cobalt and eventually promoting metal were vaporized in the flow of toluene. The toluene and solvated metal atoms were condensed into a frozen matrix by the wall of the chamber cooled with liquid nitrogen. Then the matrix was allowed to warm slowly to 178 K. The matrix melted and formed a toluene-solvated metal atom solution. This solution was stirred and warmed in the presence of a catalytic support. The solvates decomposed and deposed metal atoms on the surface of the support (Figure 9).

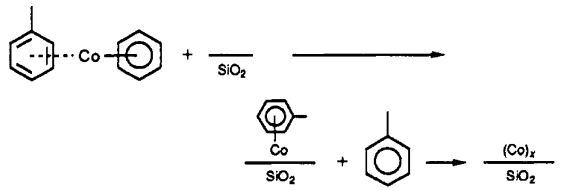

Figure 9. Deposition of metal atoms on silica support using SMAD.

Several monometallic and bimetallic cobalt[172] catalysts supported by SiO_2 and Al_2O_3 were prepared using the SMAD method. OH groups served as anchors for cobalt metal atoms solvated in toluene.[173] Nucleation of cobalt clusters proceeds on cobalt oxide species and catalyst promoters. EXAFS characterization[174] showed that a major part of cobalt atoms remains metallic. The catalytic test in a recirculating reactor showed a high activity of monometallic Co/Al_2O_3-supported catalysts in FT synthesis. The reaction rates were very high compared with those for cobalt catalysts prepared by conventional impregnation and carbonyl methods.

2.1.8. Chemical Vapor Deposition

The conventional chemical vapor deposition (CVD) method is a well-known technique for deposition of metal oxide particles on powdery supports.[175,176] CVD involves chemical reactions of gaseous reactants on or near the vicinity of a heated substrate surface. This deposition method can provide nanostructured and functionally coated materials with unique structure. The advantages of CVD are due to the uniform distribution of cobalt nanoparticles on catalyst support and possibly a narrow distribution of cobalt particle size. CVD can be performed either in vacuum or in a flow of carrier gas (Ar, He). After deposition, the precursor is decomposed at higher temperatures, yielding metallic or oxide nanoparticles.

Commercially available cobalt CVD precursors include cobalt carbonyl complexes,[177−184] cobalt acetylacetonates,[185−188] and cobalt acetate.[189] Use of these cobalt compounds for CVD could be explained by their low meting point and high vapor pressures. Recently, a novel cobalt(I) hydroxide precursor was synthesized by Choi[190] et al. It was used to deposit high-quality cobalt thin films at 573 K.

Kurhinen[177] and Pakkanen[191,192] prepared cobalt nanoparticles on Al_2O_3 and SiO_2 using chemical vapor deposition of dicobalt octacarbonyl. Cobalt carbonyl was reacted with hydroxyl groups of the support. At the surface the $Co_2(CO)_8$ rearranged to $Co_4(CO)_{12}$, and the surface was completely decarbonylated via subcarbonyl species. The amount of carbonyl adsorbed depended on the support pretreatment temperature. A considerable concentration of cobalt carbonate and bicarbonate species was observed after deposition. A higher cobalt content in the catalysts was obtained using several subsequent carbonyl deposition−decarbonylation procedures[193,194] (Figure 10).

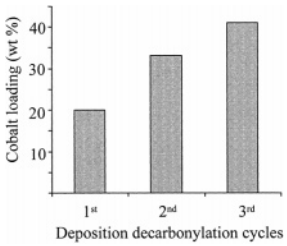

Figure 10. Cobalt loading on MCM-41 as a function of cobalt carbonyl deposition− decarbonylation cycles (reproduced from ref 194, Copyright 2000, with permission from the American Chemical Society).

Backman and Krause[185,195,196] prepared Co/SiO_2 and Co/Al_2O_3 catalysts via chemical vapor deposition of cobalt acetylacetonates (II and III). The precursor was evaporated into flowing nitrogen at 453 K. The surface of the support was saturated by an excess of precursor. The precursor was decomposed by heating the catalyst in air at 723 K. Cobalt aluminates and silicate were also formed on Co/Al_2O_3 and Co/SiO_2 samples during calcination and acetylacetonate decomposition.

Recently, Dittmar[175] et al. prepared and characterized cobalt oxides supported on titania by microwave plasma-enhanced chemical vapor deposition starting from cobalt-(III) acetylacetonate and TiO_2 (support). In this method $Co(acac)_3$ was evaporated and adsorbed on the carrier surface. Then $Co(acac)_3$ was decomposed during the microwave-plasma treatment in an oxygen atmosphere. The size of deposited cobalt oxide particles was between 2 and 10 nm as a function of plasma treatment time and cobalt content.

2.1.9. Plasma Methods

Application of plasma techniques for preparation of catalysts was initiated in the 1980s, and a few significant results have been reported in the literature.[197,198] Below two techniques are discussed based on plasma spraying and glow discharge plasma.

2.1.9.1. Plasma Spraying. A number of FT synthesis studies have been carried out using iron[199−201] and bimetallic cobalt−iron[202,203] catalysts in tube-wall reactors (TWR). Tube-wall reactor surfaces were prepared by Dalai[199] et al. using the plasma spraying of five catalysts, namely, Fe, 75Fe/25Co, 50Fe/50Co, 25Fe/75Co, and Co (weight percent basis). It was interesting to observe that despite the low BET surface areas for "plasma-sprayed" catalysts, hydrogen and carbon monoxide uptakes were found to be relatively high. XRD studies showed that various catalyst phases were stable up to 623 K; the surface consisted of particles of Fe and Co oxides and cemented particles of CoO-Fe20B. SEM studies confirmed that these particles were uniformly distributed throughout the catalyst layer. The crystallite sizes determined from hydrogen chemisorption measurements were fairly close to those obtained from X-ray line-broadening experiments. Electron probe microanalysis showed that the plasma-sprayed catalyst surface possessed a higher concentration of iron particles than that of cobalt particles, suggesting that iron

tends to migrate to the surface at the expense of cobalt. Catalyst activity was[200] a strong function of the operating conditions; a maximum of 98.5% CO conversion was achieved. The selectivity to C_5+ hydrocarbons was over 40% of the total hydrocarbons produced in the pressure range of 0.69−1.03 MPa.

2.1.9.2. Glow Discharge Plasma. In our previous work[204−206] a number of active catalysts for several catalytic processes have been developed using the glow discharge plasma technique. It was reported[204] that plasma activation of a Ni/α-Al_2O_3 catalyst was efficient for methane conversion to syngas. That was a typical example of combining plasma and chemical treatment of the catalyst. First, the radio frequency (∼13.56 MHz) plasma with argon as plasma-forming gas has been used for decomposition of $Ni(NO_3)_2$ into black Ni_2O_3. In this step, plasma served as a special energy supply. Then, hydrogen plasma at the same frequency has been applied for reduction of catalyst. The catalyst became green ($Ni_2O_3 \rightarrow$ NiO) and then changed to black (NiO → Ni) again by hydrogen plasma. The plasma-prepared catalyst showed a better activity and stability compared to a conventionally prepared sample. The total treatment time is less than 3 h at a discharge tube temperature of 338 K (plasma heat treatment for decomposition and then 65 min for plasma reduction), while conventional preparation of catalyst needs 10 h of calcination at 1173 K and 1 h of reduction at 873 K. The plasma activating process was simple, quick, audiovisual, and easy to control. The activity and stability of the activated catalyst were higher than those of conventional catalysts.

Several plasma-enhanced cobalt catalysts have been developed[162] for FT synthesis. The results of selected catalytic tests are listed in Table 3. Platinum-promoted catalyst with 15 wt % cobalt loading showed a CO conversion of 21% at 1 bar and 463 K, and the CH_4 selectivity was 8.1%. CO conversion was only 6.4% for the conventional alumina-based catalyst, which was calcined at 613 K and reduced at 673 K. On the other hand, the plasma-enhanced catalyst with platinum promoter exhibited a FT rate that was 25% higher than that of non-plasma-treated sample. The CO conversion level reached 26.3% from 21%, with a C_{5+} selectivity of 73%, slightly lower than 76 % for conventional catalyst. The cobalt time yield was 769 μmol/mol-Co/s. Glow discharge plasma treatment, therefore, could lead to higher cobalt dispersion and a high density of surface sites in cobalt FT catalysts.

Table 3. Catalytic Behavior of Plasma-Enhanced Cobalt Catalysts in FT Synthesis[a]

catalyst sample	conv. %	rate (10^2 μmol/mol Co/s)	sel. (%) CH_4	C^{5+} sel. (%)
Co15A340	6.37	1.86	7.32	78.39
CoPtA340	21.04	6.15	8.08	75.84
CoPtA-plasma-PNH	26.30	7.69	9.56	72.67

[a] Conditions: P = 1 bar, T = 463 K, GHSV = 1800 mL/g/h, H_2/CO = 2.

2.2. Promotion with Noble Metals

Numerous studies have shown that introduction of a noble metal (Ru, Rh, Pt, and Pd) has a strong impact on the structure and dispersion of cobalt species, FT reaction rates, and selectivities. The promoting metal is typically introduced via co-impregnation or subsequent impregnation. Introduction of noble metals could result in the following phenomena: much easier reduction of cobalt oxide particles, formation of bimetallic particles and alloys, a lower fraction of barely reducible mixed oxides, enhancement in cobalt dispersion, inhibition of catalyst deactivation, appearance of additional sites of hydrogen activation, and an increase in the intrinsic reactivity of surface sites.

Ease of Cobalt Reduction. Many authors have observed much easier reduction of cobalt oxides to active metal cobalt phases in the presence of noble metals. Batley et al.[207] observed that reduction of bulk Co_3O_4 occurred at much lower temperature in the presence of 0.5 wt % Pt. Van't Blik et al. [208] showed that co-impregnation of silica with solutions of cobalt nitrate and ruthenium chloride resulted in bimetallic particles, which could be reduced at much lower temperatures than the parent Co/SiO_2. Takeuchi et al.[209,210] showed that modification with ruthenium of cobalt silica-supported catalysts prepared from cobalt acetate considerably increased the extent of cobalt reduction and its activity in the synthesis of C2-oxygenates from syngas. The positive effect of ruthenium on cobalt reducibility was also observed by Reinikainen[211] et al. Okabe[100] et al. showed that addition of iridium considerably increased cobalt reducibility. Girardon[212] et al. uncovered that addition of Re and especially Ru to cobalt silica-supported catalysts considerably improved cobalt reducibility. The in-situ magnetic method (see section 3.6), which selectively detected cobalt metal particles, was indicative[212] of a higher concentration of cobalt metal phase in the promoted catalysts (Figure 11).

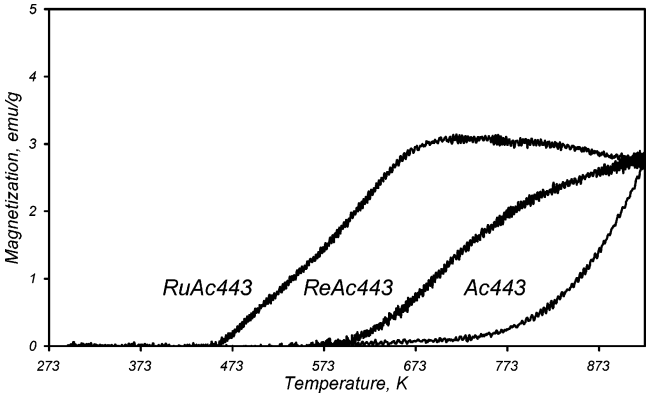

Figure 11. In-situ magnetization curves of cobalt catalysts measured during temperature-programmed reduction in pure hydrogen. The catalysts were prepared via decomposition of cobalt acetate at 443 K (reproduced from ref 212, Copyright 2005, with permission from Elsevier).

A significant effect of promotion with noble metals on the number of cobalt metal sites was observed on alumina-supported catalysts. In fact, significant shifts of cobalt oxide reduction temperature to lower values have been observed with Pt and Ru addition[213−215] (Figure 12). It was suggested that Pt was situated on the edge of the cluster and that reduction occurred on Pt first, allowing hydrogen to spill over to cobalt oxide and nucleate cobalt metal sites.[216]

Tsubaki et al.[217,218] found that addition of small amount of Ru to cobalt catalysts remarkably increased the extent of cobalt reduction, whereas modification with Pt and Pd did not have any effect on cobalt reducibility. Pt and Pd were found to promote mostly cobalt dispersion. The cobalt catalysts promoted with noble metals displayed the following order of FT catalytic activity: CoRu > CoPd > CoPt >

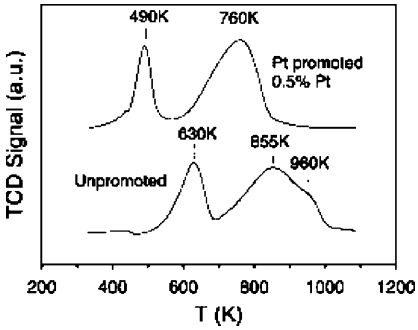

Figure 12. TPR profiles of unpromoted and Pt-promoted 15% Co/Al_2O_3 catalysts (reproduced from ref 214, Copyright 2003, with permission from Elsevier).

Co. Pd- and Pt-containing samples also showed higher methane selectivity than Co and CoRu samples.

The effect of promotion with Re on cobalt reducibility is usually less significant than with platinum and ruthenium. It is known that reduction of Co_3O_4 to metallic cobalt proceeds via intermediate formation of CoO. It was suggested that Re affected only the second reduction step: CoO to Co.[219−221] This was attributed to the fact that reduction of Re occurred above the temperature of Co_3O_4 to CoO reduction.

Formation of Bimetallic Particles and Alloys. Pt−Co alloy was observed using XRD by Dees et al.[222] at different Pt/Co ratios on silica-supported catalysts. Small amounts of cobalt had a significant impact on the selectivity of the hexene hydrogenation reaction. It was suggested that the metal surface of bimetallic Pt/Co particles was enriched by cobalt. Bimetallic particles in CoPt/NaY[213,223] and CoRe/NaY[224] zeolite were also identified by Guczi et al. Bimetallic Co/Re[225] and Co/Pt[226] particles were observed in alumina-supported catalysts. Co/Pd particles were detected in graphite[227] and silica.[228]

Promotion with noble metals could also affect **decomposition of cobalt precursor**. Our recent report[212] has shown that promotion using ruthenium nitrosyl nitrate results in a lower temperature of decomposition of cobalt acetate and a higher density of cobalt metal sites in the resulting catalyst.

Enhancement in cobalt dispersion is another effect due to introduction of noble metals to cobalt catalysts. One of the reasons responsible for the higher cobalt dispersion could be related to a higher concentration of cobalt oxide nucleation sites during decomposition of cobalt precursors in the presence of promoting noble metals. A higher concentration of Co_3O_4 nucleation sites (at the same cobalt content) would result in a larger number of cobalt particles and consequently higher cobalt dispersion in the catalysts. Another reason responsible for the higher cobalt dispersion could be related to the lower temperature of reduction of cobalt species in the presence of noble metals and, consequently, a lower probability of formation of cobalt−support mixed oxides and/or sintering of the reduced cobalt metal particles. Schanke[229] et al. showed that addition of platinum to Co/SiO_2 catalyst did not lead to a considerable increase in the extent of reduction. The total amount of chemisorbed hydrogen after promotion with 0.4 wt % Pt increased by more than 30%, while the extent of cobalt reduction was, respectively, 90% and 92% for monometallic and Pt-promoted cobalt catalysts. Higher FT reaction rates were attributed not to an easier reduction but to an increase in cobalt dispersion due to the presence of platinum.

Iglesia[230] et al. uncovered that promotion with ruthenium retarded irreversible deactivation of cobalt catalysts. **Better resistance to deactivation** led to higher concentrations of active sites in the working catalysts at FT reaction conditions. Ru-catalyzed hydrogenolysis of carbonaceous residues and reduction of surface oxygen atoms permitted regeneration of Co−Ru catalysts in hydrogen at lower temperatures. The reaction rates increased three times without apparent changes in cobalt dispersion. The data about the positive effect of the noble metal promotion on catalyst deactivation are consistent with the observation by Jongsomjit et al.[231] It was shown that promotion with ruthenium prevented catalyst deactivation due to the retarded formation of inactive mixed Co−Al oxides in the presence of water.

Guczi[232] et al. showed that addition of Pd to Co silica-supported catalysts resulted in significant modifications in the catalytic activity. Promotion with Pd resulted in an increase in the relative fraction of alkanes in the products of carbon monoxide hydrogenation. This effect was attributed to **a higher concentration of hydrogen activation sites** in the presence of promoting Pd. Bardi[233] et al. suggested, using a combination of LEED and low-energy ion-scattering spectroscopy, that formation of Co−Pt alloys modified the electronic properties of Pt atoms and the energetics of carbon monoxide adsorption. Promotion with noble metals could also lead to the increase in site reactivity.[234]

2.3. Promotion with Oxides

Promotion with oxides has been one of the methods to improve the activity and hydrocarbon selectivity of FT catalysts. Among the oxide promoters, ZrO_2, La_2O_3, MnO, and CeO_2 have been most often employed. Addition of oxide promoters could modify the catalyst texture and porosity, reduce formation of hardly reducible cobalt mixed oxides, increase cobalt dispersion, reducibility, and fraction of different cobalt metal crystalline phases, enhance mechanical and attrition resistance of cobalt FT catalysts, and improve the chemical stability of the support. The paragraphs below focus on the effects of different oxide promoters on the structure and catalytic performance of supported cobalt FT catalysts.

2.3.1. Promotion with Zirconia

The beneficial effect of promotion with zirconia has been observed on several oxide supports and even for cobalt catalysts supported by activate carbon.[235] Promotion with zirconia usually results in higher FT reaction rates; an increase in C5+ selectivity has been also reported.

Silica-Supported Catalysts. It was claimed that zirconium could enhance the activity and hydrocarbon selectivity of Co/SiO_2 catalysts. Preimpregnated zirconia could constitute a protecting layer, preventing a chemical reaction between silica and cobalt and thus formation of hardly reducible cobalt silicates.[236,237]

Feller[238] et al. showed that modification with zirconia facilitated reduction of cobalt species. An increase in zirconia content resulted in larger and easily reducible cobalt particles. The reaction rate also increased with higher zirconia contents, which was attributed to a larger concentration of cobalt metal sites in the catalysts with a higher extent of reduction. This observation is consistent with the results of Oukaci[236] et al., who found that addition of ZrO_2 to silica-supported cobalt catalysts slightly increased cobalt reducibility without any affect on cobalt dispersion. Similar results were obtained in

recent papers by Moradi,[239] Yin,[240] and Jacobs.[221] Ali[241] et al. showed that the catalytic behavior of $CoZr/SiO_2$ catalysts was strongly affected by the preparation method. The most active were catalysts prepared via sequential impregnation of silica with cobalt and zirconium nitrates.

Modification with zirconia could also modify the fraction of hexagonal and cubic phases, which constitute cobalt metal particles in the reduced catalysts. MCM-41 mesoporous silica was modified by addition of zirconium oxynitrate during hydrothermal synthesis.[242] Cobalt−iridium catalysts modified with zirconia have been shown to have higher C5+ and lower methane selectivities than pure silicaneous counterparts. These effects were attributed to a higher fraction of cubic cobalt metallic phase in the zirconia-promoted catalysts.

Alumina-Supported Catalysts. Jacobs and Davis found[221] that zirconia addition increased the cobalt dispersion and decreased the reducibility of cobalt species in alumina-supported FT catalysts. The catalysts after cobalt addition were promoted by incipient wetness impregnation with zirconium nitrate. The effect of promotion with zirconia on cobalt dispersion and reducibility in alumina-supported catalysts is illustrated in Figure 13.

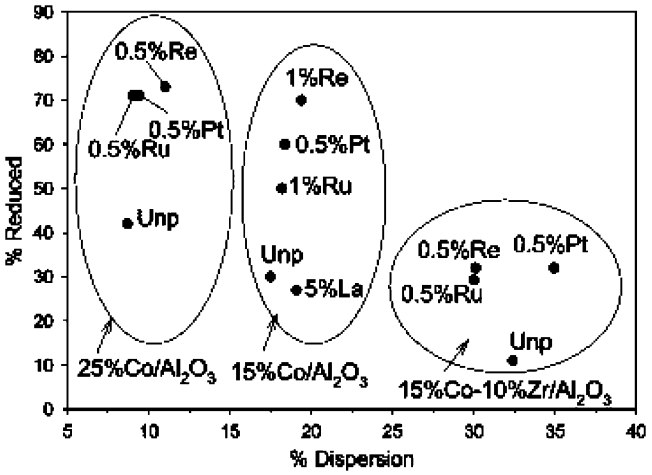

Figure 13. Extent of reduction versus cobalt dispersion in unpromoted and Zr-promoted cobalt alumina-supported catalysts. The catalysts were reduced at 623 K (reproduced from ref 221, Copyright 2002, with permission from Elsevier).

Rohr[243] et al. uncovered that addition of zirconia to alumina led to a significant increase in both activity and selectivity. This increase was attributed to the changes in surface coverage of reactive intermediates and not to changes in the intrinsic selectivity.

Jongsomjit[244] et al. showed that addition of zirconia to alumina-supported cobalt catalysts resulted in stabilization of alumina support and prevention of Co surface "aluminate" formation. SSITKA experiments indicated an increase in the number of active surface intermediates with Zr modification, while the intrinsic site activity remained constant. This suggests that the effect of zirconia is primarily due to the increase in the number of active sites without modifying the turnover rate. In agreement with these data, Xiong[245] et al. found that promotion with zirconium led to a lower content of cobalt aluminate species. This suggests that added zirconia could inhibit $CoAl_2O_4$ formation. Large cobalt particles were detected after zirconia addition.

Reduction of cobalt oxidized species supported by alumina results in cubic and hexagonal cobalt metal phase. For catalysts obtained using conventional calcinations, cobalt cubic phase seems to be more predominant on alumina than on silica. A recent study by Enache[22] et al. showed that mostly hexagonal cobalt metal phase can be obtained by direct reduction of Co/Al_2O_3 catalysts, which were prepared by impregnation with cobalt nitrate. It has been shown that the presence of zirconia in cobalt-supported catalysts promotes poorly crystallized hexagonal phase. This phase was found to be more active in FT synthesis than cobalt cubic phase. Therefore, one possible interpretation of the effect of zirconia promotion on FT reaction rate might be assigned to the higher concentration of more active Co hexagonal phase in zirconia-promoted catalysts. Promotion with zirconia does not always bring about only beneficial effects. Wei[246] et al. showed that promotion with zirconia could have a negative effect on catalyst mechanical strength.

2.3.2. Promotion with Lanthanum Oxide

Ledford[247] et al. studied the effect of promotion with lanthanum of the structure of cobalt species and their performance in carbon monoxide hydrogenation. The La/Al XPS intensity ratio in these catalysts was close to the monolayer values. This suggests that lanthanum tends to be highly dispersed on alumina support. It was found that impregnation with cobalt of alumina promoted with lanthanum resulted in higher selectivity to higher hydrocarbons, while the overall FT reaction rate was not affected. Significant fractions of La−Co mixed oxide formed at higher La contents. This led to a lower catalytic activity of these catalysts. A promoting effect of lanthanum oxide on FT reaction rates and hydrocarbon selectivities at 3 wt % La content was also observed on silica-supported catalysts by Adachi[248] et al.

Modification of cobalt silica-supported catalysts with La^{3+} was found[249] to increase FT reaction rates measured using SSITKA. The SSITKA method showed an increase in the concentration of active sites with an increase in the La^{3+} content in the samples. The effect was mostly attributed to higher metal dispersion in the modified catalysts. The catalysts in that report[249] were prepared by impregnation of reduced and passivated Co/SiO_2 catalysts with an aqueous solution of lanthanum nitrate. Haddad[250] et al. showed earlier that treatment of reduced and passivated cobalt-supported silica catalysts with water could itself modify the concentrations of cobalt crystalline phases. Modification with La^{3+} moderates[251] this effect, especially at low lanthanum loadings. At higher lanthanum loadings ($La/Co > 0.5$) the amount of cobalt hardly reducible phases increased probably due to formation of Co−La and Co−Si mixed oxides.

2.3.3. Promotion with Manganese Oxide

Mn has been described as a perspective promoter, which could enhance both the carbon monoxide conversion rate and hydrocarbon selectivity.[252−256] Zhang[257] et al. found that the presence of small amounts of Mn improved dispersion of cobalt active phases and favored formation of bridged-type adsorbed CO. A significant promoting effect of Mn was observed on titania-supported catalysts prepared by Morales and Weckhuysen.[254] The effect was more pronounced[258] in the catalysts prepared by homogenous deposition−precipitation than in those prepared by impregnation. STEM-EELS showed[259] that the oxidized catalysts prepared via impregnation contained Co_3O_4 and MnO_2 monometallic particles, while in the deposition−precipitation sample Mn cations

were incorporated into Co_3O_4 structure, resulting in the $Mn_xCo_{3-x}O_4$ mixed oxide phase. These mixed phases however could be reduced, which gives rise to cobalt metal phase and migration of MnO particles toward the TiO_2. The presence of MnO resulted in lower cobalt reducibility.[253] In the reduced catalysts electronic effects due to interaction of cobalt metal particles with MnO and possible involvement of Mn in a chain growth mechanism via CO insertion were suggested to explain an increase in the FT reaction rate and higher C5+ selectivity. Localization and transformation of these species during the reduction is shown in Figure 14.

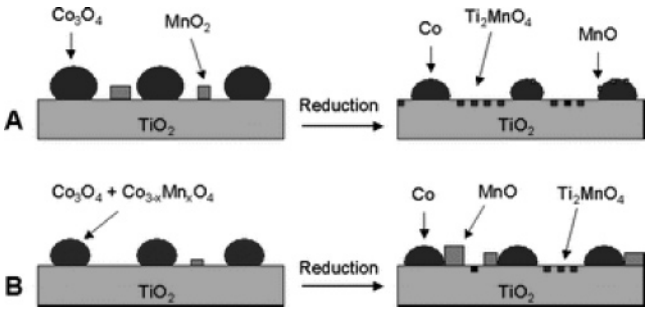

Figure 14. Localization of cobalt and manganese species in TiO_2-supported catalysts prepared via incipient aqueous impregnation (A) and deposition−precipitation (B) before and after reduction (reproduced from ref 259 by permission of the PCCP Owner Societies).

Bezemer[260,261] et al. reported the promoting effects of manganese oxide on carbon nanofiber-supported (CNF) cobalt catalysts for FT synthesis. Cobalt was introduced to the activated CNF by incipient wetness impregnation; the catalyst systems were promoted with small amounts of MnO. XPS and STEM demonstrated that manganese was closely associated with cobalt in both oxidized and reduced catalysts. Manganese retarded cobalt reduction, and the surface of the cobalt was more oxidic when MnO was added to the catalysts. The catalytic performance was affected differently in FT catalytic tests at 1 and 20 bar. The TOF increased at low MnO contents. At 1 bar chain growth probability increased, and simultaneously, the product distribution shifted toward olefinic products at increasing MnO loadings. In the experiments at 20 bar, C_{5+} selectivity increased first from 74 to 78 wt % at 0.03 wt % MnO before decreasing to 52 wt % for 1.1 wt % MnO sample.

Mn-promoted cobalt catalysts were also prepared by Martínez[262] et al. using SBA-15 silica as a catalytic support. It was found that promotion of cobalt with ca. 2 wt % Mn significantly enhanced cobalt dispersion but decreased its reducibility. The Mn-promoted catalysts were less active than the unpromoted ones. Duvenhage[263] et al. also showed that promotion with Mn led to lower reducibility of bimetallic Co/Fe catalysts and decreased their catalytic activity. More information about the effect of promotion with Mn on cobalt-based catalysts is available in a recent review by Morales and Weckhuysen.[40]

2.3.4. Other Oxide Promoters

Other oxides have been evaluated in the literature as potential promoters of cobalt catalysts. Guerrero-Ruiz[264] et al. found that promotion of cobalt and ruthenium/carbon catalysts with magnesium, vanadium, and cerium oxides enhanced the specific activity and selectivity for alkenes and long-chain hydrocarbons. The effect of promoting with oxides on the dispersion and reducibility of cobalt species was studied by Jacobs[221] et al. Addition of nonreducible oxides of B, La, Zr, and K were found to increase the cobalt reduction temperature.

Introduction of various concentrations of cerium could also increase cobalt dispersion and hinder cobalt reduction.[265] Chain growth probabilities were also lower for Ce-containing catalysts. Vanadium promotion was found[266] to increase CO conversion and hydrocarbon selectivity on cobalt catalysts supported by activated carbon. Huffman[267] et al. using XAFS studied the effect of modification of potassium on the reducibility of Co/SiO_2 and Co/Al_2O_3 catalysts. It was found that potassium hindered Co reduction in hydrogen. At the same time, CoK/SiO_2 catalysts can be reduced in synthesis gas in 473 K and remain more stable than unpromoted Co/SiO_2 catalyst. Gadolinium promotion was found[268] to increase the number of cobalt active sites in silica-supported FT catalysts. The presence of gadolinium primarily led to the enhanced cobalt reducibility. Zhang[269] et al. showed that promotion of silica-supported cobalt catalysts with 5−10 wt % of Al_2O_3 could enhance cobalt dispersion and the number of active sites. As a result, carbon monoxide conversion increased from 45% to 65%.

2.4. Effect of Catalyst Oxidizing and Reducing Pretreatments on Cobalt Dispersion and Reducibility

2.4.1. Exothermicity of Cobalt Precursor Decomposition

Cobalt precursor decomposition is an important stage in catalyst preparation. The heat released during decomposition of cobalt precursors could affect the structure of cobalt species in the final catalysts. The significance of decomposition of cobalt precursors and its effect on cobalt dispersion and reducibility was discussed by Soled and Iglesia.[16]

Cobalt nitrate and cobalt acetate are the most common precursors for preparation of FT catalysts. Decomposition of cobalt nitrate and cobalt acetate was compared in refs 270 and 271. Decomposition of cobalt nitrate in air is slightly endothermic, whereas decomposition of cobalt acetate was highly exothermic[270,271] (Figure 15). Decomposition of supported cobalt nitrate occurs at 423 K. Decomposition of supported cobalt acetate proceeds at slightly higher temperatures, the principal heat flow peak being located at 493 K.

For silica-supported catalysts, decomposition of cobalt nitrate at lower temperatures (373−423 K) resulted[271] in higher cobalt dispersion. A much smaller effect of the temperature of decomposition of cobalt nitrate on cobalt dispersion was observed in alumina-supported cobalt catalysts.[162] Highly exothermic decomposition of cobalt acetate led to higher fractions of hardly reducible cobalt silicate. The concentration of cobalt silicate could be significantly reduced if the decomposition of cobalt acetate was conducted at mild conditions. Addition of promoters significantly modifies the mechanism of cobalt acetate decomposition. It was shown, for example,[212] that nitrogen oxides released during decomposition of Ru nitrosyl nitrate reduced the temperature of decomposition of cobalt acetate.

2.4.2. Exposure to Syngas and Catalyst Deactivation

On most cobalt catalysts the FT reaction rates slowly evolve with the time on stream. Possible reasons responsible of the evolution of catalytic activity include the following: restructuring of the surface of the cobalt metal phase under the influence of syngas;[32] oxidation of the cobalt surface

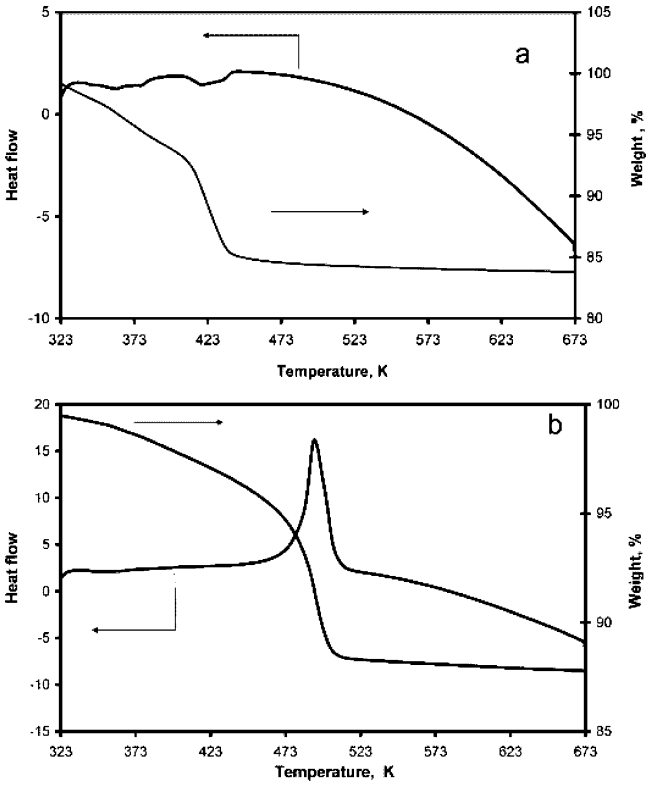

Figure 15. DSC–TGA curves of decomposition in air of cobalt nitrate (a) and acetate (b) on silica. Temperature ramp 1 K/min (reproduced from ref 271, Copyright 2005, with permission from Elsevier).

and/or small cobalt clusters and formation of mixed oxides; sintering of cobalt particles and sintering and segregation of the noble metal promoter; formation of cobalt carbide species; contamination by impurities in syngas (particularly during industrial operation).

It is usually very challenging to study the structure of cobalt FT catalysts that were exposed to syngas. The surface of FT working catalysts is covered by liquid and solid hydrocarbons and usually is not accessible for most in-situ characterization techniques. Water is one of the major products of FT synthesis. The decrease in the FT reaction rate is usually attributed to catalyst deactivation due to oxidation of small cobalt particles by water. Bulk metallic cobalt is stable to oxidation by water at the conditions typical of FT synthesis. Recently performed thermodynamic calculations[272] have shown that cobalt metal particles smaller than 4–5 nm could be oxidized by water during the FT reaction. The probability of cobalt oxidation varies as a function of catalyst support. While for alumina-supported catalysts the decrease in FT reaction rates has been observed even after addition of very small amounts of water,[220,273,274] for silica-supported catalysts several authors claim some increase[275–278] in FT reaction rate at low water levels. Note however that at high water levels significant deactivation occurs on all cobalt catalysts.[279]

Catalyst deactivation results in formation of nonreducible mixed oxides (cobalt aluminate, cobalt silicate,[280] etc.). These oxides are produced due to reaction of CoO with the oxide support (Al_2O_3, SiO_2). The mixed oxides of cobalt and support are often amorphous. This makes it rather difficult to characterize these compounds using conventional characterization techniques such as XRD diffraction. Low cobalt content and high surface area of supports favor formation of mixed oxides.[281] These mixed oxides are barely reducible; they exhibit[219] high-temperature peaks in the TPR profiles of the catalysts. They do not posses any cobalt metal sites, and thus, they are inactive in FT synthesis.

Mixed cobalt–support oxides can form during catalyst preparation, oxidative and reductive pretreatments, and in the course of the FT reaction. van Steen[282] showed that the tendency to formation of amorphous cobalt silicate increased with increasing the support surface area, the high pH of the impregnating solution, and the drying/calcination temperature. Ming[44] et al. showed that silica dissolved in water at high pH, yielding cobalt silicate species. Cobalt silicates are also generated under hydrothermal conditions during catalyst reduction and FT reaction at higher conversion levels.[283] A high calcination temperature of catalysts also results in a higher fraction of cobalt silicate or cobalt aluminate. Several reports[250,284] suggest that impregnation of reduced and passivated silica-supported cobalt catalysts followed by drying in an oxidizing atmosphere could irreversibly convert part of metallic cobalt into hardly reducible cobalt silicate.

Several types of cobalt silicate and cobalt aluminate have been postulated.[285] Three polyforms of crystalline Co_2SiO_4 are known;[286] in all of them Co atoms are located in a distorted octahedral environment. The α form has an olivine blue color[287] and orthorhombic-type structure. The β and γ forms of cobalt silicate[286] represent spinel-like (wadsleyite) and spinel structures. EXAFS characterization[271] showed that the local structure of cobalt in silicate-type species in silica-supported cobalt catalysts was similar to that in orthorhombic α silicate. Cobalt orthosilicate was also observed[288] by XRD after calcination of cobalt silica-supported catalysts at $T >$ 1000 K.

Several cobalt aluminate structures are known in the literature. These compounds usually have $Co^{2+}Co^{3+}_xAl_{2-x}O_4$ (where $x = 0-2$) spinel structure. Co^{3+} of Co_3O_4 can be gradually replaced[289] by Al^{3+} to produce the series of $Co_{3-s}Al_sO_4$ ($0 < s < 2$) spinels. They include[290,291] $CoAl_2O_4$, Co_2AlO_4, and Co_3O_4, etc. $CoAl_2O_4$ has the structure of normal spinel in which Co^{2+} ions are accommodated in tetrahedral positions while Al^{3+} ions are in octahedral positions.[292] Co^{3+} could, however, partially substitute Al^{3+} ions in an octahedral position. Generally speaking, cobalt aluminate generated during FT synthesis can contain Co^{2+} ions in tetrahedral coordination and Al^{3+} ions in octahedral coordination.

Cobalt aluminate compounds could be prepared by different methods: reaction between Co and Al oxide powders at high temperature (1073 K)[293] resulting in a blackish-blue compound or to 1473–1573 K[294] resulting on a bright blue pigment; co-precipitation of a mixed aqueous solution of Co and Al salts and subsequent calcination to 673 and 1073 K, producing a very dark blue-green-colored oxide material;[295] calcination of alumina powder soaked in cobalt nitrate solution to 1473 K, giving blue cobalt aluminate.[296] The compound can be also prepared by calcination of powdered Al_2O_3 coated with a thin film of metallic cobalt at 1273 K, yielding the characteristic bright blue color of cobalt aluminate.[297]

Arnoldy and Moulijn[298] identified on the basis of TPR measurements three different phases of cobalt aluminate in Co/Al_2O_3 catalysts. The first aluminate phase consisted of Co^{3+} ions in crystallites of Co_3AlO_6 stoichiometry or in well-dispersed surface species. The second phase consisted of surface Co^{2+} ions. The third phase consisted of either surface

Co^{2+} ions (with more Al^{3+} ions in their surrounding than in the second phase) or subsurface Co^{2+} ions occurring in diluted Co^{2+}/Al^{3+} spinel structures or in $CoAl_2O_4$. Jongsomjit[231] et al. showed using Raman spectroscopy that Co aluminate could be not identical to $CoAl_2O_4$ (spinel) but is a surface compound deficient in Co. The presence of a significant fraction of cobalt aluminate in alumina-supported catalysts can be uncovered by the color changes. Van de Loosdrecht et al.[299] observed a blue color in the reduced samples containing significant amounts of cobalt aluminate. The intense blue color typical of Thenard's blue pigment was attributed to calcined $CoAl_2O_4$.[300]

Deactivation of cobalt FT catalysts could also be due to sintering of cobalt particles. This effect is expected to be more significant on silica-supported catalysts[301] because silica is a weakly interacting support. On alumina- and titania-supported catalysts the probability of cobalt sintering is much lower.

Formation of carbide-type species was observed by Johnson et al.[302] using AES spectroscopy of submonolayer cobalt deposited on the surface after FT reaction. In-situ XRD experiments showed that[24] the decrease in the FT reaction rate over alumina- and titania-supported cobalt catalysts can be attributed to formation of cobalt carbide (Figure 16).

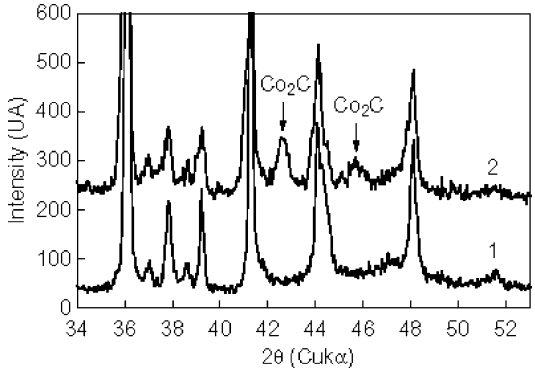

Figure 16. Diffraction patterns of Co/TiO_2 catalyst: (1) after reduction in hydrogen and (2) after 180 h in syngas ($T = 503$ K, $P = 3$ bar, $H_2/CO = 9$) (reproduced from ref 432, Copyright 2002, with permission from Oil & Gas Science and Technology—Revue de l'IFP).

Cobalt carbide itself is inactive in FT. Formation of cobalt carbide was suggested to be a major reason of catalyst deactivation on carbon-supported catalysts.[24,303]

2.5. Support Role and Influence of Support Texture

Both the structure and performance of cobalt catalysts depend on the catalytic support. The principal function of the catalyst support is to disperse cobalt and produce stable cobalt metal particles in the catalysts after reduction. The porous structure of the support could control the sizes of supported cobalt particles.

FT synthesis is an exothermic reaction. Catalytic supports also dissipate the heat released by the FT reaction and thus reduce a temperature gradient in fixed bed reactors. The support could also affect the structure and electronic properties of small cobalt metal particles. Ishihara[304] suggested that electron-donor support could enrich in electron density of the cobalt active phase and thus ease cleavage of the C—O bond in adsorbed carbon monoxide. The support could react with cobalt species forming cobalt—support mixed compounds.

The texture of the support modifies diffusion of reagents and products inside the catalyst grains. In addition, support texture could affect diffusion and capillary condensation of the reaction products in the catalyst pores. Kelvin's equation suggests that capillary condensation would occur at much lower partial pressures in narrow pores of the catalyst than in wider ones. Therefore, narrow pores are more likely to be filled by liquid reaction products than wider ones. Capillary condensation in narrow mesopores would lead to diffusion limitations[17,19] due to more difficult access for the reacting molecules to the catalyst through the gas—liquid interface.[305]

The support modifies the mechanical strength of FT catalysts. The catalyst solidity is a crucial issue for slurry FT reactors. The acidity of the catalyst support leads to olefin isomerization, lower chain growth probability, and higher selectivity to lighter hydrocarbons.[306]

A large number of reports have focused on the effect of support. Reuel and Bartholomew studied the catalytic activity of cobalt-based catalysts as a function of support[307] and found it to decline in the following order: $Co/TiO_2 > Co/Al_2O_3 > Co/SiO_2 > 100\%$ Co > Co/MgO. Iglesia[18] et al. found that at pressures greater than 5 bar and at high conversions the influence of the support on the selectivity in methane and C5+ formation could be insignificant.

Let us discuss in a greater detail the support effects in cobalt silica- and alumina-based catalysts.

2.5.1. Cobalt Catalysts Supported by Conventional Alumina and Silica

Silica-Supported Catalysts. Interaction between support and cobalt is relatively weak in silica-supported catalysts. This usually leads to better cobalt reducibility. At the same time, cobalt dispersion is much lower in silica-supported catalysts than in alumina-supported ones. Thus, high cobalt dispersion is the major challenge in the design of silica-based FT catalysts.

The effect of texture of silica-supported cobalt catalysts has been a subject of a few publications. Ernst[308] et al. studied the FT activity and selectivity of Co/SiO_2 prepared by the sol—gel technique in acid and base media. It was found that the activity in FT synthesis increased with the specific surface area, and the selectivity for higher molecular weight hydrocarbons was favored in the case of the catalyst with support pore diameter less than 4 nm. Saib[309] et al. showed that the catalyst supported by silica with an average pore diameter of 10 nm was most active and selective for hydrocarbons. Song and Li[310] also reported similar results for a series of cobalt catalysts supported on silica with different pore sizes. CO conversion first increased and then decreased with increasing catalyst pore size. The C5+ selectivity had a trend similar to CO conversion. The catalysts with a pore size of 6—10 nm displayed higher Fischer—Tropsch activity and higher C5+ selectivity.

Alumina-Supported Catalysts. Al_2O_3 has been one of the mostly used supports for cobalt FT catalysts. Cobalt oxide strongly interacts with this support, forming relatively small cobalt crystallites. Chemical reaction of small cobalt particles with the support may result in diffusion of cobalt active phase into alumina and formation of stoichiometric or nonstoichiometric cobalt aluminate spinels.[281,311] Cobalt reducibility is one of the most important problems of alumina-supported cobalt FT catalysts. Promotion with noble metals can improve cobalt reducibility (see section 2.2.1).

Several methods have been used to improve the properties of alumina support. Some of these methods address pretreatment of alumina support before deposition of active phase. Zhang[48] et al. reported that pretreatment of Al_2O_3 support with acetic acid produced a negative effect on the catalytic properties of Co catalysts, whereas pretreatment with ammonia and ammonium nitrate led to improved catalytic behavior. Another technique focused on coating alumina with a protecting layer. It has been shown[312] that oxidation of cobalt by water at higher carbon monoxide conversions could lead to formation of cobalt aluminate and reaction of cobalt ions with trace amounts of organic acids present in the reacting media. Deposition of a thin layer of silica could protect the catalyst from formation of cobalt aluminate and thus from loss of the active component during reaction. A similar effect was observed when cobalt alumina-supported catalysts were promoted with magnesia. Li et al.[313] demonstrated that formation of cobalt surface phase, which interacted strongly with the alumina support, could be effectively suppressed by modification with a small amount of magnesia (0.8 wt %). The activity of magnesia-modified catalyst in the FT reaction increased due to a lower fraction of cobalt aluminate and an increase in the overall catalyst reducibility.

The support texture represents another tool to control the structure, dispersion, and reducibility of cobalt particles. A larger size of support pores generally leads to larger Co_3O_4 crystals. Bechara et al.[314] found that alumina porosity could modify the catalytic properties through their effects on the reducibility of active phase. Li[315] et al. reported a significant effect of alumina porosity on the structure of supported cobalt catalysts and their performance in FT synthesis. The alumina carrier was calcined at different temperatures to obtain a support with different pore sizes. Larger amounts of micropores were discovered in the catalysts prepared by the support obtained by lower temperature calcination.[316] XRD and H_2 TPD suggest sintering cobalt metal particles in catalyst pores, which results in a lower number of active sites.

2.5.2. Cobalt Catalysts on Novel Mesoporous Supports

Novel mesostructured materials with adjustable porous networks have shown a great deal of promise for the design of heterogeneous catalysts,[317−320] semiconductors, low dielectric devices, and separation processes. The most common 2D hexagonal type involves MCM-41[321−326] and SBA-15.[327−329] Their surface areas are approaching 1000 m^2/g; the pore size distributions in periodic mesoporous silicas are very narrow.[321] The pore sizes from 2 to 30 nm can be adjusted at the stage of synthesis of these materials using different surfactants.

Several papers have addressed application of novel mesoporous materials as supports for cobalt FT catalysts. The catalysts have been prepared mostly by aqueous impregnation.[240,330−336] Several authors have also used ethanol impregnation,[262,337] the template ion-exchange method,[338] gas-phase incorporation (cyclooctadiene)(cyclooctenyl)cobalt ($Co(C_8H_{12})(C_8H_{13})$),[339] or $Co_2(CO)_8$ impregnation from the hexane solution.[340]

The support texture in novel mesoporous materials represents an efficient tool to control the sizes of supported cobalt particles.[305,341,342] Larger cobalt particles and higher FT reaction rates have been found in the catalysts prepared from large pore silicas[270] (Figure 17). Higher cobalt reducibility has been generally found for large cobalt particles located in large pore supports. Higher cobalt dispersion was found in periodic mesoporous silicas than in conventional silica supports. This effect was more pronounced at high cobalt contents. It appears that the narrow pore size distribution in mesoporous material prevents cobalt particles from sintering.[270,343]

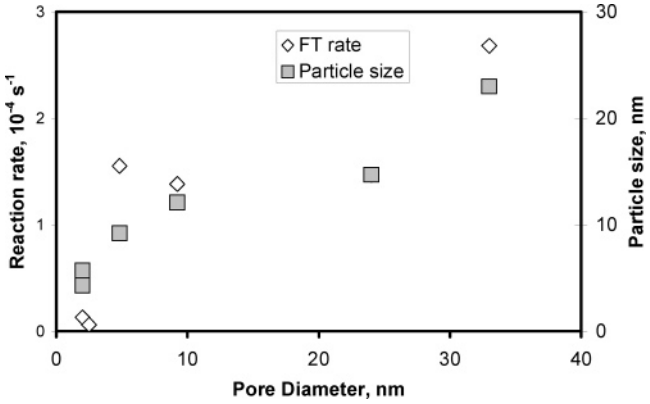

Figure 17. Relation between pore diameters, sizes of supported Co_3O_4 particles, and FT reaction rates over cobalt catalysts supported by mesoporous silicas (reproduced from ref 270, Copyright 2004, with permission from Elsevier).

The stability of the mesoporous structure in the presence of water is a crucial issue in the preparation of cobalt catalysts. SBA-15 materials seem to be much more stable relative to MCM-41. SBA-15-based materials generally conserve their structure after aqueous impregnation and thermal and mild hydrothermal pretreatments. Our recent report[332] has shown that introduction of small amounts of cobalt via aqueous incipient wetness impregnation could result in significant modification in the MCM-41 structure and loss of hexagonal ordering.

2.5.3. Cobalt Catalysts on Carbon Supports

A drawback of oxide supports (SiO_2, Al_2O_3) is their reactivity toward cobalt, which could lead to formation of mixed oxides (aluminate or silicate). These mixed oxides are not active in FT synthesis; they are reducible only at high temperatures. Carbon-based materials could possibly overcome these difficulties. Carbon supports are less stable, however, than inorganic oxides. They can gasify in the presence of hydrogen.[344]

A few reports have been published about the utilization of carbon as a support for FT catalysts. Vannice[345] et al. prepared cobalt catalyst supported by active carbon using cobalt carbonyl. The catalyst was making only saturated hydrocarbons and showed good stability on stream. Relatively moderate FT rates over Co/C catalysts were observed by Reuel and Bartholomew.[307] The catalytic performance of cobalt catalysts supported on active carbon could be modified by promotion. Addition of K resulted in much lower FT rates, whereas promotion with Ce and Zr increased carbon monoxide conversion.[235] In addition, promotion with Zr also led to higher selectivity to heavier hydrocarbons.[346]

Use of carbon nanofibers as catalyst supports has been addressed by the group of de Jong. Cobalt catalysts were prepared using fish-borne carbon nanofibers. The combination of the high mechanical strength with the high purity of graphitic carbon, the developed surface area, and the mesoporous structure makes carbon nanofibers very suitable for

supporting heterogeneous catalysts. Cobalt nanofibers are weakly interacting supports; good cobalt reducibility was usually observed.[21] The catalysts could be reduced by syngas even during FT reaction. The deposition−precipitation technique allowed making highly dispersed cobalt particles[96] (Figure 18). Because of a weak interaction between the

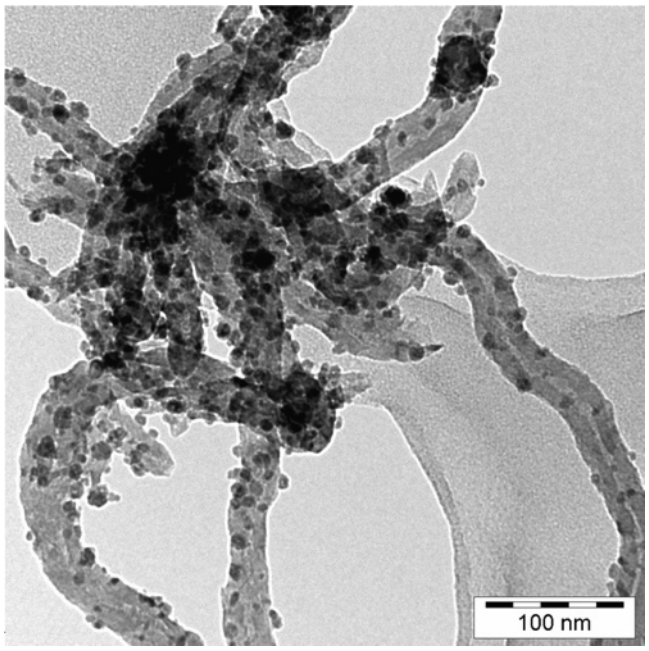

Figure 18. TEM image of carbon fish-born nanofibers showing cobalt particles with sizes of around 14 nm (reproduced from ref 21, Copyright 2006, with permission from the American Chemical Society).

carbon nanofibers and cobalt, these catalysts were recently proposed[21] as model systems to study the effect of cobalt particle sizes on FT turnover frequency. The turnover frequency was almost independent on cobalt particle size with sizes larger than 6−8 nm (Figure 19). With smaller

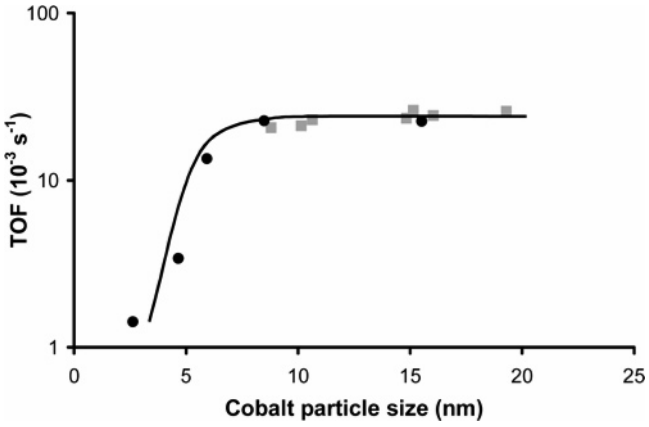

Figure 19. Influence of cobalt particle size on turnover frequency (TOF) in FT synthesis with catalysts supported by carbon nanofibers ($H_2/CO = 2$, 35 bar, 483 K; reproduced from ref 21, Copyright 2006, with permission from the American Chemical Society).

cobalt particle size FT reaction rates were much lower and significant changes in hydrocarbon selectivities were observed. Considerable restructuring of catalyst and modification of cobalt particle sizes were observed by EXAFS during the reaction.[260,261]

2.5.4. Bimodal Pore Catalysts

High cobalt dispersion could be obtained by deposition of a cobalt salt on high surface area supports, such as silica and alumina, and subsequent reduction. Conventional monomodal support with a large surface area usually contains small pores, which results in poor intrapellet diffusion of reactants and products, especially in multiphase reactors. Slow transportation of reactants and products to and from catalytic sites often controls the rate of primary and secondary reactions. The bimodal pore support[347−349] contains large pores and small pores simultaneously. The small pores yield the sites for anchoring small cobalt particles, while the large pores provide a network for fast diffusion of reacting molecules and products. The typical pore size distribution in bimodal silica is shown in Figure 20.

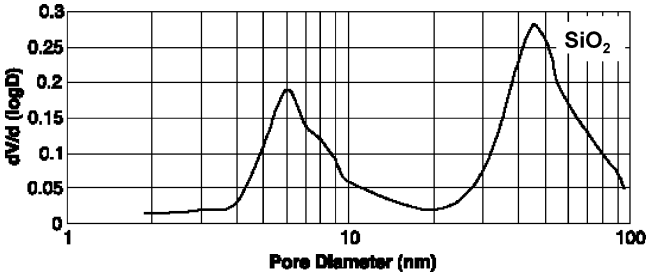

Figure 20. Pore size distribution in bimodal catalyst support (reproduced from ref 351, Copyright 2004, with permission from Elsevier).

Preparation of Bimodal Silica Supports and Bimodal Cobalt Catalysts. Recently, Tsubaki et al. reported a simple preparation method to form tailormade bimodal pore structure.[100,102,347,348, 350,351] This method was based on introduction of oxide sols (silica, alumina, or zirconia) into large-pore silica gel with pore diameters of 50 nm to form the bimodal pore supports.[347] After impregnation the support was calcined in air. Formation of new small silica pores is strongly influenced by the mechanism of interaction of silica gel with the original silica support. The sol-derived silica particles could simply block the pore structure and thus do not form any new small pores inside the large pores.

It was suggested that the following mechanism controlled the design of bimodal silica from large pore silica via addition of silica gel (Figure 21). In the calcination step small particles

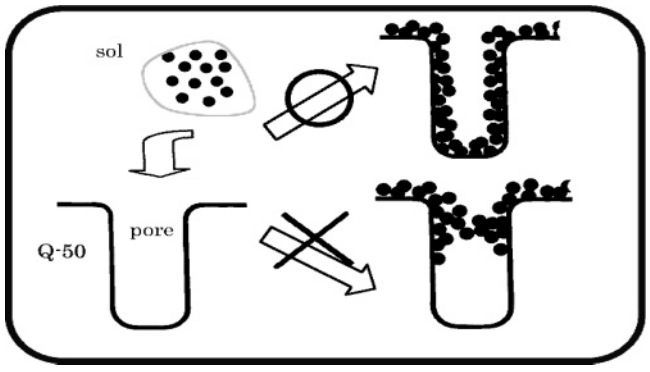

Figure 21. Scheme of synthesis of bimodal pore support using large-pore silica and silica sol (reproduced from ref 102, Copyright 2004, with kind permission from Springer Science and Business Media).

introduced from silica sols formed 6 nm small pores through condensation of the surface OH groups of silica sol particles

and narrowing the large pores of silica gel. The obtained bimodal support contained both 6 and 45 nm pores.

The catalytic performance of the cobalt prepared from the bimodal support or monomodal silica support is compared in refs 351 and 352. For the catalyst prepared from the bimodal support, CO conversion was higher and selectivities of CH_4 and CO_2 were as low as those of the catalyst prepared from the monomodal large-pore silica.

Multifunctional Alumina- and Zirconia−Silica Bimodal Pore Catalyst. Bimodal catalytic supports could also be prepared by narrowing the pores of initial large-pore silica supports with sols of other oxides, e.g., alumina and zirconia. To prepare alumina gel, the aluminum nitrate is dissolved in a 0.3 mol/L polyethylene glycol (PEG, average molecular weight of 200) aqueous solution to prepare the polymer complex solution. After stirring, the solution was impregnated into original large-pore silica gel by the incipient wetness method.[348,353] Zirconia sol was used in the preparation of zirconia−silica bimodal catalysts.[347,354] The catalysts showed enhanced catalytic performance in FT synthesis.

2.6. Preparation Methods and Properties of Cobalt-Supported Fischer–Tropsch Catalysts

The important stages for the preparation of cobalt-supported FT catalysts are displayed in Figure 22. These

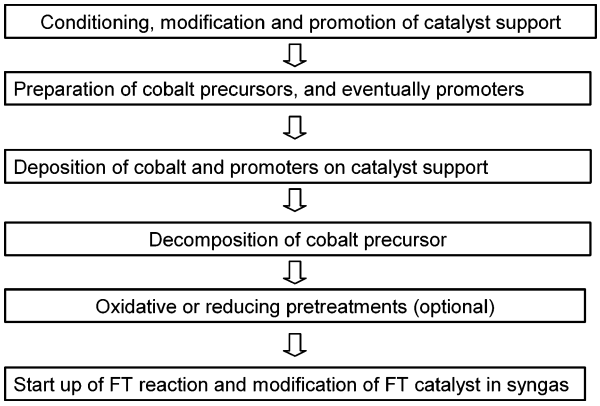

Figure 22. Principal stages in the preparation of cobalt-supported FT catalysts.

stages include conditioning, modification, and promotion of catalyst support, preparation of cobalt precursors and eventually promoters, followed by deposition of cobalt and promoters. Decomposition of cobalt precursor is an important stage in catalyst preparation. Several preparation routes require catalyst oxidative and reducing pretreatments and catalyst passivation. The catalytic performance of FT catalysts is finally adjusted during the reactor start up and on-stream during the FT reaction. The important point is to emphasize that a catalyst for FT synthesis is a result of the whole preparation procedure and each preparation step does matter in attaining the desired and lasting catalytic performance.

Let us compare different preparation routes of cobalt-supported FT catalysts. Impregnation with solutions of cobalt nitrate results in interaction between cobalt complexes and the support surface. In aqueous cobalt nitrate solutions the pH is relatively low. Cation adsorption could be rather limited at these conditions because of the repulsion between positively charged cobalt cations and the positively charged surface of the supports such as alumina, silica, and titania. Decomposition of these complexes produces cobalt oxide and cobalt metal particles of variable sizes, typically between 6 and 40 nm. Incipient wetness and slurry aqueous impregnations are most widely used for preparation of cobalt catalysts. Impregnation with cobalt carbonyls results in several cobalt carbonyl species on the surface of the support. Decomposition of the carbonyl species usually results in small cobalt metal particles. The catalyst could be immediately used in FT synthesis without calcination and reduction. Cobalt carbonyls, however, are very toxic compounds and require very careful handling during the preparation procedure.

The co-precipitation method could produce cobalt particles of different size. Note, however, that a significant fraction of cobalt could react with the support during bulk co-precipitation yielding nonactive cobalt−support compounds. Deposition−precipitation is a promising method of catalyst synthesis. It could produce very small and stable cobalt metal particles. The properties of cobalt catalyst prepared using the sol−gel technique are strongly affected by the preparation procedure. Solids with very different properties could be produced by varying the synthesis parameters. The advantage of the sol−gel method is the opportunity to control the porosity and texture of the catalysts in addition to the cobalt particle size.

Preparation of eggshell catalysts involves diffusion-limited repartition of cobalt precursor in a catalyst grain. The depth of the cobalt layer in the catalyst grain is an important parameter, which affects the selectivity of FT synthesis at the conditions when the rate of the reaction is limited by intraparticle diffusion. In the preparation of monolithic catalysts, the active phase is deposited either by aqueous (co)-impregnation or homogeneous deposition precipitation on the surface of monolith. Due to the low surface area, preparation of monolithic catalysts usually results in relatively large cobalt particles. The challenge is to obtain the monolithic catalyst with high cobalt content and high cobalt dispersion. Colloidal and microemulsion methods allow synthesis of cobalt nanoparticles with controllable particle size and shape and very narrow particle distribution curves. The crucial issue in this method is elimination of different organic and inorganic compounds involved in nanoparticle synthesis. Chloride, alkali ions, surfactants, polyols, phosphine, and products of their decomposition could irreversibly contaminate the final catalysts and alter their catalytic performance. Use of the solvated metal atom dispersion (SMAD) method for preparation of cobalt-supported catalysts remains at the present time largely exotic. The chemical vapor deposition method produces a uniform distribution of cobalt precursor on the surface of the support. The maximal deposited amount of cobalt precursor depends on the concentration of hydroxyl groups in the support. Decomposition of the preadsorbed cobalt precursors is a crucial parameter in the CVD method and usually leads to small cobalt oxide particles and a significant fraction of cobalt−support mixed oxides. The plasma-based methods allow deposition of cobalt species via the plasma spray method and also optimize the conventional preparation procedures. Decomposition of cobalt precursor in the glow discharge technique could influence the nucleation and growth of cobalt oxide particles in the catalysts and thus enhance cobalt dispersion.

Promotion of cobalt-supported FT catalysts with noble metals and oxides influences a number of catalyst properties.

The presence of promoters affects different catalyst preparation stages from deposition of cobalt active phase through reduction and evolution of catalyst structure and catalytic performance during FT synthesis. It could result in new active sites related to the promoter. The most common promotion of cobalt FT catalysts involves noble metals (Pt, Ru, Re, Pd, etc.). The important issue of promotion is its cost. Promotion with noble metals could significantly increase the cost of the catalysts and affect the economic efficiency of the overall FT technology.

In all preparation methods the catalytic behavior of the final catalysts strongly depends of catalyst pretreatments. The oxidative and reductive pretreatments convert cobalt precursor into active cobalt surface sites for FT synthesis. Though the pretreatment procedures should be adapted to each catalyst synthesis method, the general recommendation is to conduct the pretreatments at relatively lower temperatures. Higher calcination and reduction temperatures (>673 K) could result in formation of cobalt−support mixed oxides and sintering cobalt particles. The rapid temperature ramping could increase the rate of heat release and water partial pressure and thus also affect the number of cobalt active sites.

A large number of publications have shown that the chemical composition of catalytic supports significantly influences the extent of metal reduction, morphology, adsorption, and the catalytic properties of the active phase, especially in well-dispersed catalytic systems. Alumina-supported catalysts generally exhibit higher cobalt dispersion but lower cobalt reducibility than silica-supported ones. The probability of formation of mixed cobalt oxides also depends on the type of support. The support also plays an important role in the mechanical stability of cobalt catalysts and influences dissipation of heat in fixed bed reactors. The texture of the support represents an important tool to control cobalt dispersion. Narrow pore supports generally lead to small cobalt metal particles, while larger cobalt particles could be more easily obtained in large-pore supports. Bimodal supports have shown promising results for preparation of cobalt catalysts. In these supports high cobalt dispersion could be obtained via anchoring cobalt particles within small pores, while diffusion of reagents and product could proceed very rapidly in larger pores.

3. Comparative Analysis of Characterization Techniques of Cobalt-Supported Fischer−Tropsch Catalysts

Catalyst characterization provides important information about the structure of cobalt FT catalysts and their precursors. Catalyst characterization allows identification of the active sites for FT reaction and reveals possible routes for optimization of catalyst structure. A wide range of physical and chemical techniques has been used. In many cases, catalyst structure could be investigated during different pretreatments and catalytic reaction under in- situ and operando conditions. The paragraphs below address advances, challenges and uncertainties of catalyst characterization.

3.1. Optical Spectroscopy

3.1.1. UV−Visible Spectroscopy

Cobalt cation complexes are usually colored. Octahedral Co^{2+} complexes have a pink color, while tetrahedral Co^{2+} complexes are blue colored. The pink color corresponds to the absorption band at 500−510 nm in the UV−vis spectra, which is attributed to a $^4T_{1g}(F) \rightarrow {}^4T_{1g}(P)$ transition in octahedral high-spin Co^{2+} complexes. The intensity of the bands attributed to tetrahedral-coordinated cobalt complexes is usually at least two orders of magnitude higher[355,356] than those of octahedral-coordinated cobalt ions. Thus, the blue color of the sample does not necessarily mean that the catalyst contains only tetrahedral Co^{2+} species; some concentrations of cobalt octahedral complexes cannot be excluded. Co_3O_4 can be detected[271,285,357,358] in the UV−vis spectra by two very broad UV−vis bands at about 400−480 and 700−760 nm. These bands are assigned[359,360] to the ligand−metal charge transfers $O^{2-}-Co^{2+}$ and $O^{2-}-Co^{3+}$, respectively. In small Co_3O_4 particles these bands could be shifted[358] to lower wavelengths (blue shift) due to the quantum size effect of nanocrystals. A different interpretation of the broad bands at 450 and 700 nm of Co_3O_4 was suggested by Wood[361] et al. These bands were attributed[362] to the $A_{1g} \rightarrow T_{2g}$ and $A_{1g} \rightarrow T_{1g}$ transitions of octahedral-coordinated Co^{3+} ions in Co_3O_4. The presence of cobalt silicate in the calcined catalysts could be detected by the presence of bands characteristic of cobalt ions in much distorted envirionments.[286]

UV−vis spectroscopy has been used to study cobalt coordination in FT catalysts. It was found[285] that before calcination in the catalysts prepared from cobalt nitrate, cobalt kept predominately octahedral coordination. The local coordination of cobalt in silica-supported samples prepared by ion exchange changed from octahedral to tetrahedral after grinding, while in the samples prepared using impregnation with cobalt nitrate, no change in cobalt coordination was observed. Co_3O_4 was the major phase present in cobalt catalysts prepared from cobalt nitrate, while tetrahedral Co^{2+} species were dominant in the cobalt acetate derived samples. Our recent report[271] is consistent with this observation.

UV−vis spectra of impregnating cobalt nitrate and cobalt acetate solutions and dried and calcined Co/SiO_2 catalysts are shown in Figure 23a and b. In the solution of both cobalt salts Co^{2+} ions have octahedral coordination. After deposition on the silica surface via incipient wetness impregnation, Co^{2+} also keeps mainly octahedral coordination. After calcination, in the nitrate-derived samples cobalt was detected by UV−vis spectroscopy as Co_3O_4, whereas in acetate samples most of the cobalt is situated in the form of amorphous cobalt silicate. Efficient control of heat release during the decomposition of cobalt acetate could potentially increase the concentration of the Co_3O_4 phase.[271]

3.1.2. FTIR Spectroscopy

FTIR spectroscopy yields three sets of important characterization data: about the structure of supported cobalt oxides, about surface sites, and about the nature of the reaction intermediates. Let us discuss them separately.

Characterization of Supported Cobalt Oxides. Co_3O_4 in the calcined silica-supported catalysts was detected[363] using FTIR spectroscopy by the band at 660 and a broad feature at 570−600 cm^{-1} corresponding[364−367] to metal−oxygen stretching vibrations from cobalt tetrahedral and octahedral sites (Figure 24). Though it can be difficult to differentiate between the spectrum of pure Co_3O_4 and that of Co_3O_4 with CoO impurities, the vibration bands at 450 and 323 cm^{-1}, which appear after treatment of Co_3O_4 at elevated temperatures, are probably related[368] to CoO.

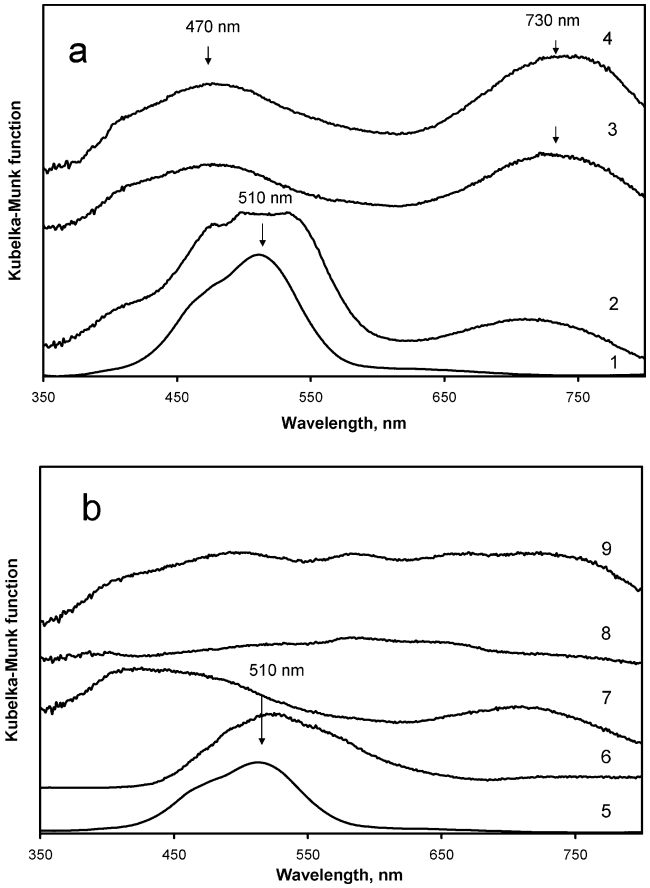

Figure 23. UV−visible spectra of cobalt precursors and silica catalysts prepared using impregnation with cobalt nitrate (a) and cobalt acetate (b): impregnating cobalt nitrate solution (1), silica after impregnation with cobalt nitrate and drying (2), samples calcined in air at 373 (3) and 673 K (4), impregnating cobalt acetate solution (5), silica after impregnation with cobalt acetate and drying (6), and samples calcined at 443 (7), 493 (8), and 673 K (9) (reproduced from ref 271, Copyright 2005, with permission from Elsevier).

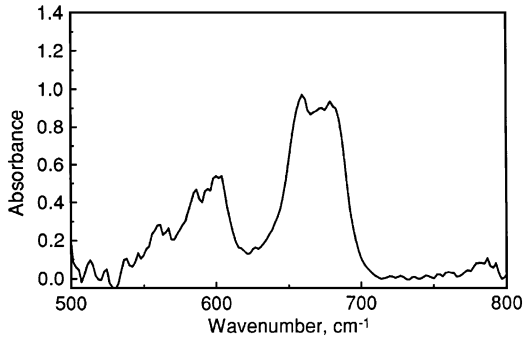

Figure 24. FTIR spectra of Co_3O_4 supported by silica (reproduced from ref 363, Copyright 1997, with permission from Elsevier).

Co_3O_4 was also identified[369] by FTIR in precipitated $Co-ZrO_2$ catalysts. Amorphous ZrO_2 did not show any remarkable adsorption. For $Co-ZrO_2$ catalysts, bands at 660 and 574 cm^{-1} appeared when the Co content exceeded 20 mol % and intensified with the further increase in Co content. The appearance of Co_3O_4 FTIR bands was indicative of the presence of rather bulky Co_3O_4 particles in the catalysts.

Characterization of Cobalt Surface Sites by Adsorption of Carbon Monoxide. FTIR spectroscopy coupled with adsorption of molecular probes is a powerful technique for investigation of the catalyst surface. Carbon monoxide is the most common molecular probe to study the nature of surface sites in cobalt catalysts. The structure of carbon monoxide complexes on the surface of cobalt-containing catalysts has been addressed in a large number of publications.

Several complexes of carbon monoxide with surface sites were detected:[48,363,370−375] carbon monoxide species linearly adsorbed on cobalt metal sites; bridged CO species on metal sites; carbon monoxide adsorbed on Co^{2+} and Co^{3+} ions on Lewis acid sites; formate, carboxylate, and carbonate species localized on the catalytic supports.[73,376] Modification of cobalt catalysts with different promoters could result in the appearance of additional FTIR bands, which are associated with CO complexes with these promoters. The position of the FTIR maxima depends on the nature of the cobalt species and support. Table 4 presents a brief summary of the spectral properties of carbon monoxide complexes in cobalt catalysts. Typical spectra of CO chemisorbed on several cobalt catalysts are shown in Figure 25. CO complexes with Co^{3+} cations and Lewis acid sites usually yield FTIR bands at 2170−2220 cm^{-1}. The bands of CO complexes with Co^{2+} ions are situated at 2150−2170 cm^{-1}. The CO frequency in

Table 4. Assignment of FTIR Bands of Carbon Monoxide Adsorbed on Co-Supported Catalysts (adapted from refs 73 and 372)

species		wavenumber, cm^{-1}
unidentate carbonate	νC−O	1040−1080
	ν_sCOO	1320−1390
	ν_{as}COO	1460−1530
carboxylate	ν_sCOO	1390
	ν_{as}COO	1580−1590
formate	ν_sCOO	1360−1400
	ν_{as}COO	1600−1625
bicarbonate		1230
		1430
		1650
carbonyl, single Co site	Co^0-CO ("nontilted" or on Co^{+d})	2050−2070
	Co^0-CO	1990−2030
	$Co^{2+}-CO$	2150−2160
	$Al^{3+}-CO$, $Co^{3+}-CO$	2180−2200
bridged carbonyl	Co−CO−Co	1800−1950
	3- and 4-fold hollow positions	1800

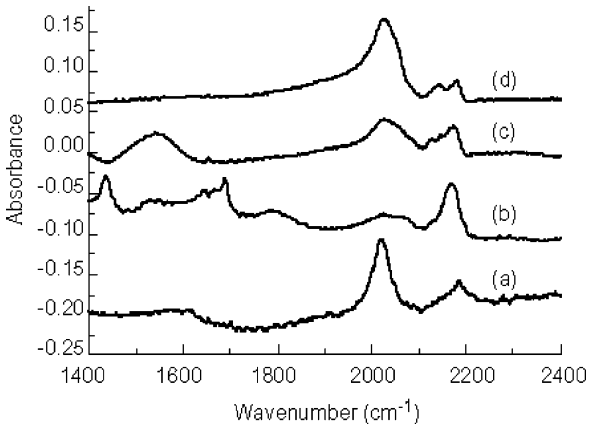

Figure 25. FTIR spectra of carbon monoxide adsorbed on 17 wt % Co/Al_2O_3 (a), 12 wt % Co/TiO_2 (b), and 23.4 wt % Co/SiO_2 (c) prepared by sol−gel and 17 wt % Co/SiO_2 (d) prepared by impregnation (room temperature, $P_{CO} = 35$ mBar) (reproduced from ref 284, Copyright 1999, with permission from Oil & Gas Science and Technology−Revue de l'IFP).

these complexes is very close to ν_{CO} in the gaseous phase; at the same time, these complexes have a significantly higher stability than the physisorbed CO species.

The bonding mechanism[377] between CO and metallic cobalt involves electron transfer from the CO(5σ) orbital into the empty bands of the metal (σ donation) and electron transfer from the occupied bands of the metal into the CO($2\pi^*$) orbitals (π back-donation). Adsorption usually proceeds via the C atom. The complexes of CO with metal particles produce FTIR bands at 1990−2100 cm^{-1}. Khassin[73] et al. tentatively attributed the FTIR bands at 1980−2040 cm^{-1} to linear Co−CO complexes, while the FTIR bands at 2050−2070 cm^{-1} were assigned to the "tilted" CO molecules with a Co−C−O angle much smaller than 180°. The FTIR bands at 2050−2070 cm^{-1} could be also attributed to CO molecules adsorbed on $Co^{\delta+}$ partially charged cobalt metal atoms.[378] In this case, the positive charging of cobalt metal particles could be related to their interaction with hydroxyl groups, Lewis acid sites, or Co cations on the catalyst surface.

In the CO complexes with metal particles the position of FTIR band varies as a function of carbon monoxide coverage due to the well-known effect of long-range dipole−dipole interaction between CO molecules;[379] the ν_{CO} bands shift to lower frequencies at low CO coverage ($\theta_{CO} \rightarrow 0$). The FTIR bands at 1950−1800 cm^{-1} are usually attributed to the bridged carbon monoxide complexes, which involve adsorption on several cobalt atoms. Carbon monoxide adsorption on the supports, especially on basic oxides (Al_2O_3, ZrO_2), yields different formate, carboxylate, and carbonate species.[376] These species exhibit FTIR bands in the 1000−1600 cm^{-1} spectral region.

The carbon monoxide complexes with different surface sites differ in their stability. Therefore, a stepwise decrease in carbon monoxide pressure and increase in temperature of catalyst evacuation could allow separation of different adsorbed CO species and selective observation of the most stable ones.

Carbon monoxide chemisorption of cobalt catalysts provides valuable tools to follow the genesis of cobalt metal sites in the catalysts. Quantitative information can be obtained about the number of cobalt metal sites, cobalt dispersion, cobalt reducibility, and structure of cobalt metal particles. The number of cobalt metal sites could be evaluated quantitatively from chemisorption measurements by simultaneously recording FTIR spectra of chemisorbed CO. The low intensity of CO bands attributed to Co^{2+} and Co^{3+} ions and very intense bands of CO chemisorbed on metal particles indicate[363] a high extent of cobalt reduction. It was also suggested[380] that the intensity ratio of the bands attributed to the linear (1990−2100 cm^{-1}) and bridged carbon monoxide complexes (ν_{CO} 1800−1950 cm^{-1}) could be used as a measure of the electronic properties of the metal particles.

In-Situ Studies of FT Synthesis on Cobalt Catalysts. FTIR provides valuable in-situ information about different intermediates present on the catalyst surface during the FT reaction. Carbon monoxide has very intense FTIR bands; the presence of hydrocarbon intermediates could be also identified by the stretching C−H bands at 2800−3100 cm^{-1}.

Earlier experiments have shown[381,382] that coadsorption of carbon monoxide and hydrogen on supported cobalt catalysts results in a red shift of the CO stretching band compared to a hydrogen-free system. The lower CO frequency was attributed to electronic modification of surface sites and weakening of CO bonds due to a higher electron dative effect of the metallic cobalt. The presence of hydrogen on the surface of the metal particle could increase the availability of d electrons for back bonding from the metal to the adsorbed CO. This would decrease the energy of C−O bonding and thus result in a lower CO frequency. Jiang[383] et al. reported a higher intensity of the CO band at 2015 cm^{-1} after CO adsorption on Co- and CoMn-precipitated catalysts in the presence of H_2 at pressures up to 1.5 MPa. The authors suggest that the influence of H_2 on carbon monoxide adsorption on cobalt catalysts could explain these phenomena. Different chemisorbed oxygenated species were uncovered on cobalt−manganese catalysts during H_2 and CO coadsorption at a wide range of temperatures.

Fredriksen[384,385] et al. studied hydrogenation of CO over supported cobalt alumina and silica catalysts using in-situ FTIR spectroscopy and gravimetric analysis at P = 6 bar, T = 473−723 K, and H_2/CO = 2−3. On both silica- and alumina-supported catalysts FTIR absorption bands corresponding to linearly adsorbed CO on metallic cobalt were observed. Bridged CO complexes were detected on alumina-supported catalysts. Conducting the FT reaction leads to the appearance of absorption bands corresponding to both adsorbed hydrocarbons (3050−2700 cm^{-1}) and oxygen-containing species (1800−1200 cm^{-1}).

3.1.3. Raman Spectroscopy

Similarly to FTIR, Raman spectroscopy allows identification of different cobalt oxidized species in cobalt catalysts. Most conventional catalytic supports (Al_2O_3, SiO_2, MgO) are weak scatters and do not produce any distinct Raman bands. This facilitates selective identification of supported cobalt oxides using Raman spectroscopy. Co_3O_4 displays[231,313] in the Raman spectra a set of bands at 684, 615, 513, 477, and 194 cm^{-1}. Due to its high sensitivity, the Raman technique could also detect the presence of cobalt mixed oxides (cobalt aluminate, cobalt silicate). Cobalt aluminate ($CoAl_2O_4$, spinel) exhibits[231] intense signals at 198, 480, 519, 619, and 690 cm^{-1} and two weak bands at 412 and 753 cm^{-1} (Figure 26).

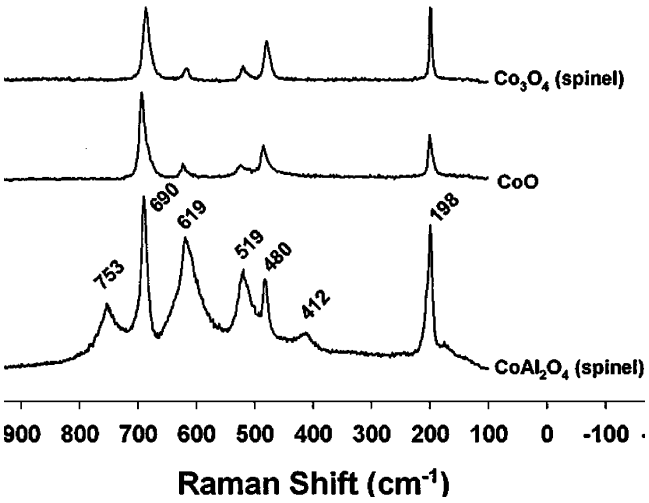

Figure 26. Raman spectra of cobalt reference compounds (reproduced from ref 231, Copyright 2004, with permission from Elsevier).

The structure of cobalt catalysts during different pretreatments can be also followed by Raman spectroscopy. Ledford[247] et al. studied the effect of promotion with La on the intensity of Co_3O_4 Raman bands. It was found that the

intensity of Co_3O_4 lines was independent of La content up to a La/Al ratio of 0.026. For higher La contents, the intensity of the Co_3O_4 Raman lines decreased with an increase in La content. In the oxidized mixed SiO_2/TiO_2 cobalt catalysts, the Co_3O_4 phase was identified[386] by Raman spectroscopy in addition to anatase TiO_2 phase. Madikizela and Coville found[387] that promotion of Co/TiO_2 catalysts with Zn led to broadening of Co_3O_4 Raman lines without affecting their intensity. Jongsomjit[231] et al. showed that in oxidized Co and $CoRu/Al_2O_3$ catalysts cobalt was primarily present in the form of Co_3O_4. After reduction, the Raman bands of Co_3O_4 totally disappeared. This suggests transformation of supported Co_3O_4 to metallic cobalt. Passivation of the reduced catalysts resulted in new broad Raman bands at 400 and 750 cm^{-1}. The authors attributed them to oxidized cobalt species "strongly interacting with alumina" different from the reference cobalt aluminate.

3.2. Diffraction Methods

X-ray diffraction (XRD) is a method of long-order characterization of solids and heterogeneous catalysts. Cobalt sites involved in FT synthesis are usually situated on the surface of relatively large crystalline cobalt metal particles (>6 nm). Thus, the XRD method can be helpful for identification and characterization of the FT active phases and their precursors. In-situ characterization of cobalt-supported catalysts using XRD leads to precious information about cobalt dispersion and reducibility during different catalytic pretreatments and under FT reaction conditions. In addition, the XRD method could detect phase transitions and phase modifications of the supports, which exhibit distinct XRD patterns such as alumina, titania, and novel mesoporous materials (SBA-15, M41S, etc.). The following sections address different aspects of application of XRD for both ex-situ characterization of cobalt phases and catalyst supports in the oxidized cobalt catalysts and in-situ characterization of cobalt phases during reduction and the FT reaction.

3.2.1. Ex-Situ Characterization of Cobalt Phases and Catalytic Supports

Oxidized cobalt catalysts supported by porous oxides typically contain Co_3O_4, CoO, intermediate cobalt oxides (Co_3O_{4-x}), mixed cobalt−support oxide phases (cobalt aluminate and silicate), and possibly nondecomposed cobalt precursors. Among all these compounds, Co_3O_4 and CoO crystallites always exhibit well-defined XRD patterns. In some cases, XRD patterns attributed to mixed cobalt−support oxides and cobalt precursors[265] could be observed, but often the mixed oxides are amorphous and do not produce any distinct XRD lines. Some XRD lines could also be attributed to the catalytic supports.

XRD is commonly used for identification of cobalt crystalline phases and evaluation of the crystallite sizes using the Scherrer equation. Let us briefly discuss the particle size analysis from XRD data. Broadening of the XRD lines is caused by structural imperfections of the sample. It has been shown that the angular breadth β of a diffraction line is given by

$$\beta = \frac{C\lambda}{L\cos\theta}$$

where C is a constant, λ is the X-ray wavelength, L is the volume-averaged size of the crystallites, and θ is the Bragg angle. In this expression either the full-width half-maximum (FWHM) or the "integral width" (area under diffraction peak divided by peak maximum) can be used[388] for definition of peak breadth. The value of the Bragg constant (C) will depend[389] on the definition of β. The uncertainty in measuring the sizes of cobalt crystallites using the Scherrer equation is often due to the fact that in the catalytic community some authors evaluate the crystallite sizes using FWHM whereas others calculate the crystallite the size using the integral width. A multimodal distribution of crystallite sizes and indistinct decomposition of the XRD signal arising from Co_3O_4 and catalyst support could also undermine the accuracy of particle size measurements.

While XRD peak broadening with a conventional diffractometer is noticeable with crystallite sizes smaller than 100−200 nm, evaluation of crystallite particle size provides relatively accurate data in the range of 6−25 nm. For very small and very large crystallites, the accuracy in measuring crystallite sizes is significantly lower. The XRD technique is not very sensitive to the presence of very small crystallites of cobalt oxides (<2−3 nm); the peaks are getting too broad to be identified and measured.

It is important to note that broadening XRD lines could be related to not only a finite size of crystallite but also the presence of strained and imperfect crystals. In this case the particle size calculated using the Scherrer equation without any corrections would be much smaller than the real sizes of cobalt oxide particles. Note that size broadening is independent of the order of reflection, while strain broadening is order dependent. The Warren−Averbach[390] and Hall−Williamson[391] approaches allow separation of broadening due to the finite size of crystallites and strain. The details of these approaches are available in previous publications.[392−394] XRD has been used to evaluate the crystallite sizes in most of publications about FT catalysts; we did not find, however, a significant number of reports which focus on the detailed analysis of XRD line broadening due to size and strain effects.

In several publications cobalt dispersion was estimated not from the sizes of metal particles but from the sizes of Co_3O_4 crystallites measured by the Scherrer equation. According to the relative molar volumes of metallic cobalt and Co_3O_4, the diameter (d) of a given Co_3O_4 particle could be converted[229,395] to the size of metallic cobalt: $d(Co^0) = 0.75d(Co_3O_4)$. This method generally provides a reasonable estimation of cobalt dispersion. Some limitations of this approach, however, should be taken into consideration. First, this approximation suggests that large and small particles of cobalt oxide have the same reducibility. Previous reports[108,363,396,397] have shown that smaller particles of cobalt oxide are much more difficult to reduce than larger ones. This could lead to underestimation of the sizes of cobalt metal particles using the method based on the average size of cobalt oxide particles. Secondly, the approximation assumes that decreasing the particle diameter during catalyst reduction proceeds according the molar volume. Castner[396] et al. showed that the decrease in the volume of silica-supported cobalt oxide particles after reduction could vary between 30% and 50%.

In addition to characterization of different cobalt species, XRD also provides information about long ordering in the catalytic supports. Different forms of titania and alumina, zeolites, and novel mesoporous materials (SBA-15, MCM-41) exhibit intense XRD patterns. XRD could be used to

follow transformation of these phases and formation of mixed oxides (cobalt silicate, cobalt aluminate). XRD, for example, showed[386] that in impregnated cobalt catalysts supported by TiO_2-SiO_2 all titania was present in the form of anatase. No phase transformation from anatase to rutile occurred during catalyst preparation. Formation of cobalt silicate was detected in the XRD patterns of the used $Co/ZrO_2/SiO_2$ catalysts by Chen[279] et al.

Small angle X-ray scattering and XRD appear to be helpful in identification of the structure and its modification of cobalt catalysts supported by mesoporous silicas. XRD data have shown[332] that SBA-15 silica is much more stable than MCM-41. Wang[398] et al. showed that addition of 20% cobalt via aqueous impregnation did not affect the intensities of small angle XRD peaks typical of SBA-15 structure, while the d(100) spacing decreased slightly from 9.9 to 9.3 nm. Our recent reports[305,343] are also consistent with those results. It was found that the hexagonal SBA-15 structure did not collapse at cobalt loadings up to 30 wt %.

Panpranot[336] et al. found that the intensity of the MCM-41 (100) XRD peak decreased after reduction and dropped considerably after conducting the FT reaction for 24 h. These observations were attributed to partial collapse of the MCM-41 structure in the presence of water vapor generated during reduction and the FT reaction. Concepción[399] et al. studied Co catalysts supported on ITQ-2, ITQ-6 zeolite-derived mesoporous materials, and MCM-41. The ordered mesoporous structure of the MCM-41 support was found to be preserved after Co loading using ethanol impregnation, as indicated by the presence of the small angle XRD peaks. Partial collapse of the cubic MCM-48 structure was observed by Li[330] et al. after modification with cobalt via aqueous impregnation. The intensity of the XRD patterns attributed to mesoporous structure also decreased[242] after conducting FT synthesis on cobalt catalysts supported by zirconium-containing mesoporous silicates.

In addition to characterization of cobalt and support phases, XRD also yields information about the build up of heavier hydrocarbons on the catalyst surface during the FT reaction. The presence of wax was observed by Bechara[400] and Ohtsuka[337] in the XRD patterns of cobalt catalysts after conducting the FT reaction test.

3.2.2. In-Situ XRD Catalyst Characterization

Most of the XRD characterization studies have been carried out using either oxidized or passivated cobalt catalysts. Note, however, that ex-situ data about the dispersion of cobalt metallic phases and cobalt reducibility might be not very accurate because of easy reoxidation of cobalt species in the presence of air. Only in-situ XRD data could probably yield reliable data about the structure of cobalt active phases present in the reduced and working catalysts.

In-situ XRD data showed[363,401] that reduction of Co_3O_4 under hydrogen proceeds via intermediate formation of CoO (Figure 27). Even heating supported particles of Co_3O_4 in nitrogen results[363] in Co_3O_4 decomposition and CoO formation in silica-supported catalysts. In the reduced catalysts in-situ XRD allows identification of cobalt cubic and hexagonal phases. Srinivasan[402] et al. identified both fcc and hcp crystalline phases of cobalt on silica after reduction, while a considerable concentration of hexagonal close-packed planes were faulty. Enache[22] et al. showed that reduction of crystallized Co_3O_4 particles supported on zirconia and alumina led to predominately cubic cobalt metal phase, while

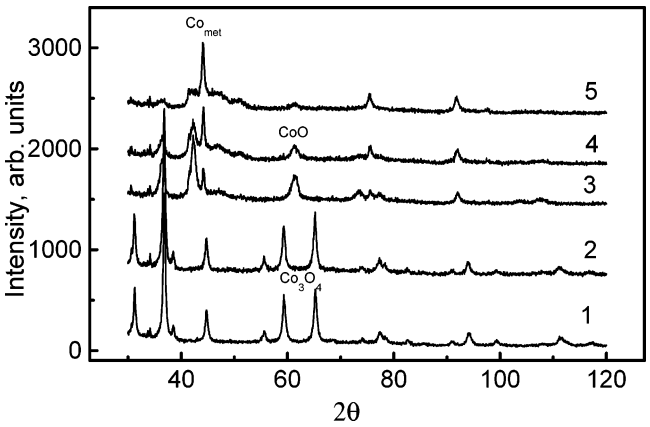

Figure 27. In-situ XRD patterns of Co/SiO_2 catalyst measured in hydrogen at room temperature (1) and 473 (2), 573 (3), 623 (4), and 723 (5) K (reproduced from ref 363, Copyright 1997, with permission from Elsevier). The patterns are offset for clarity.

direct reduction of nondecomposed cobalt nitrate resulted in a higher fraction of cobalt hexagonal phase. More cobalt hexagonal phase has been obtained after reduction of zirconia-supported catalysts. The catalysts containing hexagonal cobalt phase were found[22] to be more active in FT synthesis than those containing cubic cobalt metal phase.

The FT reaction could also have a significant impact of the fraction of different cobalt phases. Colley[403] et al. identified, using in-situ XRD, formation of the new bcc cobalt phase on Co/Al_2O_3 and Co/MnO catalysts during FT synthesis using syngas with a low H_2/CO ratio. Ducreux[24] et al. observed formation of crystalline cobalt carbide (CoC_2) on alumina- and titania-supported catalysts, whereas on silica-supported catalysts no visible phase transformation occurred. Formation of cobalt carbide in the catalysts does not result in new active sites but leads to catalyst deactivation. It was shown,[404] however, that reduction of supported cobalt carbide during catalyst regeneration selectively yielded cobalt hexagonal phase, which had a higher activity in FT synthesis than the cobalt cubic (fcc) metal phase. Thus, formation of cobalt carbide could be considered as a technique to prepare cobalt catalysts which contain high fractions of cobalt hexagonal metal phase.

3.3. X-ray Photoelectron Spectroscopy

XPS has been primarily used for identification of different phases of cobalt (Co_3O_4, CoO, metallic cobalt, and mixed oxides) and evaluation of cobalt particle sizes after different catalyst pretreatments. XPS spectra of promoting elements (Mn,[254,261] Zn,[405] Pt,[406] Ru,[211] Pd,[407] Cu,[408,409] La[247]) could also provide valuable information about the cobalt−promoter interaction and chemical composition of the surface.

Conventionally, XPS operates at ultrahigh vacuum (UHV) pressures (lower than 10^{-9} mbar) since the emitted photoelectrons are strongly scattered in gaseous phase. In these measurements the surface of cobalt catalysts can be cleaned from oxide films, contaminants, and reaction products (in the catalysts after catalytic test[410]) by argon and helium sputtering.[411,412] Argon sputtering also allows the structure of the catalyst subsurface layer to be uncovered and the structural changes in the catalysts after different pretreatments to be revealed.

It has been shown, however, that the structure of the surface layer can be modified under vacuum and thus might be not relevant to the surface of real working catalysts. To

overcome these limitations, high-pressure XPS chambers were designed in the late 1970s.[413] Note, however, that even in the high-pressure XPS set up the pressure in the measurement chamber should not exceed several mbar.[414−418]

Thus, XPS is not well suited for in-situ and operando experiments. The catalyst pretreatment, however, can be carried out at "semi-in-situ" conditions, i.e., the sample can be reduced or exposed to different gases in the pretreatment chamber of the XPS spectrometer before being transferred to the measurement chamber under vacuum or inert atmosphere without any exposure to air. Most currently this approach has been used to follow the reduction of cobalt species. XPS allows evaluation of the extent of cobalt reduction after treatment in hydrogen in the pretreatment chamber of the XPS spectrometer.[108,270,271] This technique was also used by Hilmen to study the effect of water on the oxidation of alumina-supported cobalt particles.[220] XPS can be also used for measuring cobalt catalysts, which were reduced and exposed to syngas.

In the XPS spectra of cobalt FT catalysts Co 2p XPS lines are usually the most intense; they are most commonly used for catalyst characterization (Figure 28). Co 3p XPS spectra

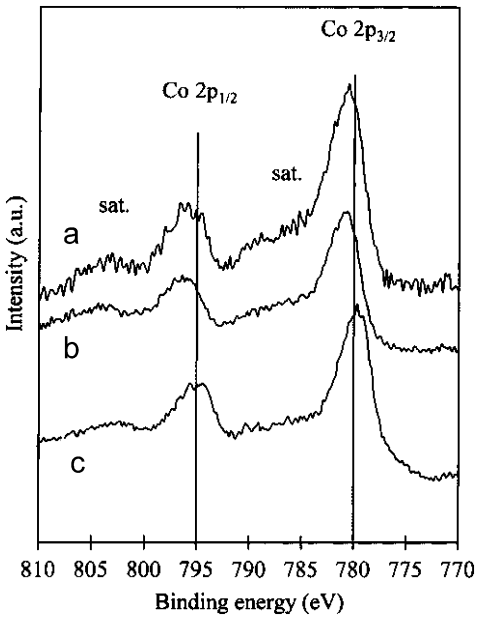

Figure 28. Co 2p XPS spectra of oxidized Co/Al_2O_3 catalysts with different cobalt contents (a) 9, (b) 16, and (c) 25 wt % (reproduced from ref 397, Copyright 1999, with permission from the American Chemical Society). At higher cobalt contents, the spectra are similar to Co_3O_4; at lower cobalt contents, the satellite structure characteristic of Co^{2+} species is observed.

are much less intense;[419] however, in conjunction with Co 2p XPS, they could provide complementary information about the cobalt oxidation state and coordination.

Most cobalt oxide compounds could be detected by XPS. Co_3O_4 is usually identified by the Co 2p XPS peak at about 780 eV; the spin−orbital splitting is 15.1 eV. Only very weak shake-up satellites are present in the Co 2p XPS spectra of Co_3O_4, which are centered at approximately 789.5 and 804.5 eV, about 10 eV from the main bands.[420] The Co^{2+} species (CoO, cobalt silicate, cobalt aluminate, etc.) exhibit XPS peaks at 797 and 804 eV;[73,420−422] the spit−orbital splitting is 15.7 eV.[423] The main $Co2p_{3/2}$ peak of Co^{2+} species shifts to higher binding energies (782−782.4 eV) relative to the spectrum of Co_3O_4. The XPS method was used by Xiong to study the inhibiting effect of promotion with zirconia[245] and magnesia[313] on formation of unreactive cobalt aluminate phase in alumina-supported FT catalysts. XPS was also used by the group of Davis[216,424] to identify the presence of cobalt aluminate phase in FT catalysts. Unfortunately, it is very difficult to distinguish from XPS data between CoO, cobalt precursor (cobalt nitrate, etc.), and mixed cobalt oxides (aluminate and silicate).

XPS also provides valuable information about cobalt metal phases. Cobalt metal phase in cobalt-supported catalysts is identified in the XPS spectra by Co 2p binding energies (Co $2p_{3/2}$ = 778 eV) and spin−orbital splitting (15.0 eV).[396,425] The fraction of different reduced and oxidized cobalt phases present in the catalysts can be calculated from decomposition of XPS spectra using the spectra of reference compounds. For decomposition of XPS spectra, the spectral background is typically subtracted using the Shirley model.[426] Then the model XPS spectra of reference compounds are used in decomposition of the XPS spectra of cobalt catalysts.[245,313]

XPS data also allow evaluation of cobalt particle sizes using the Kerkhof−Moulijn and Kuipers models. The Kerkhof−Moulijn model[427] assumes a uniform distribution of Co particles in catalyst grains, a low content of promoter, and a high specific surface area (>100 m^2/g) of the support. The Kuipers model[428,429] is based on the probability to detect cobalt atoms by XPS, which varies as a function of cobalt particle size. In that method the number of detectable cobalt atoms is strongly affected by the shape of metallic or oxide clusters. Most commonly, cobalt particles are represented by hemispheres.

While XPS provides generally acceptable values of cobalt particle sizes, some discrepancy could also be observed with the results of other characterization techniques. Several reasons could be responsible for these discrepancies. First, reliable evaluation of cobalt particle sizes using either the Kerkhof−Moulijn or Kuipers model is possible for catalysts with low cobalt content. Secondly, XPS is a surface-sensitive technique; it does not detect cobalt particles in the catalyst pores or occluded in the catalyst bulk. A nonuniform distribution of the active phase would also affect the XPS data. For example, our recent report showed that the sizes of Co_3O_4 particles evaluated from XRD were much larger than those calculated from XPS using the Kerkhof−Moulijn method.[320] The validity of the Kerkhof−Moulijn model rests on the assumption of a uniform distribution of the supported phase between the bulk and outer surface of catalyst grains. Previous work,[430] however, showed that impregnation of silicas followed by calcination could lead to enrichment of Co_3O_4 particles on the exterior of SiO_2 grains. A higher concentration of Co_3O_4 near the outer surface of catalyst grains would result in a higher intensity of the Co 2p XPS signal and, therefore, to underestimating Co_3O_4 particle sizes using the Kerkhof−Moulijn model.

3.4. X-ray Absorption Spectroscopy (XANES and EXAFS)

X-ray absorption spectroscopy (XAS) is a powerful method of local order characterization in catalytic systems. XAS has been extensively used for identification of the type of neighboring atoms, measuring interatomic distances, and evaluation of coordination number and structural and thermal disorder. The rapid expansion of XAS is due to the growing availability of synchrotron radiation.[431] XAS incorporates the XANES and EXAFS techniques. EXAFS carries information

on the short-range order around a target atom.[432,433] This is particularly useful in the case of particles whose size is 1 or 2 nm. Electronic state information can also be obtained by analyzing the near-edge structure or XANES. Both synchrotron-based XANES and EXAFS are well suited[434,435] for determining local structures of amorphous and polycrystalline materials.[436] Since the pioneering work of Tohji,[437] XAS has provided a lot of valuable information about the structure of cobalt-supported FT catalysts and their evolution during different pretreatments and catalytic reactions.

XAS measurements of cobalt catalysts are typically conducted at the K edge of cobalt (7709 eV). The relatively high photon energy at the cobalt K edge allows both in-situ and operando studies during catalyst preparation and chemical reaction. Bazin[438] et al. demonstrated the feasibility of extracting information about the structure of Co silica-supported catalyst from cobalt L_{II} and cobalt L_{III} absorption edges. Note that at these photon energies, due to strong absorption of the X-ray beam by air, the experiments have to be carried out at very low pressures. This limits application of this approach for in-situ experiments.

Several difficulties in evaluating the phase composition of cobalt FT catalysts from XANES and EXAFS should be taken into consideration.

First, it is known that the relative fraction of different cobalt phases present in the catalyst can be measured from decomposition of near-edge X-ray absorption (XANES) using X-ray absorption data of the relevant reference compounds. Note, however, that very often the structure of amorphous cobalt silicate or cobalt aluminate is uncertain. This limits the information which can be obtained using the XANES spectra of reference crystalline cobalt aluminate and silicate. Secondly, it is known that EXAFS is very sensitive to the presence of heavy atoms in the cobalt coordination sphere, while the contribution arising from lighter atoms (O, C, Al, and Si) could be calculated less accurately. This could lead to not very reliable EXAFS Co−O and Co−C coordination numbers in partially reduced or carburized catalysts.

Thirdly, EXAFS has some difficulties in identification of cobalt metallic phases. Three cobalt crystallographic phases have been described in the literature: cubic fcc cobalt, cobalt in hexagonal packing (hcp), and recently discovered epsilon cobalt.[439] The fcc structure is favored above 723 K, while the hcp phase is more stable at lower temperatures. The epsilon cobalt is a cubic metastable phase which could be obtained via decomposition of dicobalt octacarbonyl in the presence of trioctylphosphane oxide.[439] The fcc and hcp phases of cobalt are close-packed structures which differ only in the stacking sequence of atomic planes in the 111 direction. The epsilon phase is considerably less dense than either cubic or hexagonal cobalt. In the epsilon cobalt phase there are two types of atoms which differ in their local coordination.[439] Unlike ideal close-packed structures (fcc or hcp), ϵ-cobalt has three nearest neighbors for type 1 atoms and two nearest neighbors for type 2 atoms.

Unfortunately, from XANES and EXAFS it is rather difficult to distinguish between the most common cobalt hcp and fcc phases. Indeed, the Co—Co coordination number and interatomic distances are the same in the first and second coordination shells in both cubic and hexagonal phases. Simulation[436] using the FEFF package yielded (Figure 29) exactly the same Fourier transform patterns for the first and second coordination shells of fcc and hcp phases of metallic cobalt. The third peak in the hcp structure has a lower

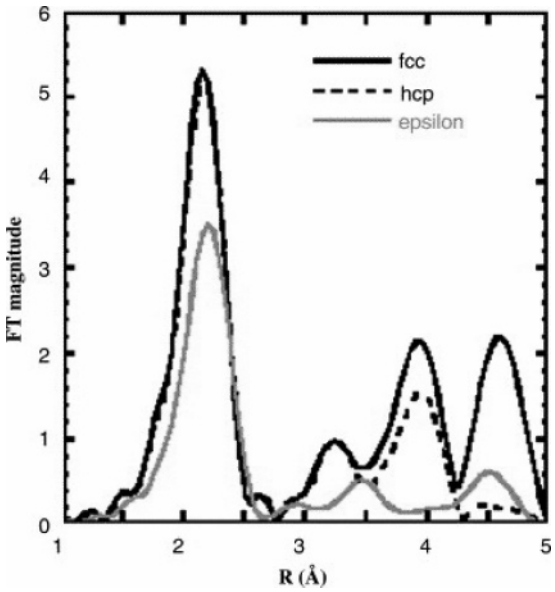

Figure 29. Simulated FT moduli of cobalt fcc, hcp, and ϵ metallic phases (reproduced from ref 436, Copyright 2004, with permission from Elsevier).

intensity, and no obvious peak is observed in the fourth coordination shell. In the fcc cobalt phase the fourth peak is rather intense due to the multiple scattering. Provided that the cobalt metal phase is well crystallized, identification of the fcc and hcp cobalt phases could be done using the fourth coordination shell. In real disordered catalytic systems the accuracy in evaluation of the fraction of different cobalt metallic phases from EXAFS using the third and fourth coordination shells is relatively low. The EXAFS Fourier transform modulus of the ϵ-cobalt phase is much different from that of hcp or fcc cobalt.[436] The magnitude of all peaks is much lower, and the positions for the second and higher coordination shells are different. This suggests that EXAFS could distinguish the ϵ-cobalt phase from hcp and fcc cobalt.

XAS yields very essential information about cobalt species during catalyst preparation, pretreatments, and the FT reaction. Very often the information could be obtained in situ[440] when the catalyst is inaccessible to most spectroscopic or surface analysis techniques. XAS has been used for characterization of the structure of cobalt catalysts through their preparation. First, valuable information was obtained about cobalt phases in the cobalt precursors deposited on the support. Our recent work[271] showed that after deposition from cobalt nitrate and cobalt acetate cobalt ions had mostly octahedral coordination, similar to that in the precursors.

Decomposition of cobalt precursor (cobalt salt or cobalt carbonyl) leads to several cobalt species: Co_3O_4, CoO, and mixed oxide (silicate or aluminate) or metallic cobalt. XAS spectroscopy provided quantitative information about the concentration of each cobalt compound present in the catalyst.[441]

XAS undoubtedly showed that reduction of Co_3O_4 to metallic species proceeded via intermediate formation of CoO[108] (Figure 30). The XANES spectra and EXAFS Fourier moduli obtained after reduction of Co/SiO_2(SBA-15) catalysts in hydrogen at 473 K were identical to those of the reference CoO. Reduction at higher temperatures led to metallic cobalt.

XAS seems to be very helpful in evaluating the extent of cobalt reduction. The XANES spectra could be decomposed using a linear combination of XANES spectra of reference

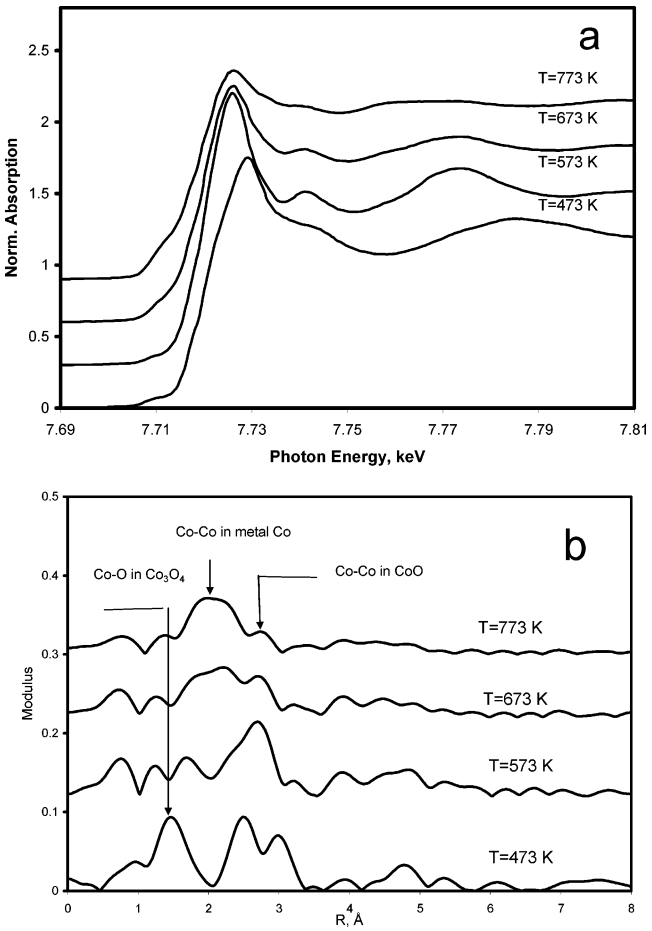

Figure 30. XANES spectra (a) and moduli of Fourier transform of EXAFS (b) for the cobalt catalysts supported by SBA-15 mesoporous silica reduced in hydrogen at different temperatures. The X-ray absorption spectra were measured in situ at corresponding temperatures (reproduced from ref 341, Copyright 2001, with permission from the American Chemical Society).

metallic cobalt, CoO, and mixed Co−Si and Co−Al compounds. Due to the relatively large cobalt oxide and cobalt metallic particles in FT catalysts, the X-ray absorption edge should not be much affected by the cluster size. Provided the structure of all phases in the cobalt catalysts has been established and the references are available, the phase composition of the partially reduced catalyst could be estimated from XANES data. As for oxidized catalysts, the principal problem in such evaluation is related to the lack of information about the structure of mixed oxides and cobalt metallic phases (cobalt silicate, cobalt aluminate, fcc, hcp, or ϵ-cobalt).

XAS provides valuable information about the reduction and structure of bimetallic cobalt catalysts. The X-ray absorption data could be measured at adsorption edges of both cobalt and promoting metals. These experiments could possibly identify formation of monometallic and bimetallic cobalt particles.[442] Theoretical calculations using molecular dynamics[443] showed a significant effect of Pd in cobalt clusters on both EXAFS of cobalt and palladium. The most important information about the presence of bimetallic particles could be collected at the absorption edge of the promoter. Note, however, that the concentration of the promoting metal (Pt, Pd, etc.) should be high enough to collect a measurable EXAFS signal. Guczi et al. showed that EXAFS at the Pt L_{III} absorption edge could identify the presence of bimetallic particles in CoPt/NaY[213,223] and CoRe/NaY[224] zeolites. Holmen[225] et al. also showed using Re L_{III} edge absorption that Co and Re formed bimetallic particles in alumina-supported FT catalysts. EXAFS analysis of the Pd and Co K adsorption edge indicated formation of bimetallic particles in the catalysts supported by graphite[227] and silica.[228] The presence of bimetallic cobalt−platinum particles was also identified from EXAFS in $CoPt/Al_2O_3$.[226] Bimetallic Co−Ru and Co−Re particles were not however detected in CoRu/NaY zeolite[444]

Previous reports[174,262] have shown that addition of Mn to cobalt catalysts results in lower cobalt reducibility. In the oxidized cobalt catalysts supported by titania[259] and carbon nanofibers,[260] which were prepared via deposition−precipitation technique, EXAFS and scanning transmission electron microscopy−electron energy loss spectroscopy (STEM−EELS) have shown the presence of mixed Mn−Co oxides. Treatment of these catalysts under hydrogen results in partial reduction of cobalt, while manganese atoms remain mostly in the oxidized state.

Several attempts were made to investigate, using X-ray absorption spectroscopy, the structure of cobalt species in situ under FT reaction conditions. Ernst[108] et al. showed that the reduced cobalt on silica-supported catalysts kept its metallic state in CO/H_2 mixtures. Huffman[267] et al. showed that addition of water to syngas ($H_2/CO = 3$), which corresponded to operating at higher carbon monoxide conversions, resulted in oxidation of cobalt on silica- and alumina-supported catalysts. The effect of water on the structure of cobalt species in FT catalysts has been extensively studied by the group of Davis. XAS analysis was performed with the samples withdrawn from the liquid phase of the laboratory slurry reactor. In the reactor and after their withdrawal the catalyst samples were suspended in FT wax. The authors suggest that coating in wax prevents cobalt catalysts from oxidation. Analysis of the XANES derivatives was indicative of partial oxidation of cobalt metal particles during FT synthesis.[445] The increase in the intensity of the Fourier transform patterns of metallic cobalt during the FT reaction also suggests sintering of cobalt metallic particles in $CoPt/Al_2O_3$ catalysts.[445] Cobalt sintering was probably the main cause of deactivation of Co/Al_2O_3 catalysts promoted with rhenium.[446]

Jacobs[214,447] and Saib[401] showed that the extent of cobalt oxidation depended on the partial pressure of water in the reactor. At relatively low water concentrations ($H_2O/CO = 1.2$; $H_2O/H_2 = 0.6$) no changes were detected in the XANES spectra of cobalt alumina-supported catalysts promoted with platinum. At higher water levels, a significant fraction of cobalt aluminate may be produced. This resulted in the abrupt drop in the FT reaction rate. The in-situ XAS experiments[401] with model cobalt silica-supported catalysts showed partial oxidation of cobalt particles in the presence of a low pressure of water ($P_{H2O} = 0.04$ bar) at 373 K. It was found that oxidation with water depended on the sizes of cobalt particles and their possible encapsulation in silica matrix.

EXAFS also could be used for measuring sizes of small metallic clusters. Note that it can be very rarely done accurately with cobalt-supported FT catalysts. The Co−Co coordination number obtained from EXAFS is sensitive to particle size for very small particles (1−2 nm). FT catalysts characteristically involve larger cobalt metal particles (6−30 nm). For larger particles, the accuracy in measuring sizes from EXAFS is much smaller due to an insignificant dependence of metal coordination number on particle size.[448]

Cobalt particles supported on porous supports usually display significant structural disorder and often consist of several structurally ordered domains. In this case, the EXAFS Co−Co coordination number can be obtained only for a single ordered cobalt domain. The size of these domains is much smaller than the overall size of cobalt metal particles. A significant discrepancy was observed by Barbier[449] et al. between cobalt particle sizes evaluated from the Co−Co coordination number and microscopic and magnetic data. This discrepancy was attributed to the presence of larger cobalt agglomerates attached to each other by a small fraction of their surface.

3.5. Temperature-Programmed Reduction

Among the thermoanalytical methods, temperature-programmed reduction is most commonly used for characterizing heterogeneous catalysts.[450] The temperature-programmed reduction (TPR) method is a catalyst characterization method based on measuring consumption of hydrogen during heating a catalyst with a linear temperature rate under continuous gas flow. The flow typically consists of 5−10% of hydrogen in argon. The chemical composition of the gas mixture at the reactor inlet and outlet is continuously monitored by a catharometer or a mass spectrometer. Interaction of hydrogen with the catalysts leads to reduction of different species. In the TPR method all the information is extracted from hydrogen consumption profiles. This gives "fingerprints" information about the catalyst redox properties. The TPR was proposed in its current version by Robertson[451] et al. in 1975.

Application of TPR techniques to different catalytic systems has been examined in several reviews.[452−455] Careful selection of the experimental conditions is essential to ensure sufficient detector sensitivity and avoid mass- and heat-transfer limitations. The reactor is usually operating in a differential mode with constant gas velocity and pressure along the catalyst bed.

TPR also has several shortcomings. The TPR profiles do not provide direct information about the modification of catalyst structure; hydrogen consumption could be attributed to different reduction processes. Use of diluted hydrogen in TPR experiments makes direct extrapolation of the TPR data about the extent of reduction to the catalysts reduced in pure hydrogen questionable. A higher partial pressure of hydrogen could lead to higher extents of catalyst reduction. During TPR measurements the catalyst is exposed to high temperatures (973−1273 K). High-temperature treatments during TPR measurements could alter the structure of the original catalyst samples.

The method has been largely applied for investigation of cobalt-supported catalysts. It has been shown that reduction of unsupported cobalt oxide (Co_3O_4) is a two-stage process[456,457] which could be ascribed to successive reduction of Co_3O_4 to CoO and then to Co.[458,459] The TPR profiles obtained for cobalt silica-supported catalysts prepared via impregnation using different cobalt salts[460] are shown in Figure 31. Several TPR peaks have been detected usually. Though it is usually difficult to attribute these peaks unambiguously, the low-temperature peaks at 373−623 K are commonly assigned to either partial reduction of Co_3O_4

$$Co_3O_4 \rightarrow CoO$$

or reduction or decomposition in hydrogen of residual cobalt

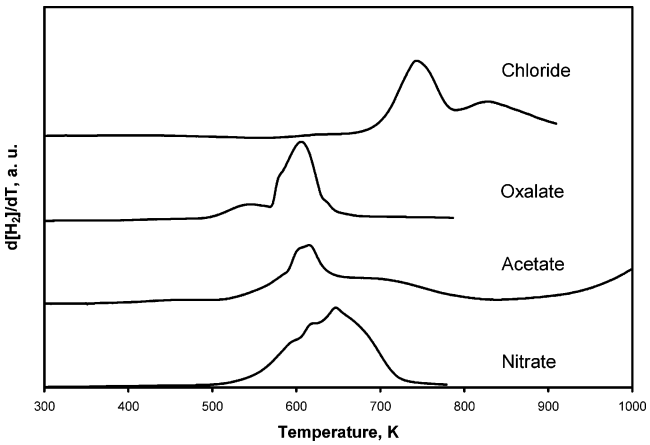

Figure 31. TPR profiles of 10 wt % Co silica-supported catalysts prepared using aqueous impregnation with different cobalt salts (5% H_2/Ar, ramping rate 0.4 K/s).

precursors (cobalt nitrate, chloride, acetate, etc.). The low-temperature TPR peaks could be also attributed[461] to reduction of surface carbonate species usually present in strongly basic oxides (La_2O_3, ZrO_2, etc.). Enache[22] and Van Berge et al.[462] assigned several low-temperature peaks to reduction of amorphous surface cobalt oxide and hydroxide species (CoO_aH_b, $a \geq 1.7$, $b \geq 0$) different from well-known crystalline Co_3O_4. Medium-temperature peaks at 673−873 K are attributed to the emergence of cobalt metallic phases

$$CoO \rightarrow Co$$

while peaks at temperatures higher than 873 K are usually related to reduction of barely reducible mixed cobalt oxides (cobalt silicate, cobalt aluminate).

It has been shown that cobalt reducibility is affected by the nature of the support. It is generally found[445,463] that cobalt species are much more difficult to reduce in alumina than in silica, titania, and zirconia supports. Below is the brief review of TPR data obtained for silica, alumina, and other supported FT catalysts.

Silica-Supported Cobalt Catalysts. A detailed TPR study of cobalt silica-supported catalysts has been performed by van Steen[282] et al. First, reduction of supported cobalt nitrate, cobalt acetate, cobalt chloride, and cobalt sulfate was examined. It was found that TPR profiles of cobalt catalysts starting from chloride or sulfate were essentially the same as for the unsupported metal salt, showing negligible interaction between the support and salt. In the case of nitrate or acetate precursor, however, a number of peaks were observed in the TPR spectra indicating formation of different cobalt species during preparation. The silica source, impregnation solvent, and temperature of drying and calcination had a significant impact on TPR profiles. van Steen[282] et al. found that low-temperature calcination (473−523 K) of silica-supported cobalt catalysts resulted in a higher intensity of low-temperature hydrogen consumption peaks in TPR profiles. This suggests that extended drying and low-temperature calcination of cobalt catalysts reduce the concentration of barely reducible cobalt silicate. The effect of calcination temperature on the reducibility of cobalt silica-supported catalysts was also a subject of our recent report.[271] The data obtained using TPR in combination with in-situ magnetic measurements are consistent with the results of van Steen about the beneficial effect of low-temperature calcination on the fraction of reducible cobalt species.

The TPR method has also been used for characterization of cobalt catalysts supported on mesoporous silicas (MCM-41, MCM-48, SBA-15). Several TPR peaks were usually observed.[330] Martinez[399] et al. reported TPR profiles for a series of mesoporous materials (Figure 32). TPR profile of

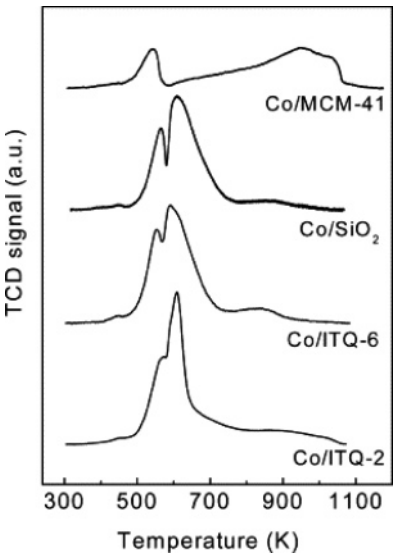

Figure 32. TPR profiles for a series of mesoporous materials (reproduced from ref 399, Copyright 2004, with permission from Elsevier).

Co/MCM-41 showed a first reduction peak with a maximum at about 543 K, most likely related to reduction of larger Co_3O_4 particles located on the external surface. This sample also exhibited a second broad reduction at higher temperatures with maximum hydrogen consumption above 900 K, which is typical of reduction of cobalt silicates.[308]

Alumina-Supported Cobalt Catalysts. Arnoldy and Moulijn[298] have shown that TPR is a sensitive technique in identification of different cobalt phases present in alumina-supported catalysts. Four different reduction regions (600, 750, 900, and 1150 K, ramping rate 10 K/min) were observed, which were assigned to four Co phases. Similar TPR results for Co/Al_2O_3 catalysts have been observed in more recent publications. Enache et al. uncovered[464] four reduction peaks at 497, 623, 973, and 1243 K in TPR profiles of 10 wt % $Co-A1_2O_3$ catalyst. The first peak resulted from reduction of Co_3O_4 to CoO. The second one was attributed to CoO reduction into metallic cobalt. The two other peaks, at higher temperatures (973 and 1243 K), were ascribed to cobalt aluminate species. The TPR curves reported by Li[245,315] show similar reduction behavior of Co/Al_2O_3. The peak at 533−673 K was attributed to reduction of bulk Co_3O_4 ($Co^{3+} \rightarrow Co^{2+} \rightarrow Co^0$), and the high-temperature peak (673−1023 K) was attributed to reduction of cobalt oxide and cobalt aluminate. The small peak at ca. 513 K was attributed to reductive decomposition of residual $Co(NO_3)_2$.

Titania- and Zirconia-Supported Catalysts. Strong metal−support interaction (SMSI) is a specificity of titania-supported metal catalysts. SMSI is usually observed when the reduction is performed at temperatures higher than 573 K.[465] At these conditions, heating in hydrogen may reduce TiO_2 to (TiO_x) suboxide.[466] Thus, in addition to reduction of cobalt oxidized species, reduction of TiO_2 can contribute to the TPR peaks. This could explain the high extent of reduction calculated for these systems using TPR data. It has been found that the metal−support interactions are weaker for rutile titania than for the anatase phase.[465,467] The presence of water vapor during reduction could result in formation of hardly reducible cobalt titanate.[468]

Zirconia is a well-known promoter of cobalt-supported FT catalysts. However, very few studies have focused on the TPR behavior of zirconia-supported cobalt catalysts. For a series of cobalt catalysts supported on zirconia, Chernavskii[469] et al. showed that TPR profiles were strongly affected by the support porous structure. The presence of small pores resulted in an appearance of low TPR temperature peaks. These peaks were attributed to reduction of cobalt species located within narrow pores. Cobalt reduction proceeded[464] differently in TPR experiments on tetragonal, monoclinic, or amorphous zirconia. Cobalt catalysts supported on monoclinic zirconia exhibited four reduction peaks with the maxima situated at 398−673 K. These peaks were attributed to the gradual reduction of Co_3O_4 into CoO and then into metallic cobalt. The catalysts supported on high surface area amorphous zirconia exhibited very small shoulders indicating hydrogen consumption at a wide range of temperatures (373−573 K) with maxima situated at 403 and 483 K. This suggests a wide range of Co_3O_4 particle sizes. The high-temperature TPR peak (1038 K) observed during reduction of cobalt catalysts supported on amorphous zirconia is attributed to reduction of cobalt zirconate.[470] Panpranot et al.[471] showed that TPR profiles are also affected by the methods of zirconia preparation. Glycothermal synthesis of zirconia results in higher cobalt dispersion and reducibility and thus better catalytic performance in FT synthesis.

3.6. Magnetic Methods

Let us first briefly recall the magnetic properties of oxidized and reduced cobalt species. It is known that both Co_3O_4 and CoO are antiferromagnetic at lower temperatures. At the Néel temperature (30 K for Co_3O_4;[472] 288 K for CoO[473]) they undergo an antiferromagnetic−paramagnetic transition. Thus, at ambient and higher temperatures both Co_3O_4 and CoO exhibit paramagnetic behavior. This leads to very small magnetization of oxidized cobalt catalysts in the magnetic field. Thus, the magnetic method does not seem to be very sensitive to the presence of cobalt oxidized species. Nevertheless, Dutta et al.[474] showed that the dependence of magnetization on temperature could provide information about the number of paramagnetic ions in the oxidized catalysts when no other information about the localization and coordination of cobalt atoms could be obtained by other characterization techniques.

Cobalt metallic particles could be of three different sorts:[475] superparamagnetic and single- and multidomain ferromagnetic. Small superparamagnetic cobalt particles behave as an ensemble of paramagnetic atoms which have a significant magnetic momentum.[476−478] These particles do not have any residual magnetization (no remittance). The upper limit of superparamagnetic particles can be determined from the relation[479]

$$KV = 25k_bT \quad (1)$$

where K is the cobalt anisotropy constant, k_b is Boltzmann's constant, V is the volume of the cobalt particles, and T is the temperature of the measurements. The calculation shows that at ambient temperatures the maximal size of cobalt superparamagnetic particles is about 7 nm. Cobalt metal particles larger than 7 nm constitute a single ferromagnetic

domain. The maximal size of a single-domain ferromagnetic particle for metallic cobalt is about 20 nm.[480] Larger cobalt particles have multidomain ferromagnetic structure. The ferromagnetic structure disappears when the sample has attained the Curie temperature. The Curie temperature for bulk metallic cobalt is 1388 K.[481]

The magnetic method could provide two sorts of information about cobalt FT catalysts. First, the extent of reduction could be quantitatively measured in situ from the magnetic data. Second, in some particular cases, the sizes of cobalt metal particles could be evaluated.

Reduction of cobalt species could be followed in situ using the magnetic method coupled with conventional TPR. The principal advantage of this technique is due to the fact that magnetic method selectively identifies cobalt metal particles. Since the magnetic method is very sensitive to the presence of ferromagnetic and superparamagnetic phases, formation of cobalt metal particles could be detected at relatively low concentrations. For example, the presence of a low fraction of cobalt metallic particles in La(Co,Fe)O_3 perovskites after reduction was uncovered by in-situ magnetic measurements.[482,483] The decrease in magnetization during catalyst reduction at higher temperatures could be related to the physical effect of temperature on ferromagnetic structure or indicate formation[484] of cobalt silicate or cobalt aluminate.

All magnetic measurements can be done in pure hydrogen. This leads to more reliable data about cobalt reducibility than those obtained from conventional TPR. Note that the TPR method usually operates with H_2/Ar mixtures, while FT catalysts for catalytic tests are commonly reduced in pure hydrogen. Our recent report[485] has shown that use of diluted hydrogen in TPR experiments could lead to significantly lower extents of reduction than those normally attained in pure hydrogen.

Determination of sizes of superparamagnetic and ferromagnetic particles is based on the relation between the magnetization and intensity of the magnetic field (field dependence curve). The field dependence can be characterized by three important parameters: σ_s, saturation magnetization; σ_r, residual magnetization; and H_c, coercive force (Figure 33a). Different types of cobalt metal particles exhibit different behavior in magnetic field. The small superparamagnetic particles[476−478] (size < 7 nm at room temperature) do not produce a hysteresis in the field dependence curve (see Figure 33b). For these particles the field dependence curve represents a sigmoid with zero residual magnetization and zero coercive force. Particles larger than 7 nm could have single-domain and multidomain ferromagnetic structure. The coercive force increases with the size of single-domain cobalt particle and reaches[475,479,480] a maximum for the size of cobalt metal particles of about 20 nm. Then the coercive force decreases to the limit typical of bulk metal cobalt. Therefore, the absolute value of the coercive force provides a method of preliminary evaluation of cobalt particle size.[486] The method based on the absolute value of coercive force was employed by Rana et al.[487] to evaluate the sizes of cobalt metal particles encapsulated in carbon nanotubes. A more accurate method of measurements of cobalt metal particle sizes has been proposed by Chernavskii.[475] It has been shown that at relatively low temperatures oxidation of cobalt metal particles follows the Cabrera−Mott mechanism.[488] In this mechanism the oxidation proceeds via formation of thin oxide layers of the surface of metal particles. Formation of CoO/Co bilayers during partial oxidation of metallic cobalt

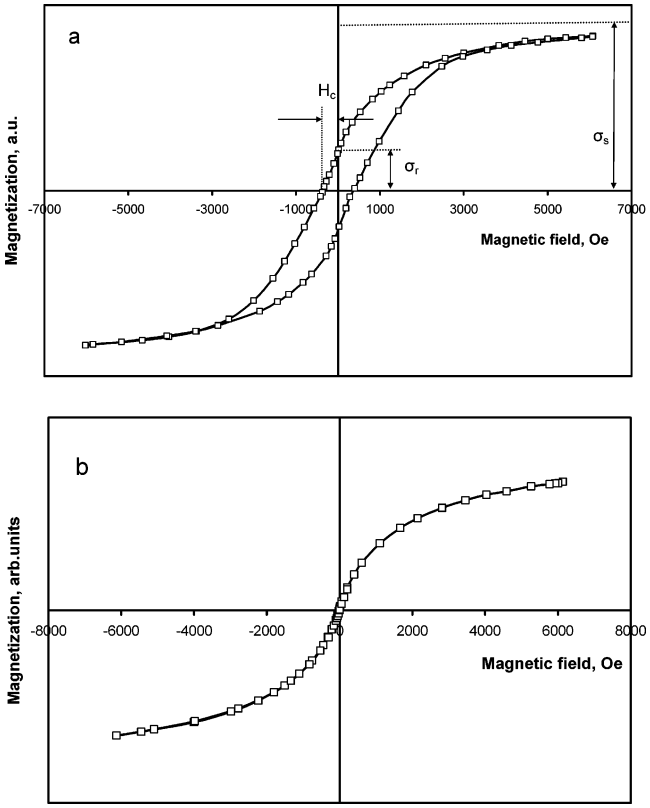

Figure 33. Field dependences measured for $CoRe/SiO_2$ (a) and $CoRe/SiO_2$ catalyst promoted with sucrose (b) (reproduced from J.-S. Giradon, E. Quinet, A. Griboval-Constant, P.-A. Chernavskii, L. Gengembre, and A. Y. Khodakov, *J. Catal.* **2007**, http://dx.doi.org/10.2016/j.cat.2007.03.002, Copyright 2007, with permission from Elsevier).

was confirmed by Gruyters[489] and Elbashir.[490] Therefore, oxidation at mild conditions reduces the apparent size of cobalt metal particles. If the average size of cobalt particles is larger than 20 nm, the decrease in the apparent size of cobalt metal particles would result in an increase in coercive force. If the average size of cobalt particles is smaller than 20 nm, oxidation would lead to a decrease in coercive force.

The choice of method for particle size analysis is strongly affected by the nature of the cobalt metal particles. When the catalyst contains only superparamagnetic cobalt particles, magnetization is expressed by the Langevin function

$$J = J_s\left(cth\,\frac{M_s VH}{k_b T} - \frac{k_b T}{M_s VH}\right) \qquad (2)$$

where J_s is the saturation magnetization (at infinite magnetic field), M_s is the magnetic momentum, V is the particle volume, H is the magnetic field intensity, T is the temperature, and k_b is Boltzmann's constant. The cobalt particle diameter can be therefore calculated from the particle volume V assuming a spherical morphology of the particle. When both superparamagnetic and single-domain ferromagnetic particles are present in the catalyst, the fraction of superparamagnetic particles (γ) can be determined from the simple relation proposed by Martin and Dalmon[491,492]

$$\gamma = 1 - \frac{2J_r}{J_s} \qquad (3)$$

where J_s is the saturation magnetization and J_r is the residual

magnetization. Note that when multidomain ferromagnetic cobalt particles are present in the catalysts, eq 3 does not yield accurate information about the fraction of superparamagnetic particles.

The magnetic method has been very valuable for characterizing different cobalt FT catalysts. The in-situ magnetic method was used[270] to follow the genesis of cobalt metal catalysts in silica-supported FT catalysts. It was shown that promotion with noble metal resulted[212] in a decrease in the temperature of appearance of cobalt metallic species. Chernavskii[486] et al. evaluated the fraction of superparamagnetic and ferromagnetic particles in bimodal silicas from magnetic measurements. The magnetic method indicated the presence of cobalt small superparamagnetic particles in the silica-supported catalysts prepared using impregnation with cobalt acetate. Larger ferromagnetic cobalt particles were found in the silica-supported catalysts prepared with cobalt nitrate. Addition of sucrose during catalyst impregnation resulted in a significant decrease in the cobalt particle size.[485] The relevant field dependence curves are displayed in Figure 33. Cobalt catalysts prepared without sucrose showed a field dependence curve with a hysteresis characteristic of ferromagnetic particles (Figure 33a). Addition of sucrose leads to superparamagnetic particles which do not exhibit any hysteresis loop.

3.7. Analytical Electron Microscopy

Transmission electron (TEM), scanning electron (SEM), scanning transmission electron (STEM), and scanning tunneling electron (STM) microscopies provide detailed information about the composition and electronic structure of heterogeneous catalysts with real-space resolution down to the atomic level.[493] Conventional transmission electron microscopy does not require special pretreatment of the catalysts; it operates in UHV and at room temperature. Recent development of high-voltage electron microscopes (>200 kV) allows[494] resolution of atomic structure. The accelerating voltage of 200 kV considerably reduces[495] the beam damage of the sensitive specimens by the ionization process. For the new TEM microscopes the point resolution is not limited by the wavelength of the electrons but by the optics, electronics stability, and mechanical vibrations of the apparatus. Improvements in electron optics have allowed a resolution of 0.18 nm to be reached. In SEM and STEM microscopes the resolution is limited by the size of the electron probes. For a long time SEM has been considered to have only very modest resolution. With the development of novel instrumentation, the resolution of SEM has been also considerably improved. In the past decade probe sizes of 0.5 nm at 30 kV and 2.5 nm at 1 kV have been reported.[496]

Conventional electron micrographs have been obtained in UHV ($10^{-6}-10^{-7}$ mbar). Currently, the new environmental high-resolution electron microscopy[497,498] (EHREM) allows measuring high-resolution images under oxidizing and reducing atmospheres and in the presence of condensable vapors at pressures of several mbar. The STM technique is also very promising. Recent studies[499−502] showed the feasibility of in-situ STM imaging real metal-supported catalysts at high pressures and temperatures.

Interaction of the electron beam with the sample results in several phenomena: emission of photons and Auger, secondary, and back-scattered electrons. Several techniques, which involve these phenomena, have been developed recently. Electron energy loss spectroscopy (EELS) is one of them. In combination with electron microscopy it provides space-resolved information about the chemical composition and atoms coordination in the catalysts.

The limitations of electron microscopic methods have been summarized by Lynch.[432] Microscopy is a local technique which does not provide global vision of the sample. The accuracy of TEM data depends on the number of images taken. The statistics problem can be crucial with nonuniform samples. Measuring cobalt particle size is based on reconstitution of particle size distributions (histograms). Particle size measurements from electron microscopy could be performed accurately only for relatively dilute samples. Formation of particle agglomerates in the catalysts with high cobalt contents makes it difficult to evaluate the sizes of primary cobalt particles. The technique is not selective for a given atom or phase. In many cases mapping using energy dispersive spectrometry might be required to discern the active phase from the support. The electron beam is potentially destructive; it could modify the catalyst structure and size of nanoparticles. All measurements in transmission and scanning electron microscopies have to be carried out in UHV, while it has been largely accepted that the presence of reacting molecules could affect the catalyst structure. In addition, it is also difficult to evaluate the extent of cobalt reduction from TEM data. Cobalt metal and cobalt oxide particles look rather similar in the microscopic images.

Electron microscopy has been used to study the structure of both cobalt active phase and catalytic supports of FT catalysts. The size of cobalt particles in the supported FT catalysts has been measured using TEM in a large number of publications.[240,330,386,395,503−508] Cobalt particles of spherical, hexagonal, oval, or irregular shapes have been detected. In most cases useful information about cobalt dispersion was obtained and TEM data were consistent with the results of other characterization techniques.

The electron microscopic measurements have been generally performed with oxidized catalysts. In the oxidized catalysts the cobalt particles detected by microscopy are mostly particles of Co_3O_4. The absence of Co_3O_4 crystallites detectable by TEM usually suggests that most of the cobalt is present in the form of cobalt mixed oxides (silicate, aluminate). For example, in our recent report[270] no Co_3O_4 particles were detected by TEM in the silica-supported catalysts prepared using high-temperature decomposition of cobalt acetate, while in the catalysts prepared via cobalt acetate decomposition at low temperatures, a considerable concentration of Co_3O_4 crystallites was observed. This indicates a low concentration of Co_3O_4 phase in the catalysts prepared via high-temperature treatment. A combination of characterization techniques uncovered that cobalt silicate was the major phase in the sample prepared via high-temperature cobalt acetate decomposition.

Several authors did their measurements on reduced and passivated catalysts. Storsæter[509] et al. showed, however, that passivated cobalt catalysts in the presence of air could be readily oxidized to cobalt oxide. This would definitely affect the accuracy of particle size measurements using electron microscopy. As with XPS, which is also an UHV-based technique, the best approach would be to reduce the catalyst in situ in the pretreatment chamber and then transfer it to the microscope vacuum chamber. This type of set up was used by Castner[396] et al. for evaluation of the sizes of cobalt oxide particles in the oxidized catalysts and cobalt metal particles in the reduced catalysts.

In addition to measuring supported cobalt particles, microscopy has also been used to study the structure of catalyst supports. Iwasaki[340] et al. prepared supports for FT catalysts using mesoporous silicates by hydrothermal treatment of Si-, Mg-, and/or Al-containing hydroxide precipitates. TEM showed that Si−Mg−Al and Si−Mg hydroxides were composed of homogeneous disk-shaped particles of about 5 nm in diameter. During the hydrothermal treatment the particles became about 8 nm in diameter. Microscopy has been particularly helpful[262] for determination of the structure of cobalt catalysts supported by SBA-15 mesoporous silica. The images show the presence of both a highly ordered hexagonal arrangement of the channels and cobalt oxide particles. Concéption[399] et al. measured cobalt particle sizes in ordered mesoporous silicas (MCM-41, ITQ-2) and amorphous SiO_2. The distribution of cobalt particle sizes was much narrower in the mesoporous silicas than in the amorphous counterparts.

Encapsulation of cobalt particles in silica matrix was observed by Saib[401] et al. A thick layer of amorphous silica around the cobalt crystallites indicated that silica could undergo migration during reduction.

Several recent papers have addressed investigation of cobalt active phase in manganese-promoted catalysts using STEM-EELS. The STEM-EELS method provided detailed information about localization of cobalt, manganese, and support (TiO_2 or carbon nanofibers) in the oxidized, reduced, and passivated catalysts. STEM-EELS images of calcined titania-supported catalysts prepared via deposition−precipitation suggest[254,259,510] (Figure 34A and B) association of cobalt

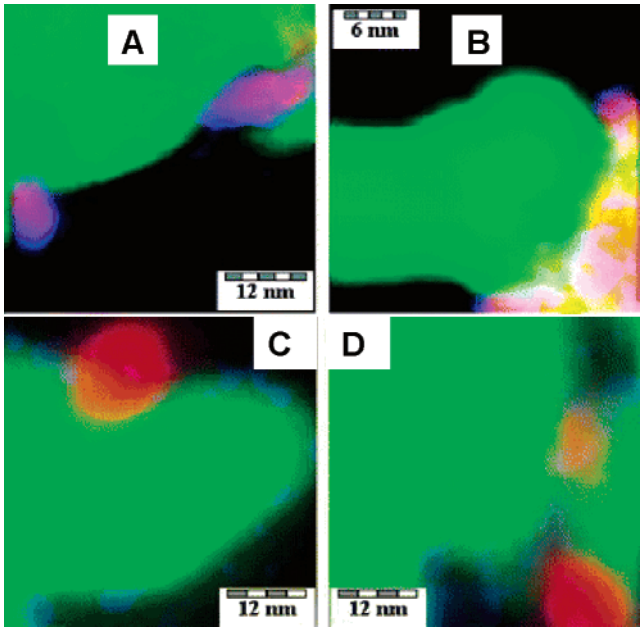

Figure 34. STEM-EELS images of CoMn after calcination (A, B), reduction at 623 K, and passivation at 423 K (C, D): Ti (green), Co (red), and Mn (blue) (reproduced from ref 259, Copyright 2005, by permission of the PCCP Owner Societies).

and manganese atoms and possible formation of mixed Co/Mn oxide. In the reduced and passivated catalysts, redispersion of MnO_x species on titania support was observed and Mn species were no longer mixed with Co (Figure 34C and D).

In the oxidized catalysts supported by carbon nanofibres Bezemer[260,261] et al. using STEM-EEELS also showed close association of cobalt and manganese atoms. In contrast to titania-supported catalysts, catalyst reduction and passivation did not lead to redispersion of manganese on the support. The presence of Mn retarded cobalt reduction, while close association of Co and Mn existed in the reduced cobalt catalysts.

Information about the surface structure of cobalt catalysts can be obtained using STM. This technique offers excellent opportunities since it is not limited by UHV conditions. STM has been used by Wilson[32,511] et al. to study restructuring of the Co (0001) surface. A terrace-type Co (0001) surface with atomic steps of 0.2−1 nm was observed following annealing (Figure 35). After 1 h of FT reaction ($H_2/CO = 2$, $P = 4$

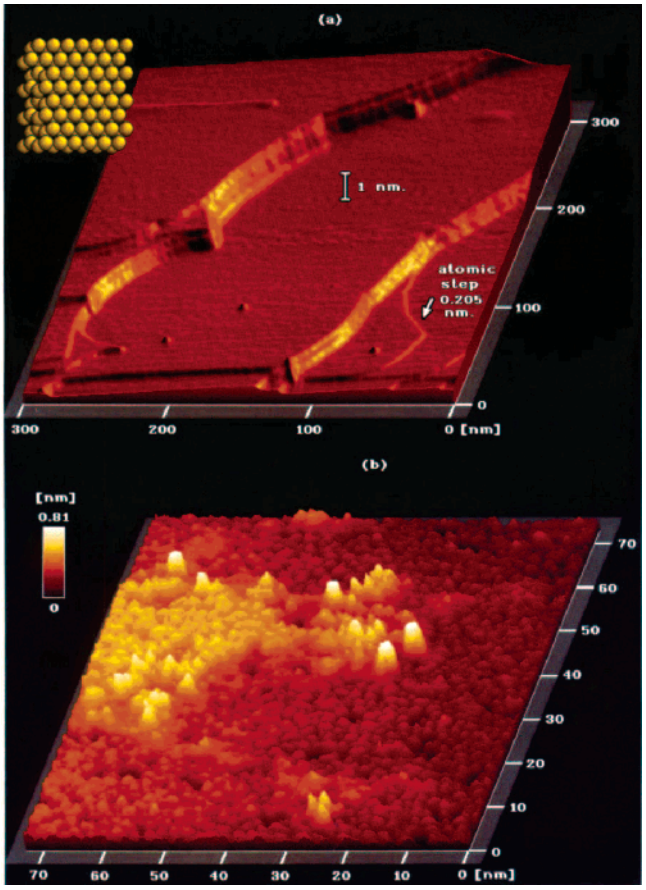

Figure 35. (a) STM image of the clean Co(0001) surface (prior to reaction) showing atomically flat terraces 150 nm (ca. 600 atoms) in width (tunneling current $I_t = 2$ nA, sample bias $V = 0.05$ V). (b) STM image of the Co(0001) surface after 1 h exposure to high-pressure CO hydrogenation conditions ($I_t = 0.5$ nA, $V = 0.5$ V). (Insert) Hard-sphere model of the bulk-terminated Co(0001) surface (reproduced from ref 511, Copyright 1995, with permission from the American Chemical Society).

bar, $T = 523$ K) small islands of cobalt atoms occupying the three-fold hollow sites of the underlying close-packed cobalt terrace were detected. Surface restructuring could result from exposure of the catalyst to carbon monoxide, water, high pressure, and high temperature.

3.8. Chemisorption Methods

Chemisorption provides important information about cobalt FT catalysts. While many characterization techniques yield data about the structure of different cobalt species, only chemisorption measurements give direct information about the number of active sites. This method is directly related to activation of molecules in the FT catalytic process.[512] The

information about the number of cobalt surface sites is essential for description of the catalytic performance. Four key parameters should be taken into consideration while using chemisorption methods.

(1) Stoichiometry of chemisorption. The stoichiometry of chemisorption corresponds to the ratio between the number of adsorbed molecules and cobalt surface atoms at monolayer coverage.

(2) Reversibility of chemisorption. Chemisorption is reversible at a given temperature if all chemisorbed molecules could be removed from the surface at a partial pressure close to zero. If chemisorption is to a larger extent reversible, the pulse and flow adsorption methods, which measure only irreversible uptakes, are not well suited for evaluating the number of cobalt active sites. These adsorption methods would result in underestimated values of the cobalt surface area. If chemisorption is reversible, only static adsorption techniques provide relevant information about the number of cobalt surface sites.

(3) Chemisorption could be an activated or a nonactivated process. If chemisorption is activated, the kinetics of chemisorption can be slow; the amount of chemisorbed molecules is more significant when the chemisorption is conducted at higher temperatures.

(4) Restructuring catalyst surface. Adsorption of molecules strongly interacting with cobalt atoms could modify metal dispersion, shape, and morphology of metal nanoparticles.

The following sections address chemisorption of hydrogen, carbon monoxide, and hydrocarbons on cobalt catalysts.

3.8.1. Hydrogen Chemisorption

Hydrogen chemisorption is a widely used method for characterization of the surface of metal-supported particles. Molecular hydrogen adsorbs[513] dissociatively on the surface of transition metals, including cobalt, at temperatures higher than 80−90 K.

Reuel and Bartholomew[514,515] systematically studied hydrogen chemisorption on supported cobalt catalysts. It was found that chemisorption of hydrogen at elevated temperatures was greater than at room temperature. This suggests[516,517] that hydrogen chemisorption is an activated process. The stoichiometry of total hydrogen chemisorption was one hydrogen atom per cobalt surface site. Figure 36 shows typical adsorption isotherms obtained on cobalt-supported catalysts at room temperature. Hydrogen chemisorption on Co/Al_2O_3, Co/SiO_2, and Co/C catalysts was to some extent reversible at room and higher temperatures. The extent of reversibility and activation of hydrogen adsorption increased with decreasing metal loading and increasing the extent of interaction between metal and support.[518] Our recent report[519] is consistent with the results of Bartholomew and Reuel. We found that hydrogen chemisorption on cobalt silica- and alumina-supported catalysts was partially irreversible at temperatures below 373 K. At the conditions of FT synthesis (T > 423 K), hydrogen chemisorption was essentially reversible.

The reversibility of hydrogen adsorption suggests that flow and pulse hydrogen adsorption methods are not well suited to measure cobalt dispersion. Extrapolation of hydrogen chemisorption isotherms to zero pressure does not provide reliable information about the number of cobalt active sites either because it takes into consideration only irreversibly chemisorbed hydrogen. The reversibility of hydrogen chemisorption also suggests that TPD methods cannot provide accurate information about the number of cobalt metal surface sites. The TPD peaks of hydrogen could also arise from desorption of hydrogen species spilled over support or reoxidation of small cobalt metal particles by hydroxyl groups of the support

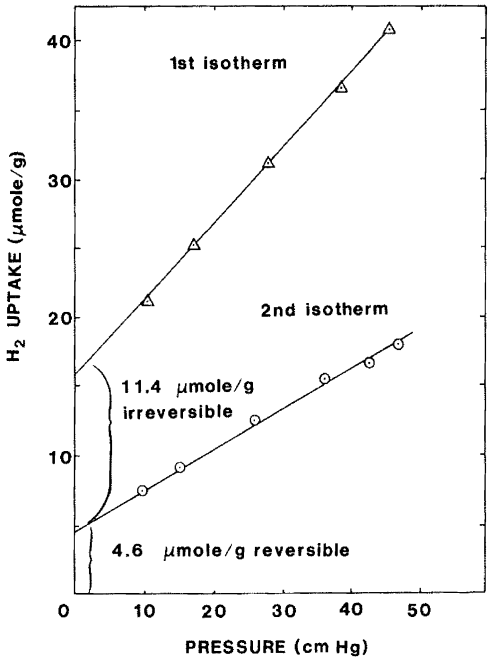

Figure 36. Reversible and irreversible H_2 adsorption on impregnated 3 wt % Co/SiO_2 at room temperature (reproduced from ref 514, Copyright 1984, with permission from Elsevier).

$$Co + 2T{-}OH \rightarrow CoO + T{-}O{-}T + H_2,$$ where T is a support atom (T = Al, Si, Ti, etc.)

Several more reliable approaches have been suggested to measure cobalt dispersion in FT catalysts using hydrogen chemisorption. These approaches are summarized as follows. Measurement of total H_2 uptake at static conditions at temperatures of maximum hydrogen chemisorption. This technique has been used by Bezemer,[260] Jongsomjit,[231] Niemelä,[301] Reinikainen,[211] Belambe[520] and others. Measurement of total hydrogen uptake during cooling in H_2 from the reduction temperature to 298 K. This approach was adopted by Ernst and Kiennemann.[265] Measuring the amount of irreversibly chemisorbed hydrogen at 190−200 K using the improved flow method. Bartholomew[521] et al. showed that hydrogen chemisorption at 190−200 K was mostly irreversible.

3.8.2. Carbon Monoxide Chemisorption

Carbon monoxide chemisorption plays a key role in FT synthesis. It is known that the metals that do not dissociate CO are inactive in FT synthesis. It was found[514,519] that carbon monoxide chemisorption on cobalt catalysts was inactivated and less reversible than that of hydrogen. Carbon monoxide adsorption on cobalt catalysts is more reversible (T < 423 K). Carbon monoxide adsorption is almost irreversible at FT reaction conditions because of the irreversibility of carbon monoxide dissociation. If the catalysts before carbon monoxide adsorption were exposed to hydrogen, carbon monoxide can substitute[519] hydrogen atoms at cobalt metal sites. This leads to carbon monoxide assisted hydrogen desorption. The stoichiometry of carbon monoxide adsorption

varies from 0.4 to 2.3 as a function of cobalt dispersion, support, and catalyst preparation.

Three important issues about carbon monoxide adsorption on cobalt catalysts should be taken into consideration. First, it has been established that in contrast to hydrogen chemisorption, carbon monoxide can adsorb on different types of catalyst surface sites: metallic sites, unsaturated ions (Co^{2+}), Lewis acid sites, hydroxyl groups of the support, etc. Second, it is known that carbon monoxide can dissociate and disproportionate on cobalt metal sites at elevated temperatures according to the Boudouard reaction

$$2CO \rightarrow CO_2 + C$$

Third, it is known that carbon monoxide strongly adsorbs on cobalt catalysts. Carbon monoxide adsorption can irreversibly modify the catalyst surface. These modifications could be attributed to both carbon monoxide disproportionation and possible sintering of very small cobalt and noble metal particles, formation of metal carbonyls in the presence of CO.

All these issues affect the stoichiometry of carbon monoxide chemisorption and consequently the results of evaluation of cobalt surface metal sites. Since carbon monoxide can react on cobalt catalysts, detection of desorbing products by mass spectrometry can yield additional valuable information. The great advantage of carbon monoxide as an adsorption probe is the opportunity to conduct the adsorption measurements with simultaneous detection of the adsorbed species by FTIR spectroscopy. Both gaseous and adsorbed carbon monoxide species exhibit distinct and intense FTIR bands. More information about identification of different carbon monoxide species adsorbed on cobalt FT catalysts is available in section 3.1.

A number of techniques based on carbon monoxide chemisorption and disproportionation have been developed to characterize cobalt metal sites in FT catalysts. Since carbon monoxide chemisorption on cobalt metal sites is to a larger extent irreversible, both dynamic and static adsorption methods can be used to measure the metal surface area. Holmen[229,522,523] et al. suggested that carbon monoxide chemisorption at 373 K was a more realistic measure of cobalt surface metal sites than volumetric H_2 chemisorption. Carbon monoxide adsorption in a pulse mode was used by Niemelä[301] and Spadaro[524] to calculate the number of cobalt metal sites in ceria-promoted Co/SiO_2 catalysts. TPD of carbon monoxide chemisorbed at room temperature was used to calculate the number of metal sites in the catalysts[525] supported by Na forms of different zeolites, in MCM-41-supported catalysts[505] and in silica- and alumina-supported catalysts modified by Zr and La.[526] Kienneman[239,482] et al. proposed the rate of carbon monoxide disproportionation for evaluation of the number of cobalt metal sites. In a typical experiment the catalysts were reduced in hydrogen and then cooled to 503 or 623 K. Pulses of carbon monoxide were admitted to the catalyst until stabilization of the amount of formed CO_2. Carbon monoxide conversion was found to correlate with the cobalt metal surface area.

3.8.3. Propene Chemisorption

Readsorption of olefins is commonly hypothesized as one of the principal stages of FT synthesis on cobalt catalysts; it influences both the selectivity of the reaction and the yield of higher hydrocarbons. Chemisorption of methane and ethene has been extensively studied on transition metals, while studies of chemisorption of propene and higher hydrocarbons have been mostly limited to monocrystals and Pt catalysts. Propene hydrogenation as a model reaction of secondary olefin readsorption and hydrogenation has been proposed by Aaserud[527] and Schanke.[528] The lower activity of the catalysts in propene hydrogenation favors propene readsorption and leads to a higher C5+ selectivity in the FT reaction.

Our recent report[529] has shown that adsorption of propene on FT catalysts results in its autohydrogenation, source of propane, and CH_x species adsorbed on the catalyst surface. Analysis of the propene chemisorption data and results of other characterization techniques suggests[271,530] that propene chemisorption could be also a useful tool for estimation of the number of metal sites and FT reaction rates over cobalt-supported catalysts. It was found that the FT rate was a function of the number of cobalt surface sites detected in the catalysts by propene chemisorption (Figure 37).

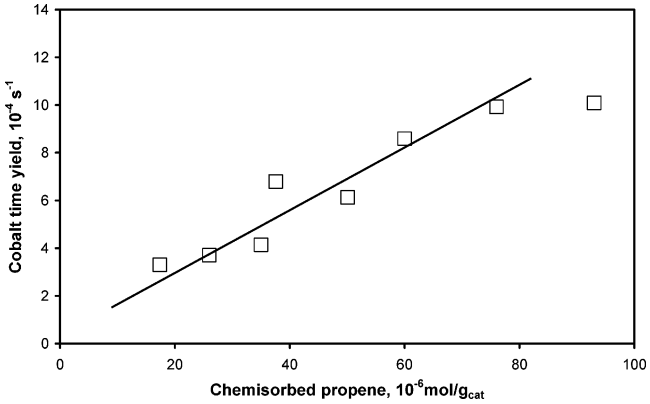

Figure 37. FT reaction rates as a function of propene chemisorption at 323 K over a series of cobalt-supported catalysts.

3.9. SSITKA for Characterization of Cobalt Catalysts

The steady-state isotopic transient kinetic analysis (SSITKA) method[531−534] involves the transient response of isotopic labels at the reactor outlet following an abrupt change (switch) in the isotopic composition of one of the reactants. The reactant concentrations, product concentrations, and gas flow rates remain unchanged during and after the isotopic switch; only the isotope composition is changing. It is generally considered that the steady state of the catalyst and reactor is not perturbed by the changes in the isotope composition of the reactant. An overview of the SSITKA method was given by Shannon and Goodwin.[535] Details of the SSITKA mathematical analysis are available in refs 536 and 537.

SSITKA yields a set of parameters such as kinetic constants, abundance and mean-surface residence time of the adsorbed surface intermediates, surface coverage, site heterogeneity, activity distribution, and concentration of adsorbed reaction intermediates. SSITKA has been used for studying FT synthesis over cobalt catalysts since the early 1980s. SSITKA has provided[538−540] valuable information about the FT reaction mechanism and chain growth on cobalt-supported catalysts. Though SSITKA is a kinetic method, it is also convenient for evaluating the number of active sites in heterogeneous catalysts. Two types of quantitative catalyst characterization information can be ob-

tained: about the number of active intermediates involved in the catalytic reaction and about the kinetic constants characteristic of these sites (intrinsic site activity).

Promotion of cobalt catalysts could result in either an increase in the concentration of the active sites in cobalt catalysts or/and an increase in the intrinsic activity of a given active site. The SSITKA method decouples these two effects. These effects are usually very difficult to separate in conventional characterization and kinetic experiments.

A brief summary about calculating the number of active surface intermediates and kinetic constants from SSITKA data is given below. The number of active intermediates involved in a catalytic reaction can be determined from integration of non-normalized transient response curves after the switch in isotope composition. This yields the amount of ^{12}C or ^{13}C atoms present in the active surface species.

The intrinsic kinetic constants characteristic of a given catalytic site could be calculated from the mean residence time of surface intermediates. Most SSITKA publications suggest that the reaction proceeds in a CSTR or in a series of CSTR reactors. Assuming that the reaction has first-order kinetics, the reaction rate (R) can be represented by the following equation

$$R = kN$$

where k is the intrinsic kinetic constant characteristic of the catalytic site and N is the number of the sites.

It has been shown that integration of the normalized transient curve yields the overall mean residence time of all adsorbed surface intermediates

$$\tau_p = \int_a^\infty F^p(t)\, dt$$

The first-order kinetics suggests that the rate constant is the reciprocal of the mean surface residence time of the active intermediate

$$k = \tau_p^{-1}$$

Thus, in this approximation the intrinsic kinetic constant can be readily evaluated from the normalized transient isotopic response and mean surface residence time. Note, however, that this SSITKA kinetic analysis is not relevant when the catalytic reaction involves a complex mechanism and especially reversible reaction pathways.

Two types of SSITKA experiments have been carried out to characterize cobalt catalysts: CO chemisorption and CO hydrogenation studies.

The carbon monoxide chemisorption experiments allowed measuring the number of sites of reversible carbon monoxide adsorption. In the chemisorption experiments the transient switch is carried out between ^{12}CO/inert gas and ^{13}CO/inert gas or between $^{12}CO/H_2$ and $^{13}CO/H_2$ at low temperatures (Figure 38). At these conditions no carbon monoxide hydrogenation occurs. The lag in transient responses of carbon monoxide relative to that of an inert gas is related to the kinetic effect of carbon monoxide adsorption and desorption. Frøseth[541] et al. showed using SSITKA that H_2 did not influence carbon monoxide chemisorption on cobalt catalysts at lower temperatures. The limitations of SSITKA for measuring carbon monoxide chemisorption are due to the fact that only reversible carbon monoxide chemisorption is measured. This technique does not take into consideration the presence

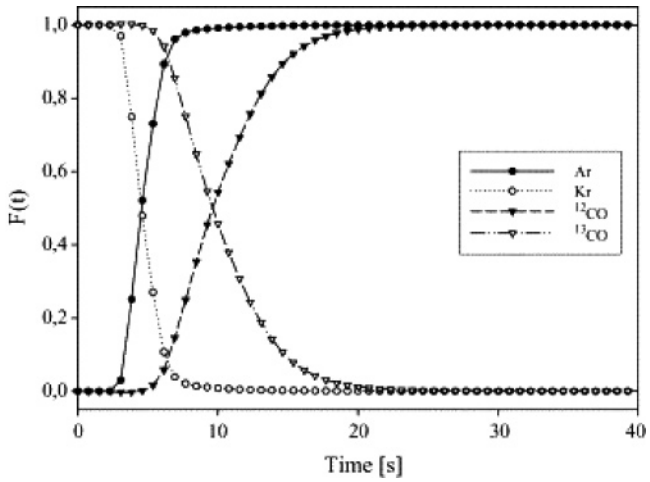

Figure 38. Transients of a CO/inert switch ($^{13}CO \rightarrow {}^{12}CO$) at 373 K and 1.85 bar for Co/Al_2O_3 catalyst promoted with rhenium (reproduced from ref 541, Copyright 2005, with permission from Elsevier).

of cobalt active sites, which could irreversibly chemisorb carbon monoxide molecules at a given temperature.

The second set of SSITKA experiments addresses carbon monoxide hydrogenation. For simplicity of data analysis and in order to avoid catalyst deactivation most of SSITKA experiments have been carried out at reaction conditions favoring methanation, i.e., at high H_2/CO ratio and low total pressure. The effect of promotion with La, Zr, and noble metals on the number of surface active intermediates and site intrinsic activity has been investigated. Haddad[249] et al. studied the effect of promotion of Co/SiO_2 catalysts with La^{3+} ions. It was found that La^{3+} ions did not affect the intrinsic site activity but led to a higher number of surface intermediates. Rothaemel[542] et al. conducted carbon monoxide hydrogenation ($H_2/CO = 10$, diluted in He) on Co/Al_2O_3 and $CoRe/Al_2O_3$ catalysts in the presence of water. Lower reaction rates were observed when the catalyst was exposed to water vapor before or during the CO hydrogenation reaction. The normalized methane transient responses $^{12}CO/H_2 \rightarrow {}^{13}CO/H_2$ were[542] the same on $CoRe/Al_2O_3$ catalyst before and after water treatment (Figure 39). The

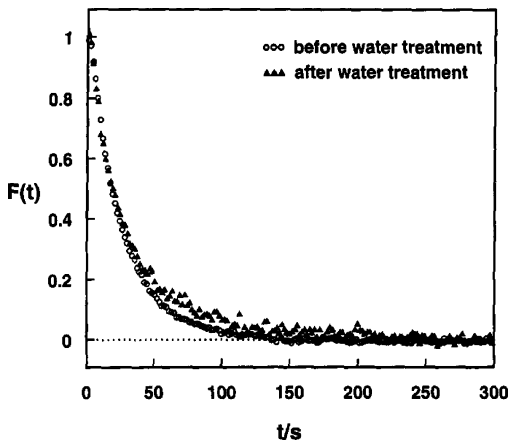

Figure 39. Normalized methane transient responses $^{12}CO/H_2 \rightarrow {}^{13}CO/H_2$ at 473 K before and after water treatment of $CoRe/Al_2O_3$ catalyst (reproduced from ref 542, Copyright 1997, with permission from Elsevier).

SSITKA experiments show that this deactivation is due to loss of active sites without affecting the specific site activity

by water treatment. Essentially the same site intrinsic activity was detected using SSITKA by Rohl[243] et al. on zirconia- and platinum-promoted Co/Al_2O_3 catalysts. The increase in the CO hydrogenation rate over the promoted catalysts was attributed to different coverages with active intermediates. The results are consistent with the more recent data by Jongsomjit[244] et al. They found that in the catalysts promoted with zirconia the surface abundance of intermediates was almost twice as high as in the unpromoted Co/Al_2O_3 catalysts. Promotion with Zr did not alter, however, the intrinsic activity of cobalt sites. Panpranot[336] et al. characterized Ru-promoted Co/MCM-41 catalysts using SSITKA. Higher methanation rates were observed on catalysts supported by narrow and wide pore MCM-41 than on those prepared using conventional amorphous silica. In agreement with the SSITKA results, higher CO hydrogenation rates were attributed to a higher concentration of active sites, while the intrinsic activity of the sites remained unchanged after catalyst promotion. A higher concentration of active surface intermediates was also observed[336] on CoRu/MCM-41 at a wide range of hydrogen pressures without affecting the intrinsic site activity.

3.10. Modeling Active Sites

Modeling cobalt FT catalysts represents a formidable and unique opportunity to study the nature and reactivity of active sites at molecular and atomic levels. It has been largely shown that the properties of nanoparticles dramatically differ from bulk metal. Because of nanosizes and interaction with catalyst support, the supported metal nanoparticles may have an unusual morphology and electronic, magnetic, chemical, and catalytic properties. Experimental studies of supported metal nanoparticles represent an extremely difficult task. Quantum chemical calculations yield important and sometimes crucial information about active sites in metal-supported catalysts, which cannot be obtained by experimental techniques. Modern density functional theory (DFT) calculations have been most often used. The modeling gives information about the elementary steps of FT synthesis on cobalt catalysts, such as adsorption, desorption, bond cleavage, surface reactions, and hydrocarbon chain growth. The FT reaction network is very complex and involves several kinetic constants. Provided that the structure of the active sites has been established, the kinetic constants of different elementary steps can be calculated ab initio. The calculated kinetic constants can be then employed for predicting the reaction rates and hydrocarbon selectivities.

The principal difficulty in modeling active sites of FT catalysts is the uncertain structure of the catalyst surface. The catalytic supports are usually amorphous; a large number of different surface species and phases can coexist simultaneously. The second difficulty is due to computing. DFT methods are still computationally demanding,[543] especially for catalytic systems involving a lot of atoms of transition metals. Despite considerable progress in computing methods, obtaining reasonable accuracy requires a high volume of numerical calculations. Cobalt particles involved in FT synthesis typically contain several thousands of cobalt atoms. The structure of these clusters cannot be calculated accurately at the present time using DFT. This is the reason why the catalyst surface is often modeled with clusters and fragments which only scarcely represent the structure of a real FT catalyst.

Several papers have addressed the processes of preparation of cobalt catalysts, interaction, and adhesion of cobalt metal atoms on the oxide supports. Suvanto[544] et al. studied the interaction of cobalt carbonyls with SiO_2 surface sites. The silica surface was represented with clusters of silica. These clusters were cut from the bulk crystal structure. The interaction of these silica clusters with $Co(CO)_4$ and $Co(CO)_3$ species was optimized using the 6-31G* basis set. The strongest adsorption was found for negatively charged $Co(CO)_3$ and $Co(CO)_4$ species bonded to the silica surface via Si−O−Co bonds. DFT calculations of deposition of Co, Rh, and Ir atoms on the alumina α-Al_2O_3 (0001) surface uncovered[545] a strong interaction of metal atoms with oxygen sites. The DFT method showed that a three-fold oxygen site was[546] the most stable adsorption site for Co atoms at low metal contents. A significant displacement of the alumina outermost layer was detected upon deposition of metal atoms. Similar cobalt preferential adsorption sites were also found by the same authors[547] on SiO_2. An increase in the cobalt content resulted[548] in metal clustering and formation of layered structures with strong metal−metal bonds and weak interaction between cobalt and silica. Active sites located on a flat and stepped Co(0001) surface were modeled by four layers of cobalt atoms by Gong[549] et al.

Deactivation of cobalt catalysts under FT reaction conditions is often attributed to oxidation of small cobalt particles. Thus, theoretical modeling of the interaction between cobalt clusters, oxygen atoms, and water is of significant interest for predicting the performance of FT catalysts. Mikhailov et al. studied[550] the interaction of Co_6 clusters with γ-Al_2O_3 surface using DFT with exchange and correlation potentials. Cobalt cluster interaction with a partially dehydroxylated alumina surface resulted in a thermodynamically favored proton transfer from alumina to the surface of metal particles. The modeling identified positive charging cobalt metal clusters (0.3−0.57 q/e) and partially oxidized electronic states of cobalt.

The thermodynamic approach was employed by van Steen[272] et al. to evaluate the stability of cobalt metallic nanocrystals in the presence of water and hydrogen. It is known that small cobalt metal nanoparticles could be less stable than bulk metal due to the significant contribution of the surface energy. The surface energy of cobalt metal nanoparticles was estimated from the number of "broken" Co−Co bonds on the particle surface. The thermodynamic calculations showed that with increasing crystallite diameter the stability of Co fcc crystallites also increased (Figure 40). Assuming a spherical morphology of the nanoparticles, under

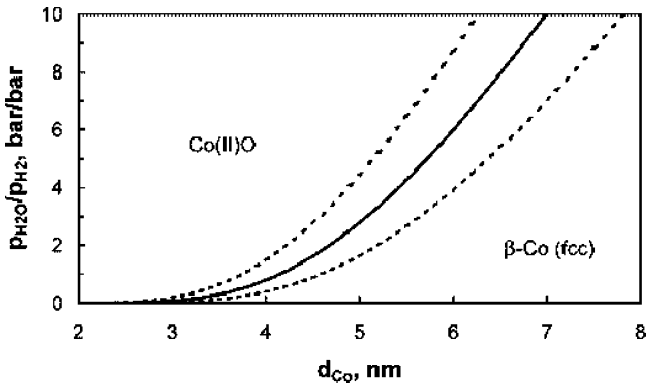

Figure 40. Stability region of spherical Co (fcc) and $Co^{2+}O$ crystals in H_2O/H_2 atmosphere at 493 K as a function of the diameter of a spherical metal Co-crystallite (dotted lines ± 15%) (reproduced from ref 272, Copyright 2005, with permission from the American Chemical Society).

realistic FT synthesis conditions ($p_{H2O}/p_{H2} < 1.5$) metal cobalt crystallites smaller than 4−5 nm were expected to be unstable and could be readily reoxidized to CoO.

Quantum chemical modeling could give valuable information about the structure of intermediate species and elementary steps of FT synthesis. The report by Klinke[551] et al. focused on the structure of hydrogen adsorption complexes on the Co(0001) surface. The binding energy of all possible high-symmetry adsorption sites was calculated to determine the most energetically favorable site. Similarly to Ni monocrystals, the most stable configuration for hydrogen atoms on the Co(0001) surface at all surface coverages was adsorption on three-fold hollow sites.

3.11. Evaluation of Attrition Resistance

Catalyst attrition is a commonly encountered problem in fluidized bed reactors and particularly in the fluid catalytic cracking (FCC) units.[552] Attrition could be a major problem in commercialization of FT catalysts for slurry bubble columns. The term "attrition" describes[553] all phenomena of unwanted degradation of catalyst particles. Degradation of catalyst particles could occur at all stages of catalyst preparation and catalytic reaction. Attrition leads to generation of fine powders and loss of valuable catalysts. Attrition reduces the quality of final products, hinders operation of filtration system, and could plug downstream lines and affect fluidization properties of the reaction medium. Two modes of attrition are distinguished: abrasion and fragmentation. Abrasion generates a lot of very fine material from the surface of catalyst grains, while the grains themselves keep their shape but get slightly smaller. Abrasion is particularly undesirable in FT slurry reactors.

Fragmentation destroys particles and produces a number of particles which are slightly smaller than the original ones. Fragmentation broadens the original particle size distribution with a shift of the mean particle size to smaller values. Catalyst attrition in a catalytic reactor usually represents a combination of abrasion and fragmentation processes. Attrition resistance of solid particles depends on several parameters which can be related to both particle and process parameters: particle structure, size, size distribution, morphology, pretreatment and preparation, gas and solid velocity, solid residence time, temperature, pressure, wall hardness, and chemical reaction.

Thus, evaluation of attrition resistance is an important issue in the development of cobalt FT catalysts for slurry bubble column reactors. Evaluation of attrition could be done in the laboratory before envisaging larger scale attrition test. Since catalyst attrition is strongly affected by the reaction and process parameters, the principal issue in evaluating attrition is whether the laboratory attrition tests are relevant to represent the attrition behavior of FT catalysts in a slurry bubble column reactor. The laboratory attrition scale tests should imply the high intensity and the same mechanism of catalyst attrition as large commercial reactors. The evaluation should involve comparison of newly developed FT catalysts with the known attrition resistance of a commercially acceptable catalyst. Several laboratory-scale methods have been proposed for evaluation of attrition resistance of FT catalysts: CSTR test, ultrasonic fragmentation, uniaxial compaction, ASTM-D-5757-95 method, fluidized bed test, jet cup, and collision test.

A few tests to evaluate the attrition resistance of FT catalysts have been proposed by the research group of Oukaci and Goodwin. Below is the brief presentation of these tests. The CSTR attrition test consists of conducting FT synthesis at realistic FT reaction conditions in a CSTR reactor and measuring the particle size distribution curves before and after the test. Uniaxial compaction is a method in which a sample confined in a cylindrical die is compressed uniaxially under a load. The ultrasonic method involves exposing a powder to a calibrated ultrasonic field and following the changes via particle size analysis. Ultrasonic fragmentation of agglomerates is caused by interaction of cavitation bubbles with adjacent agglomerated particles. Ultrasonic fragmentation coupled with particle size distribution measurements was found in a recent report by Pham[554,555] et al. to be more sensitive to differences in catalyst strength than the conventional approach involving uniaxial compaction.

The conventional ASTM-D-5757-95 attrition test is applicable[556−558] to spherically or irregularly shaped particles that range in size between 10 and 180 μm and have skeletal densities between 2.4 and 3.0 g/cm^3. During a typical test a representative dry sample of the granular material (approx. 50 g) is subjected to attrition by means of three high-velocity jets of air. The fine powder generated by attrition is continuously removed from the attrition zone by elutriation into a fine collection assembly. The fluidized bed test (Figure 41) and jet cup test are also based[559] on the ASTM design.

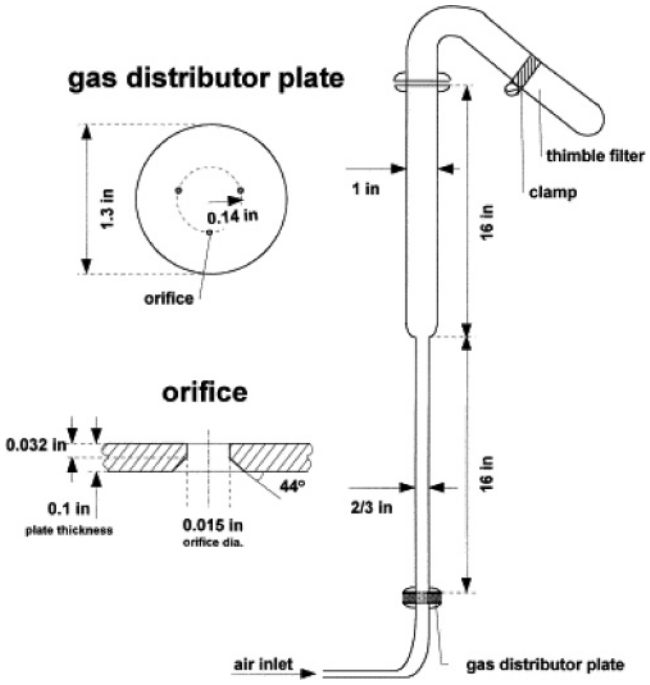

Figure 41. Fluidized bed attrition test (reproduced from ref 559, Copyright 1999, with permission from Elsevier).

They involve, however, a single high-velocity air jet and a smaller catalyst amount (1−2 g) than the conventional ASTM-D-5757-95 test. To prevent the particles from sticking to the tube as a result of static electricity, humidified air can be used in the fluidized bed and jet cup tests as a gas medium. In the collision test[559] the catalyst particles are accelerated and carried by air jet. Then they drop onto a flat surface. The particles are collected by the thimble. The collection assembly is removed after the test and analyzed for changes in the particle size distribution.

It has been shown[559] that the particle break-down mechanisms were different in different attrition tests. In the CSTR test catalyst particles were subjected to fragmentation more

than abrasion. Fragmentation was also the dominant mechanism of attrition in the collision test. For the fluidized bed, jet cup, and ultrasonic tests the large remaining catalyst particles were obviously smoother on the surface and more spherical compared to the fresh ones, which suggests[559] a significant contribution of abrasion. Though all attrition tests produce particle size distribution curves similar to those obtained after the attrition tests in CSTR, the collision test better represents the mechanism of catalyst attrition in the CSTR reactor during FT synthesis.

The attrition resistance of typical cobalt FT catalysts has been studied by Wei[246] et al. using the ultrasonic method. The catalysts were prepared via aqueous impregnation, aqueous kneading, and impregnation with a solution of acetone and ethanol. As expected, Al_2O_3 was more resistant to abrasion and produced less fine particles, while SiO_2 was less attrition resistant

$$Al_2O_3 > TiO_2(\text{rutile}) > SiO_2$$

Rutile had a much better attrition resistance than anatase. Cobalt addition improved the attrition stability of Al_2O_3 and SiO_2 without any significant effect for TiO_2 (both rutile and anatase). The attrition resistance of cobalt-supported catalysts decreased in the sequence

$$Co/Al_2O_3 > Co/SiO_2 > Co/TiO_2(\text{rutile}) > Co/TiO_2(\text{anatase})$$

Catalyst attrition resistance could be also affected, however, to a much lesser extent by promoters (Zr, Ru−La).

3.12. Summary Characterization of Cobalt Fischer−Tropsch Catalysts

Characterization of Cobalt Fischer−Tropsch Catalysts. A number of methods can be used for characterization of cobalt-supported catalysts at different preparation stages and during the FT reaction. Table 5 summarizes the capabilities, challenges, and difficulties of these techniques.

Optical spectroscopy provides information about the structure of cobalt precursors and oxidized cobalt species. All optical spectroscopy measurements can be performed in situ provided the spectrometer has been equipped with the appropriate cells and attachments. UV−vis spectroscopy yields data about the coordination of cobalt atoms in cobalt salts, cobalt oxides, and cobalt support mixed compounds. Cobalt oxides exhibit intense FTIR and Raman bands and thus could be detected in the cobalt catalysts. Unfortunately, no information about cobalt metal species can be obtained directly from optical spectroscopy. Nevertheless, FTIR combined with carbon monoxide adsorption could identify various cobalt surface sites which interact with CO adsorbing molecules. The attribution of FTIR bands of chemisorbed carbon monoxide is shown in Table 4.

X-ray diffraction methods are suitable for qualitative and quantitative identification of different cobalt oxides and metal crystalline phases. Broadening of XRD peaks is due to the finite size of nanocrystals and crystal faults. The size of the cobalt crystallites and the presence of faults and strains could be evaluated from the width of the XRD patterns using the Scherrer equation and Warren−Averbach and Hall−Williamson methods. XRD could also measure the extent of reduction of crystalline oxides to cobalt metallic phases. XRD provides useful information about the structure and stability of catalytic supports and can reveal the presence of solid hydrocarbons in the catalysts after exposure to syngas. At the same time, the structure of cobalt amorphous phases has not been satisfactorily characterized using XRD data.

Both reduced and oxidized cobalt phases in cobalt FT catalysts could be identified using XPS data. Decomposition of the XPS spectrum provides information about the extent of cobalt reduction. In the catalysts with low cobalt contents, the size of the cobalt metal and cobalt oxide crystallites could be evaluated using this technique. Note, however, that the sensitivity of XPS is a function of the electron mean path in the solids and all the information about the catalyst structure is only relevant to the surface and subsurface layers. All XPS measurements have to be carried out in vacuum or under very low pressure; this limits application of XPS for in-situ and operando experiments. The method is not very sensitive to cobalt local coordination; it is very difficult to distinguish Co^{2+} species in CoO and Co^{2+} ions in cobalt−support mixed oxides (aluminate, silicate, etc.). The accuracy in evaluating the extent of reduction is a function of the quality of XPS spectrum decomposition. The model (Kerkhof−Moulijn, Kuipers, or others) strongly affects the results of the particle size measurements using XPS.

X-ray absorption spectroscopy is sensitive to the bulk composition of the sample. The method detects both cobalt crystalline and amorphous phases. Most X-ray absorption measurements can be carried out in situ. The possibility of in-situ and operando information represents one of the principal advantages of this technique. The extent of cobalt reduction can be estimated at different stages of catalyst preparation and reaction. In addition, this method can identify the presence of cobalt bimetallic particles if the concentration of the metallic promoter is above the detection limit.

Analysis of the phase composition in XANES is based on reference compounds. The uncertain structure of cobalt−support mixed oxides makes this analysis rather tricky. EXAFS analysis is not very sensitive to the presence of light atoms around the central cobalt atoms. The EXAFS Fourier moduli are nearly the same for cobalt hpc and fcc phases; these phases cannot be clearly distinguished in cobalt FT catalysts. EXAFS does not provide reliable information about the sizes of cobalt metal particles larger than 1−2 nm, which are typically involved in FT synthesis.

The redox fingerprints of cobalt FT catalysts could be measured using TPR. This method is very useful to confirm the reproducibility of catalyst synthesis. It evaluates the fraction of easily and hardly reducible cobalt species. The attribution of TPR peaks is rather intricate; it should be based on the results of other characterization techniques. All TPR experiments have to be carried out in diluted hydrogen, while cobalt FT catalysts are usually reduced in pure hydrogen prior to the FT reaction. The reduction in diluted hydrogen could lead to a lower extent of cobalt reduction than that normally attained after pretreatment in pure hydrogen. Conducting TPR analysis at high temperatures could alter the catalyst structure.

The high sensitivity of the magnetic method to ferromagnetic and superparamagnetic phases allows detection of cobalt metal particles at different stages of catalyst reduction and FT reaction. Valuable in-situ information could be obtained about the extent of cobalt reduction and in some cases about the sizes of cobalt metal particles. The method provides little information about cobalt particle sizes when

Table 5. Comparative Analysis of Techniques for Characterization of Cobalt-supported FT Catalysts

technique	acquired information about FT catalysts	challenges and uncertainties
UV−visible	coordination of cobalt ions in cobalt precursors and oxidized cobalt catalysts	conventional UV−visible spectroscopy does not provide information about cobalt metal species
FTIR	identification of supported cobalt oxides characterization of cobalt suface sites using adsorption of molecular probes in-situ studies of FT reaction intermediates	only cobalt oxidized species could be directly observed by FTIR; detection of cobalt metal surface sites requires adsorption of molecular probes
Raman	characterization of cobalt oxide species	cobalt metal species are not seen by Raman spectroscopy
diffraction	in-situ identification of different cobalt oxidized and reduced crystaline phases measuring extent of cobalt reduction measuring sizes of cobalt crystallites characterization of the structure of catalyst supports (Al_2O_3, TiO_2, SBA-15, MCM-41, etc.) detection of hydrocarbon built up in the catalysts	very little information about structure of amorphous compounds; poorly crystallized and polycrystalline cobalt particles
X-ray photoelectron spectroscopy	identification of cobalt oxidized and reduced phases	information only about subsurface layer
	measuring cobalt particle size (catalysts with low cobalt contents)	UHV-based technique; unfeasibility of in-situ measurements
	evaluating extent of cobalt reduction	not enough sensitive to cobalt local coordination quality of XPS spectrum decomposition strongly affects the accuracy of quantitative analysis choice of model affects values of cobalt particle size
X-ray absorption spectroscopy	identification of cobalt oxidized and reduced crystalline and amorphous phases	difficulty to find appropriate references for amorphous mixed oxide compounds (aluminate, silicate)
	detection of bimetallic clusters	lower sensitivity to the presence of light atoms in the cobalt coordination spheres
	evaluating extent of cobalt reduction	lower sensitivity to cobalt particle sizes for cobalt particles larger than 1−2 nm
	possibility of in-situ and operando experiments	difficulties in distinguishing between cobalt metal phases (fcc and hcp)
temperature-programmed reduction	redox finger prints of catalysts	uncertain interpretation and attribution of TPR peaks
	detection of easily and hardly reducible cobalt phases	low extent of cobalt reduction in TPR experiments because of use of diluted hydrogen
magnetic methods	evaluation of cobalt reducibility and fraction of cobalt metal phase	unfeasibility of cobalt particle size measurements in the presence of cobalt multidomain ferromagnetic particles
	measuring cobalt metal particle size	
analytic electron microscopy and related techniques	measuring size and morphology of cobalt particles	absence of global vision of the sample; statistics dilemma
	characterization of support structure qualitative evaluation of the fraction of cobalt oxide phases and cobalt-support amorphous compounds	difficulties in evaluation of primary cobalt particle sizes in the presence of particle agglomerates low selectivity to a given atom or phase; mapping is required to discern active phase from support and promoters
	information about localization of cobalt and promoter	difficulties in distinguishing between cobalt oxidized and reduced species potential destructivity of electron beam; possible modification of catalyst structure and nanoparticle sizes need for UHV in most microscopic measurements
chemisorption methods	number and type of cobalt surface sites	choice of chemisorption method depends on the prerequisite information about the chemisorption: reversible/irreversible, activated/nonactivated, possible effect on catalyst (sintering, redispersion, etc.) uncertain stoichiometry of chemisorption uncertain attribution of chemisorption to a specific cobalt site without supplementary spectroscopic data
SSITKA	number of active sites intrinsic site activity	not sensitive to irreversible adsorption very complex mechanism of FT synthesis may affect the results of common SSITKA analysis
modeling active sites	information about elementary steps of FT reaction	uncertain structure of active sites in FT catalysts high volume of numerical calculations for rigorous models of cobalt clusters
evaluation of attrition resistance	characterization of fragmentation and abrasion of cobalt catalysts	uncertain representation in laboratory tests of attrition behavior of FT catalysts in slurry bubble column reactors

larger multidomain ferromagnetic cobalt particles are present in the catalyst.

Analytical electron microscopy allows obtaining space-resolved information about cobalt catalysts at the atomic level. The size, shape, and morphology of cobalt particles and catalyst support could be evaluated. The method could qualitatively measure the relative fraction of cobalt oxide and cobalt−support mixed oxides. The absence of distinct cobalt oxide particles suggests that amorphous cobalt−support mixed compounds constitute the dominant phase. Electron microscopy combined with electron energy loss spectroscopy (EELS) provides information about the mech-

anism of catalyst promotion. The STEM-EELS mapping detects localization of cobalt and promoting elements in the catalysts at different preparation stages.

Note, however, that electron microscopy does not provide a global vision on the sample. This issue is particularly significant with nonuniform samples. Evaluation of the cobalt particle size is difficult in samples with high cobalt loadings when large cobalt agglomerates are present. The method is not selective to a given metal atom or phase. This complicates detection of cobalt particles in promoted cobalt catalyst containing several electron-dense phases. Currently the method has been mostly used for ex-situ measurements; mostly oxidized or passivated cobalt catalysts were studied. It is known, however, that exposure of the catalyst to oxygen during passivation could affect the extent of reduction and cobalt particle size. Analytical microscopy does not distinguish cobalt oxidized and reduced phases and does not provide information about the extent of cobalt reduction. The electron beam is potentially destructive and could affect the catalyst structure. While development of scanning tunneling electron and environmental high-resolution electron microscopies seems to be very promising, most electron microscopy methods involve UHV. The vacuum-based methods are not suited for in-situ and operando experiments.

Chemisorption methods evaluate the number of cobalt surface sites in FT catalysts; information about cobalt active sites is essential for understanding and predicting the catalytic performance. Note that the choice of static or dynamic chemisorption method strongly depends on the prerequisite information about the chemisorption. If chemisorption is to a larger extent reversible, static chemisorption measurements are more suited than dynamic ones to measure the number of cobalt metal sites. If chemisorption is activated, the measurements should be carried out at elevated temperatures. The effect of chemisorption on restructuring the catalyst surface should be also taken into consideration. The uncertain stoichiometry of chemisorption is one of the most serious problems in measuring the number of cobalt metal sites. Note that molecules involved in chemisorption, e.g., carbon monoxide, can adsorb on several different sites (cobalt metal sites, acid Lewis and Bronsted sites, etc.). This suggests that the number of cobalt metal sites is not necessarily equal to the number of chemisorbed molecules. Other characterization techniques such as FTIR of chemisorbed carbon monoxide could provide supplementary information about chemisorption.

SSITKA proposes a methodology to evaluate separately the number of active intermediates and intrinsic site activity. This method has been used to study the number of carbon monoxide adsorption sites and kinetics of carbon monoxide hydrogenation at conditions favoring methanation. Note that in carbon monoxide chemisorption experiments SSITKA generates information only about the sites of reversible carbon monoxide adsorption without taking into consideration the sites of irreversible carbon monoxide chemisorption. Common analysis of SSITKA data involves a model based on the CSTR reactor and first kinetic order. It is known, however, that FT synthesis has a very complex mechanism and kinetics; use of simplified kinetic approaches could possibly alter the results of SSITKA analysis.

Most of the methods of modeling active sites involve the DFT approach. Modeling provides important and unique information about the structure of cobalt active sites and their interaction with adsorbing and reacting molecules. Quantum chemical modeling could evaluate the kinetic constants of many elementary steps. Difficulties in modeling cobalt active sites are due to the uncertain structure of actives sites and the high volume of numerical calculations.

Attrition represents a challenge for utilization of cobalt FT catalysts in slurry reactors. Several laboratory-scale attrition tests have been proposed in the literature. While valuable information has been obtained, resemblance of attrition phenomena in the laboratory-scale test and in a larger slurry bubble column reactor has not been always confirmed. The choice of the test for measuring catalyst attrition probably requires preliminary comparison of the mechanism of catalyst attrition and catalyst hydrodynamics at laboratory conditions and in a slurry bubble column reactor.

4. Strategies in the Initial Evaluation of the Catalytic Performance of Cobalt Fischer–Tropsch Catalysts

4.1. Catalyst Design and Evaluation of Catalytic Performance

Elaboration of a new heterogeneous catalyst usually involves several important steps[560,561] (Figure 42). After the new catalyst has been synthesized, its catalytic performance has to be tested and compared with that of conventional and commercial catalysts. This stage of catalyst development is called catalyst screening. As the catalytic performance is being evaluated, the catalyst has to be characterized by a number of different techniques. Catalyst synthesis, activations, pretreatments, evaluation of catalytic performance, and characterization are the primary steps in the catalyst design. In-situ and operando studies yield in-depth information about the state of the catalyst during its activation or catalytic reaction. Comparison of characterization data and results of catalyst testing is a very important task; it allows the nature of the active sites to be identified and catalyst synthetic routes to be optimized. Thus, the primary stages of catalyst design generate catalytic systems whose structure, composition, active sites, and catalytic performance have been qualitatively defined by characterization and screening.

Kinetic investigation is often the next step in catalyst design. In contrast to the screening, which allows principally qualitative ranking of different catalysts, the kinetic studies provide not qualitative but quantitative relations between the intrinsic chemical rates and composition of the fluid around the catalyst. Different from catalyst screening, in the kinetic studies the intrinsic reaction rates, instead of conversions and selectivities, are measured or computed. Ideal reactors with well-defined hydrodynamics are preferred (plug flow or perfectly mixed). These reactors allow easier computation of kinetic rates and concentrations of reacting molecules. The best reactor dedicated to kinetic studies is certainly a perfectly mixed reactor, which could involve either internal (CSTR) or external recycling (fixed bed reactor with external recycling). Usually, several kinetic models are considered; their discrimination is based on fitting with the experimental data. Detection of various reaction intermediates by in-situ and operando characterization techniques is usually helpful in choosing the most appropriate kinetic model. The kinetic stage of catalyst design ends up with the quantitative kinetic model of catalytic reaction on a given catalyst.

The intrinsic kinetic model of the catalytic reaction will eventually lead to the next step of catalyst design, which

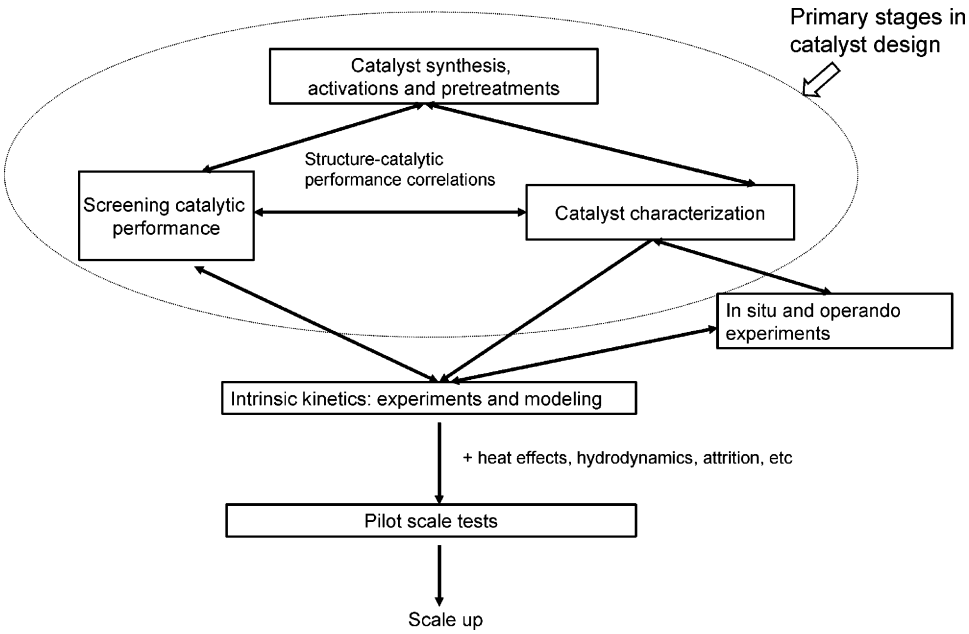

Figure 42. Schematic presentation of principal stages in the design of a new heterogeneous catalyst.

involves modeling and evaluation of the performance of pilot catalytic reactors. More comprehensive models will account for nonideality of the flows and reactors, complex hydrodynamics, coupling between mass/heat transfer, and chemical kinetics.

Thus, the performance of catalysts is evaluated at different stages of catalyst design (Figure 42), though these evaluations are performed at different conditions. The goals of these evaluations are also different. The following sections address principally the early evaluation of catalytic performance of cobalt FT catalysts (catalyst screening), which is usually performed right after catalyst synthesis and activation. Large-scale development of FT catalysts, kinetics, mass and heat transfer, and hydrodynamic phenomena have been addressed in previous publications and reviews.[8,13,14,17,19,26−30]

4.2. Challenges: Choice of Reactor and Operating Conditions

Conventional FT catalyst screening consists of comparing the catalytic performance at the same experimental conditions (temperature, pressure, space velocity, amount of catalyst or active phase). The measured output values of catalyst screening are typically overall activity (syngas conversion), selectivities (methane, light and heavy hydrocarbons, carbon dioxide), stability, and catalyst behavior during the start-up/activation steps.

The choice of operating conditions and reactor represents the major challenge of FT catalyst screening. The reactor for screening FT catalysts should involve a small amount of catalyst; it should have relatively low syngas consumption. At the same time, operating conditions for the laboratory FT test (temperature, pressure, inlet syngas composition, syngas conversion) should be as close as possible to the operating conditions of a large catalytic unit, while the time of the experiment should be possibly reduced relative to the tests in larger reactors. The principal concern of catalyst screening is that the results obtained in the laboratory FT reactor should be transferable to other FT reactors. In other words, it is desirable that the catalyst, which exhibits the highest activity and selectivity in FT reaction in the laboratory reactor, remains the most active and selective in other reactors. This is not always the case with FT catalysts. Oukaci[236] et al. measured the activity of several patented cobalt catalysts (Figure 43) in both fixed bed and slurry

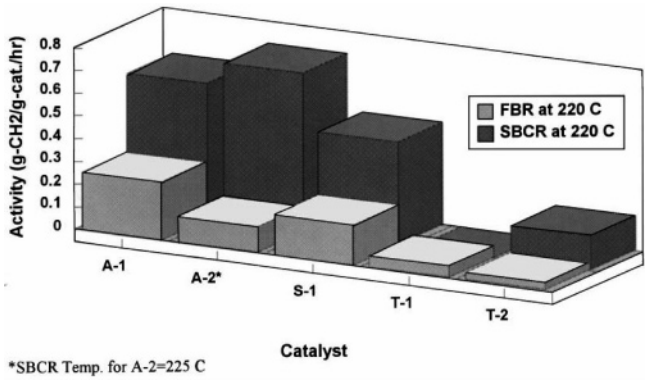

Figure 43. Comparison of FT activity of different cobalt catalysts in fixed bed and slurry bubble column reactors (reproduced from ref 236, Copyright 1999, with permission from Elsevier). The fixed bed and slurry reactors operate at atmospheric pressure and at 3.2 MPa, respectively.

bubble column reactors (SCBR). It was found that the most active catalyst in the slurry bubble column reactor operating at 3.2 MPa was the less active one in the fixed bed reactor at atmospheric pressure. The experiments of Oukaci suggest that catalyst screening should be performed at the same conditions and in the same reactor. The results of Oukaci[236] et al. would have been even more rigorous if the experiments in fixed bed and SCBR reactors were performed at the same total pressure. Often FT synthesis is an interplay of chemical kinetics, interphase, and mass- and heat-transfer phenomena. Even in the same reactor use of different reactor startup procedures could significantly affect the performance of FT catalysts. Note that catalyst screening never provides absolute ranking of catalytic performance but allows classification of catalysts on the categories (active catalysts, less active catalysts, inactive catalysts).

A fixed bed reactor is often selected for FT catalyst screening because it represents the easiest and cheapest

technical solution to perform catalytic evaluation. Other reactors are sometimes also used such as slurry continuous stirred tank reactor (CSTR) for specific objectives (design of attrition resistant catalyst, etc.). Relative to the fixed bed reactor, the slurry reactor has a few advantages relevant to catalyst screening: better control of the temperature, especially at high syngas conversions; possibility to extract the catalyst from the reactor without perturbing the reaction; better control of reactor hydrodynamics; suitability of slurry reactor for intrinsic kinetic measurements.

However, despite these advantages, a fixed bed reactor is often preferred. The slurry reactor is more expensive (cost of the technology, high amount of loaded catalyst). Gas−liquid−solid mass transfer may be rate limiting. The local concentration of the catalyst can be nonuniform inside the slurry. Catalyst in the slurry reactor can undergo attrition. Catalyst activation (calcination and reduction) in a slurry reactor cannot always be performed in situ and requires additional pretreatments (reduction ex-situ, passivation, etc.). The time to attain steady-state conditions is usually more significant in slurry than fixed bed reactors.

4.3. Atmospheric or High-Pressure Test?

Industrial FT units with cobalt catalysts operate at 493−513 K, a total pressure of 2−3 MPa, and an inlet $H_2/CO = 1.7-2.2$ ratio. Laboratory screening FT catalysts under a total syngas pressure of 2−3 MPa increases the risks for experimentalists; it requires sophisticated safety systems and adequate experimental procedures. Let us consider the influence of the total syngas pressure on both FT kinetics and the structure of FT catalysts.

(1) Influence of total pressure on FT kinetics and heat and mass transfer. An increase in total pressure would generally result in condensation of hydrocarbons, which are normally in the gaseous state at atmospheric pressure. Higher pressures and higher carbon monoxide conversions would probably lead[305] to saturation of catalyst pores by liquid reaction products. The presence of liquid products on the catalyst surface and in catalyst pores would affect heat and mass transfer and chemical kinetics. Fewer problems with heat transfer can be expected for high-pressure tests due to more rapid heat transfer in liquids than in the gaseous phase, while mass transfer could be slower in the presence of liquid phase. Chemical kinetic rates are functions of the local concentration of reacting molecules. This suggests that FT kinetics could be also affected when the catalyst is filled with liquid wax. A different composition of the liquid phase in catalyst pores at atmospheric and high syngas pressures could affect the rate of elementary steps and carbon monoxide and hydrogen concentrations. For example, Bremaud[562] et al. found that the computed Henry coefficient (defined as the ratio between the partial pressure and the molar liquid fraction) for H_2 was around 43 MPa and for CO around 35 MPa, leading to a ratio of solubility between H_2 and CO of about 1.23 (computed at 493 K and 2 MPa). In this example, if the molar ratio of H_2/CO in the gaseous phase is 2, the resulting molar ratio in the liquid phase would be only 1.6.

(2) Influence of total pressure on catalytic surface restructuring at the atomic level. The surface of FT catalysts could significantly evolve under the influence of syngas and FT reaction products. Previous STM reports[32,511,563,564] revealed significant restructuring of the cobalt Co (0001) surface in the presence of $H_2/CO = 2$ mixture at 0.4 MPa and 523 K (see Figure 35). The restructuring could affect the number of active sites in cobalt catalysts. Water produced by syngas conversion is often reported to be responsible for the initial deactivation which is probably due to a partial reoxidization of the metallic cobalt particles. Total syngas pressure may influence the concentration of liquid and gaseous water in contact with cobalt particles and, thus, the rate of deactivation. Due to the lower concentration of reagents and water, restructuring the surface of cobalt catalysts is generally less significant at atmospheric pressures than at 2−3 MPa.

Thus, total syngas pressure is an important catalyst screening parameter. The results of FT catalyst screening at atmospheric and higher pressures could yield different results. These differences could be interpreted in terms of different concentrations of reagents in gaseous and liquid phases, different mass- and heat-transfer conditions, catalyst restructuring, and deactivation.

4.4. Screening Fischer−Tropsch Catalysts in Fixed Bed Reactor

The fixed bed reactor represents a reasonable compromise for preliminary screening of FT catalysts. A wide range of experimental conditions (temperature, pressure, space velocity, syngas conversion) can be obtained at both differential and integral modes. To conduct preliminary screening of FT catalysts, several additional conditions, however, should be fulfilled: simple, controlled, and reproducible hydrodynamics, and the fixed bed reactor should exhibit plug flow behavior for gaseous and liquid phases; the reactor should operate at the kinetic regime without any significant mass- and heat-transfer effects; the isothermal mode is preferred instead of the adiabatic one in order to have good reproducibility.

While the fixed bed reactor could provide valuable qualitative information about the catalytic performance of FT catalysts, it is not very well suited for intrinsic kinetic studies. The fixed bed reactor exhibits considerable gradients of concentration of liquid and gaseous components along the catalyst bed. The nonuniformity of the catalyst bed also implies that different portions of the catalyst work at different conditions and may evolve differently during the reaction. The sections below address the choice of operating conditions for screening cobalt FT catalysts in the fixed bed reactor.

4.4.1. Plug Flow Hydrodynamics

During catalyst screening the hydrodynamics of the reactor should be relatively simple and most importantly reproducible. The plug flow hydrodynamics requires that the slices of the fluids inside the reactor are not mixing and are "pushing" each other along catalyst bed. Several criteria can be applied to check the plug flow regime provided that a Reynolds number based on particle diameter is larger than 10 (turbulent flow). These criteria are relevant to the size of the catalyst particles and diameter of the reactor. To obtain plug flow regime, the following simplified relation between catalyst bed length (L_b) and mean catalyst particle diameter (d_P) should be fulfilled

$$\frac{L_b}{d_p} > 50$$

To avoid the wall effect on catalyst performance, the diameter of the reactor (d_R) should considerably larger

than the catalyst particle size

$$\frac{d_R}{d_p} > 10$$

If a thermometric well is placed in the center of the reactor, the reactor diameter should be correspondingly corrected.

More rigorous verification of the plug flow regime in a fixed bed reactor requires evaluation of the residence time distribution (RTD). RTD studies involve measuring the transient response at the reactor outlet. The RTD is usually obtained by introduction of a pulse tracer or introduction of a step change in the concentration at the reactor inlet. If the reactor does not deform the trace transient curve, the reactor operates in plug flow regime. RTD may also be used for reactor diagnostics: the presence of back mixing and dead zones will result in broadening the trace transient, while the appearance of very early peaks will indicate the presence of shut cuts. The method of RTD measurements has been largely described in the literature.[565−568]

When a significant amount of liquid is synthesized, a trickle flow hydrodynamic regime can exist in several parts of the bed. Due to the specificity of FT synthesis (conversion of gas to liquids), the gas phase and liquid phase are moving in the same direction. While the criteria presented here are still relevant, the hydrodynamic complexity of the trickle bed does not guarantee full ideality of the reactor.

4.4.2. Intraparticle Mass-Transfer Limitations: Maximal Catalyst Particle Size

If the reactor has plug flow hydrodynamics and operates in the kinetic regime, no concentration gradients should be present inside the catalyst particle. If intraparticle mass-transfer limitations occur, this suggests that transport of the reactants/products in the catalyst particle is not sufficiently fast relative to their consumption by the chemical reaction. Internal mass-transfer limitations result in lower syngas conversions and could also affect hydrocarbon selectivities. Screening a series of FT catalysts in a fixed bed reactor with the intraparticle mass-transfer limitations will lead to severe mistakes in evaluating catalyst performance.

The kinetic network of the FT reaction is rather complex, and prediction of intragranular transport is rather difficult. This uncertainty is due to a complex dependence of mass transport inside the porous solid particles on the geometry, porosity, tortuosity of the catalyst, and diffusivities of the reagents and reaction products. It is known that gas and liquid diffusivities are a function of the temperature, pressure, and composition of the reacting medium.

Conventional experimental verification of the influence of intraparticle diffusion on the reaction rates usually involves variation of catalyst particle size while keeping other conditions constant (mass of catalyst, temperature, pressure, inlet composition, and flow rate). Steadiness of selectivity (see further) and conversion (or apparent rate of syngas consumption) while varying catalyst particle size suggests the absence of internal and fluid−solid external mass-transfer limitations. Note, however, that variation of catalyst particle size can induce an additional pressure drop and modify reactor hydrodynamics (see criteria above). In addition, an apparent activation energy lower than that usually expected for a chemical reaction could also indicate the possibility of intraparticle mass-transfer limitations with an internal concentration gradient.

If no general rules can be postulated concerning the maximal particle size for screening FT catalysts in the fixed bed reactor, several experimental and computational studies suggest that generally no internal mass-transfer limitations occur with a size between 50 and 200 μm. For most laboratory fixed bed reactors this is an acceptable catalyst particle size.

Note that intraparticle diffusion influences hydrocarbon selectivity to a greater extent than carbon monoxide conversion. The intraparticle diffusion affects differently intraparticle concentrations of carbon monoxide and hydrogen. This leads to different H_2/CO ratios at the outer surface and in the bulk of catalyst particles. Intraparticle diffusion limitations generally lead to a higher H_2/CO internal ratio and consequently a higher probability of methanation. In addition, water produced by FT synthesis for the highest pellet size has difficulties in being removed from the center to the external surface of the catalyst. It can enhance the rate of the water gas shift (WGS) reaction

$$CO + H_2O = CO_2 + H_2$$

Iglesia[17] et al. experimentally studied the effect of pellet size on the syngas consumption rate and selectivity in an isothermal fixed bed reactor (60−65 % CO conversion, 474 K, 2 MPa total pressure, inlet $H_2/CO = 2.08$) with Co/SiO_2 catalysts. For the range of catalyst diameter from 130 μm to 1.5 mm, CH_4 selectivity varied as a function of pellet size with the maximal methane selectivity obtained for a 1.5 mm diameter of catalyst pellets. Production of α-olefins is also drastically affected. The ratio of 1-hexene/hexane decreased from 1.25 to 0.06 with increasing of pellet size. While that experimental study clearly revealed that the internal mass transfer affected the selectivity, the syngas consumption rate was not altered much at these conditions. Several kinetic studies showed that the FT reaction had an apparent negative kinetic order relative to CO.[569,570] The decrease in the overall concentration of reagents inside the catalyst particles is often accompanied by an increase in the H_2/CO ratio. This seems to be the reason why the apparent rate of CO consumption could be relatively constant even when severe internal mass-transfer limitations occur; depletion of CO intraparticle concentration leads to a higher reaction rate. Thus, FT hydrocarbon selectivity is much more sensitive to intraparticle mass-transfer limitations than the overall CO conversion.

Computation of the Thiele modulus (based on the intrinsic rate) or the Weisz modulus (based on the apparent rate) also could be helpful in order to detect intraparticle mass-transfer limitations. Sie and Krishna,[28] using the data of Post[115] et al., computed the internal efficiency (calculation of the active part of the catalyst). The Thiele−Wheeler plot (Figure 44)

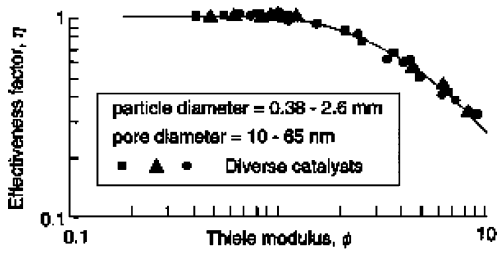

Figure 44. Catalyst effectiveness η as a function of the Thiele modulus μ for various cobalt and iron catalysts. $H_2/CO = 2$, $P =$ 2.1 MPa, $T = 473-513$ K (reproduced from ref 28, Copyright 1999, with permission from Elsevier).

correlates data obtained with different catalysts under different operating conditions. Catalyst effectiveness starts to drop significantly when the Thiele modulus φ becomes greater than 1. It was estimated that for usual FT conditions the internal mass transfer could interfere with the chemical reaction above a mean diameter of 500 μm. Wang et al.[571] with a complete kinetic model simulated the concentration profiles inside a catalyst pellet filled by liquid wax and found that a mass-transfer limitation could occur if catalyst particles were larger than 150 μm.

4.4.3. External Mass-Transfer Limitations

Transport of each species in the interface around the catalyst particle or between gaseous and liquid phases may also limit the activity and selectivity of FT catalysts. The presence of external mass-transfer limitations in a fixed bed reactor can be detected using a simple experimental test. The test consists of simultaneous variation of the mass of the catalyst and inlet syngas flow rate while keeping the space velocity and other experimental conditions (temperature, pressure, and inlet H_2/CO molar ratio) constant. The reaction rate and especially selectivities should remain constant until the superior limit where extragranular mass-transfer limitations can be observed.

In order to keep the plug flow regime of the reactor during this test dilution of the catalyst in an inert material may be required. To avoid possible segregation of the catalyst and inert material in the reactor, the diluting inert material should have a density close to that of the catalyst. Note, however, that dilution may lead to bypassing[572] and can decrease the apparent activity of the catalyst. Previous reports suggest that catalyst dilution should not exceed 5−10 catalyst volumes.[561,573]

As with intraparticle diffusion limitations, the presence of external mass-transfer limitations could be also detected via measuring the apparent activation energy. An external mass-transfer control regime could lead to the apparent energy activation of just a few kJ mol^{-1}.

4.4.4. Heat Transfer and Hot Spots

Since FT synthesis is highly exothermic, heat transfer can be problematic even in a laboratory fixed bed reactor, especially operating at gas−solid mode. In gas−solid mode the heat removal capacity can be low because of low heat conductivity of the gaseous phase. This would lead to axial and radial temperature gradients in the reactor. The presence of temperature gradients in the catalyst bed could be detected via direct temperature measurements.

The heat release is proportional to the FT reaction rate. At high conversion levels, different parts of the fixed bed reactor could be affected differently by heat-transfer problems. Thus, high heat release could occur in the catalyst layers where most of carbon monoxide and hydrogen are converted, while heat production in other parts of the fixed bed reactor could be significantly lower. In addition to a nonhomogeneous temperature distribution in the reactor, intraparticle temperature gradients also can be present; a catalyst particle may have different temperatures on the outer surface and inside the pores. The variation of catalyst temperature both in the catalyst bed and inside the catalyst particle could affect the results of FT catalyst screening.

The temperature gradient in the catalyst bed can be reduced or eliminated using dilution of catalyst with a smaller inert solid (maximal ratio of size between 5 and 10 depending on the size of the catalyst) while keeping unvaried all the other parameters. The system of heating should be homogenous in the axial direction, and the presence of a guard bed for syngas preheating is recommended. The diameter of the heater in the case of a band heater (metallic or ceramic) should be as close as possible to the outside wall of the reactor to prevent the heat-transfer problem in the gap between the reactor and heater.

4.5. High-Throughput Experimentation

Combinatorial techniques developed in biology have inspired high-throughput experimentation (HTE) for evaluating the performance of heterogeneous catalysts. In these experiments several heterogeneous catalysts can be evaluated simultaneously instead of testing catalysts one by one.[574,575] The principle is to multiply the reactors and reduce the laboratory space. Small reactors called "microreactors" are often used. The advantages of HTE are as follows: shorter experiment times because several catalytic tests can be performed in parallel in a single experimental setup; economy of laboratory space because of reactor miniaturization; smaller amounts of catalyst for catalyst tests and economy of catalyst samples.

The drawbacks of HTE are also summarized: High cost of the HTE setup; high probability of technical problems because of miniaturization (plugging of the tubes, loading/removing the catalyst, etc.); possible low reproducibility because of the small amount of samples, especially if the catalyst sample is nonuniform; the method is not well suited when analysis of reaction products is rather complex and time consuming.[561]

While several parallel systems have been proposed for many applications in catalysis, very few HTE attempts have been made for screening FT catalysts. Ouyang[576] proposed a microreactor system which involves 16 parallel reactors. Although the authors claimed that this system was very promising, only hydrogenation of carbon monoxide to methane was studied. Moulijn[561] et al. proposed a more realistic system with six fixed bed reactors placed in parallel. This system was used to carry out FT catalyst screening and study the effect of bed dilution on the catalytic performance of the fixed bed reactor. The same research group also proposed an identical system for screening the catalytic performance of FT monolith catalysts.[134] The work of Moulijn and co-workers represents a rare demonstration of HTE approach efficiency for screening the catalytic performance of FT catalysts under high pressure.

HTE is probably well suited for screening catalyst performance when the catalytic reaction could be carried out under atmospheric pressure and analysis of products can be performed on-line. FT synthesis produces a wide range of products (hydrocarbons, C1−C100, paraffins, olefins, oxygenates, etc.). The steady-state conditions of the FT reactor could be usually attained after several hours and days of operation. FT tests are usually conducted under elevated pressures and require additional experimental set-up such as condensers in order to separate liquid, solid, and gaseous products. Analysis of liquid hydrocarbons and especially wax is rather complex and cannot always be performed on-line. It can be suggested, therefore, that HTE would probably be less efficient for evaluating the performance of FT catalysts than for many other catalytic reactions, especially at the conditions favoring waxes and higher hydrocarbons.

5. Summary and Outlook

Catalyst synthesis, catalysts characterization, and evaluation of catalytic performance are the primary and probably most important stages in the design of cobalt FT catalysts (Figure 42). Different catalyst synthesis routes, promotion with noble metals and metal oxides, catalyst pretreatments, and support effects provide efficient tools to control the structure and chemical, physical, and mechanical properties of cobalt catalysts. The bulk and surface structure of cobalt-supported catalysts could be identified by a wide range of characterization techniques. The most relevant information about the active phases could be extracted from in-situ and operando measurements because the catalyst structure and catalytic performance can evolve during different pretreatments and FT reaction. A fixed bed reactor with plug flow hydrodynamics which operates in the kinetic regime and in the isothermal mode at $H_2/CO = 2$ and 2−3 MPa of total pressure probably provides the most suitable methodology for preliminary evaluation of the performance of cobalt FT catalysts.

Several specific requirements for cobalt FT catalysts can be formulated. To attain a high and stable yield of long-chain hydrocarbons, FT catalysts should have an optimal density of cobalt metal active sites. The active component (cobalt) should be used very efficiently; loss of cobalt in the support matrix should be avoided. The catalyst should exhibit high stability during FT synthesis. The cost of the catalyst should be moderate to allow possible industrial utilization.

Thus, the first objective of any catalyst preparation is to generate the optimal number of active sites. It has been largely accepted that FT synthesis proceeds on cobalt metal particles. Thus, the goal of FT catalyst preparation is to generate a significant concentration of stable cobalt metal surface sites. The number of cobalt metal sites depends on the size of cobalt particles and their reducibility. An optimal equilibrium between cobalt dispersion and reducibility can be obtained using different catalytic supports, methods of cobalt deposition, pretreatments, and promotion with noble metals and metal oxides.

There is generally a consensus in the literature that the FT reaction is structure insensitive at least for cobalt particles larger than 6 nm. Though several methods of deposition of the active phase could generate very small cobalt particles (<4−6 nm), the catalysts containing these very small particles do not normally exhibit adequate catalytic performance. First, it has been shown that very small cobalt particles are not stable at the conditions of FT synthesis; they could be reoxidized, sinter, carburize, and react with the support, which leads to formation cobalt−support mixed oxides. Second, when particles are very small, their electronic, magnetic, optical, and adsorption properties could be dramatically altered[577−579] because of the quantum size effect. The quantum size effect on the structure of metal and oxide particles is usually observed when the particle is getting smaller[580] than 10 nm. Therefore, the intrinsic catalytic activity of cobalt sites located in smaller cobalt particles could be different from that in larger ones, even provided no deactivation occurs.

In addition to the overall number, repartition of cobalt surface sites in a catalyst grain could be essential in attaining a high yield of hydrocarbons. No intraparticle diffusion limitations have been usually reported for slurry phase catalytic reactors operating with catalyst grains of about 50 μm. In fixed bed tubular reactors,[17,19] which involve catalyst particles of 1−3 mm, diffusion of reagents, intermediates, and final products could be relatively slow and affect the FT reaction rate and selectivity. The methods of eggshell catalyst synthesis seem to provide a solution, which could optimize the efficiency of cobalt catalysts in fixed bed reactors.

The goal of catalyst preparation is also to avoid loss of cobalt atoms in the support matrix during catalyst preparation, pretreatments, and FT reaction. Cobalt oxide could react with most oxide supports yielding cobalt−support mixed compounds. These compounds are not reducible at moderate reduction temperatures and do not produce any active sites for FT synthesis. Production of undesired mixed compounds could be minimized by adjusting the parameters of catalyst synthesis and pretreatments.

It has been largely shown that the performance of FT catalysts evolves with time on stream. Several days and weeks may be required to attain the steady-state conditions even in a laboratory-scale reactor. Significant modifications of catalyst structure could occur during the FT reactor start up and on-stream during FT synthesis. These modifications could be related to different phenomena: exothermicity of the reaction, temperature control, impurities in the feed, and presence of water, carbon dioxide, heavier hydrocarbons, and organic compounds in the reaction products. Catalyst attrition also could be one of the reasons responsible for the drop in catalytic performance in a slurry reactor. This suggests that cobalt active sites generated in cobalt-supported catalysts should be stable during FT synthesis. Understanding and controlling the phenomena that occur in the catalyst during FT reaction represent a significant challenge. Catalyst modifications under the influence of the FT reaction medium seem to be currently the most obscure area in the design of FT catalysts.

FT synthesis is an industrial process. Because of the relatively low space velocities, a significant amount of catalyst is required for a slurry bubble column and fixed bed multitubular reactor. This involves the requirement to the catalyst cost. Promotion with even small amounts of noble metals and sophisticated methods of cobalt preparation could spectacularly increase the cost of cobalt FT catalysts and overall technology.

6. Acknowledgments

Wei Chu thanks the CNRS and University of Sciences and Technologies of Lille for providing financial support during his stay as an associated researcher and invited professor in the Unité de Catalyse et de Chimie du Solide, UMR CNRS 8181. He also acknowledges partial financial support in the area of plasma-enhanced catalysts by the NNSFC of China (Project 205903603) and the Ministry of Sciences and Technologies of China (2005CB221406).

7. References

(1) Fischer, F.; Tropsch, H. *Brennst. Chem.* **1923**, *4*, 276.
(2) Fischer, F.; Tropsch, H. *Brennst. Chem.* **1926**, *7*, 97.
(3) Fischer, F.; Tropsch, H. *Ber. Dtsch. Chem. Ges.* **1926**, *59*, 830.
(4) van Dyk, J. C.; Keyser, M. J.; Coertzen, M. *Int. J. Coal Geol.* **2006**, *65* (3−4), 243.
(5) Fischer−Tropsch Technology (Steynberg, A. P., Dry, M., Eds.) *Stud. Surf. Sci. Catal.* **2004**, 152.
(6) Batholomew, C. H. AIChE Spring Meeting, New Orleans, LA, 2003; paper 83b.
(7) Vannice, M. A. *J. Catal.* **1975**, *37*, 449.

(8) Jager, B. *Stud. Surf. Sci. Catal*. **1998**, *119*, 25.
(9) Espinoza, R. L.; Steynberg, A. P.; Jager, B.; Vosloo, A. C. *Appl. Catal. A* **1999**, *186* (1−2), 13.
(10) Jager, B.; Espinoza, R. *Catal. Today* **1995**, *23*, 17.
(11) Dry, M. E. *Catal. Today* **2002**, *71*, 227.
(12) Bromfield, T. C.; Vosloo, A. C. *Macromol. Symp.* **2003**, *193*, 29.
(13) Jager, B.; van Berge, P.; Steynberg, A. P. *Stud. Surf. Sci. Catal*. **2001**, *136*, 63.
(14) Steynberg, A. P.; Espinoza, R. L.; Jager, B.; Vosloo, A. C. *Appl. Catal. A* **1999**, *186* (1−2), 41.
(15) Geerlings, J. J. C.; Zonnevylle, M. C.; de Groot, C. P. M. *Surf. Sci.* **1991**, *241* (3), 315.
(16) Soled, S. L.; Iglesia, E.; Fiato, R. A.; Baumgartner, J. E.; Vroman, H.; Miseo, S. *Top. Catal.* **2003**, *26* (1−4), 101.
(17) Iglesia, E.; Reyes, S. C.; Madon, R. J.; Soled, S. L. *Adv. Catal.* **1993**, *39*, 221.
(18) Iglesia, E.; Soled, S. L.; Fiato, R. A. *J. Catal.* **1992**, *137*, 212.
(19) Iglesia, E. *Appl. Catal. A* **1997**, *161* (1−2), 59.
(20) Boudart, M. *Adv. Catal. Relat. Subj.* **1969**, *20*, 85.
(21) Bezemer, G. L.; Bitter, J. H.; Kuipers, H. P. C. E.; Oosterbeek, H.; Holewijn, J. E.; Xu, X.; Kapteijn, F.; van Dillen, A. J.; de Jong, K. P. *J. Am. Chem. Soc.* **2006**, *128* (12), 3956.
(22) Enache, D. I.; Rebours, B.; Roy-Auberger, M.; Revel, R. *J. Catal*. **2002**, *205*, 346.
(23) Van Berge, P. J.; Van De Loosdrecht, J.; Visagie, J. L. U.S. Patent 6,835,690, 2004.
(24) Ducreux, O.; Lynch, J.; Rebours, B.; Roy, M.; Chaumette, P. *Stud. Surf. Sci. Catal*. **1998**, *119*, 125.
(25) Steynberg, A. P.; Dry, M. E.; Davis, B. H.; Breman, B. B. *Stud. Surf. Sci. Catal*. **2004**, *152*, 64.
(26) Schulz, H. *Appl. Catal. A* **1999**, *186*, 3.
(27) Davis, B. H. *Top. Catal.* **2005**, *32*, 143.
(28) Sie, S. T.; Krishna, R. *Appl. Catal. A* **1999**, *186*, 55.
(29) Davis, B. H. *Catal. Today* **2002**, *71*, 249.
(30) Dry, M. E. *J. Chem. Technol. Biotechnol.* **2002**, *77*, 43.
(31) Dry, M. E. *Appl. Catal. A* **1999**, *189*, 185.
(32) Geerlings, J. J. C.; Wilson, J. H.; Kramer, G. J.; Kuipers, H. P. C. E.; Hoek, A.; Huisman, H. M. *Appl. Catal. A* **1999**, *186*, 27.
(33) Adesina, A. A.; Hudgins, R. R.; Silveston, P. L. *Catal. Today* **1995**, *25*, 127.
(34) Dry, M. E. *Catal. Today* **1990**, *6*, 183.
(35) Davis, B. H.; Iglesia, E. *Technology Development for Iron and Cobalt Fischer−Tropsch Catalysts*; Final Technical Report DE-F26−98FT40308, June 2002; http://www. fischer-tropsch. org/DOE/DOE_reports/40308/FC26-).
(36) Schulz, H. *Top. Catal*. **2003**, *26*, 73.
(37) Davis, B. H. *Fuel Process. Technol.* **2001**, *71*, 157.
(38) Overett, M. J.; Hill, R. O.; Moss, J. R. *Coord. Chem. Rev*. **2000**, *206−207*, 581.
(39) van der Laan, G. P.; Beenackers, A. A. C. M. *Catal. Rev.-Sci. Eng*. **1999**, *41*, 255.
(40) Morales, F.; Weckhuysen, B. M. *Catalysis (R. Soc. Chem.)* **2006**, *19*, 1.
(41) Lee, S.-Y.; Aris, R. *Catal. Rev. Sci. Eng.* **1985**, *27*, 207.
(42) Schwarz, J. A. *Catal. Today* **1992**, *15* (3−4), 395.
(43) Park, G. A. *Chem. Rev.* **1965**, *65*, 177.
(44) Ming, H.; Baker, B. G. *Appl. Catal. A* **1995**, *123*, 23.
(45) van Berge, P. J.; van de Loosdrecht, J.; Caricato, E. A.; Barrradas S. Patent WO99/42214.
(46) Zhu, Z.-Q.; Fang, K.-G.; Chen, J.-G.; Sun, Y.-H J. *Fuel Chem. Technol.* **2005**, *33* (4), 506.
(47) Zhang, Y.; Hanayama, K.; Tsubaki, N. *Catal. Commun*. **2006**, *7*, 251.
(48) Zhang, J.; Chen, J.; Ren, J.; Sun, Y. *Appl. Catal. A* **2003**, *243*, 121.
(49) Barradas, S.; Caricato, E. A.; van Berge, P. J.; van de Loosdrecht, J. *Stud. Surf. Sci. Catal*. **2002**, *143*, 55.
(50) van de Loosdrecht, J.; Barradas, S.; Caricato, E. A.; Ngwenya, N. G.; Nkwanyana, P. S.; Rawat, M. A. S.; Sigwebela, B. H.; van Berge, P. J.; Visagie, J. L. *Top. Catal*. **2003**, *26*, 121.
(51) van Berge, P. A.; van de Loosdrecht, J.; Caricato, E. A.; Barradas, S.; Sigwebela, B. H. U.S. Patent 6455462 B2, 2002.
(52) Bailey, D. C.; Langer, S. H. *Chem. Rev.* **1981**, *81*, 109.
(53) Lapidus, A. L.; Ihm, S.-K.; Krylova, A. Yu.; Kondrat'ev, L. T.; Minachev, Kh. M. *Russ. Solid Fuel Chem*. **1983**, *17*, 1.
(54) Yermakov, Y. I. *J. Mol. Catal*. **1983**, *21*, 35.
(55) Roeper, M.; Hemmerich, R.; Keim, W. *German Chem. Eng*. **1984**, *7*, 329.
(56) Nakamura, R.; Oomura, A.; Echigoya, E. *Chem. Lett*. **1982**, 1463.
(57) Nakamura, R.; Okada, N.; Oomura, A.; Echigoya, E. *Chem. Lett*. **1984**, 119
(58) Iwasawa, Y.; Yamada, M.; Sato, Y.; Kuroda, H. *J. Mol. Catal*. **1984**, *23*, 65.
(59) Armstrong, R. S.; Bell, T.; Chaffee, A. L.; Chin, V. W. L.; Loeh, H. J.; Lucchese, A. B. J.; Masters, A. F.; Williams, M. A. *Appl. Catal*. **1989**, *47*, 243.
(60) Niemelä, M. K.; Krause, A. O. I.; Vaara, T.; Kiviaho, J. J.; Reinikainen, M. K. O. *Appl. Catal. A* **1996**, *147*, 325.
(61) Kiviaho, J.; Reinikainen, M.; Niemelä, M. K.; Kataja, K.; Jääskeläinen, S. *J. Mol. Catal. A* **1996**, *106*, 187.
(62) Withers, H. P., Jr.; Eliezer, K. F.; Mitchell, J. W. *Ind. Eng. Chem. Res.* **1990**, *29*, 1807.
(63) Johnson, B. G.; Rameswaran, M.; Patil, M. D.; Muralidhar, G.; Bartholomew, C. H. *Catal. Today* **1989**, *6*, 81.
(64) Lee, D.-K.; Ihm, S.-K. *Appl. Catal.* **1987**, *32*, 85.
(65) Bergmeister, J. J.; Hanson, B. E. *Organometallics* **1989**, *8* (2), 283.
(66) Schweyer, F.; Braunstein, P.; Estournès, C.; Guille, J.; Kessler, H.; Paillaud, J.-L.; Rosé, J. *Chem. Commun.* **2000**, 1271.
(67) Huang, L.; Xu, Y. *Catal. Lett.* **1998**, *53*, 177.
(68) Huang, L. *J. Mol. Catal. A* **1997**, *125*, 47.
(69) Huang, L. *J. Mol. Catal. A* **1996**, *112*, 69.
(70) Kiviaho, J.; Niemelä, M. K.; Morioka, Y.; Kataja, K. *Appl. Catal. A* **1996**, *144*, 93.
(71) Khomenko, T. I.; Kadushin, A. A.; Khandozhko, V. N.; Kolobova, N. E.; Davydova, S. L. *Kinet. Catal*. **1989**, *29*, 853.
(72) Duvenhage, D. J.; Coville, N. J. *J. Mol. Catal. A* **2005**, *235*, 230.
(73) Khassin, A. A.; Yurieva, T. M.; Kaichev, V. V.; Bukhtiyarov, V. I.; Budneva, A. A.; Paukshtis, E. A.; Parmon, V. N. *J. Mol. Catal. A* **2001**, *175*, 189.
(74) Khassin, A. A.; Anufrienko, V. F.; Ikorskii, V. N.; Plyasova, L. M.; Kustova, G. N.; Larina, T. V.; Molina, I. Yu.; Parmon, V. N. *Phys. Chem. Chem. Phys.* **2002**, *4*, 4236.
(75) Khassin, A. A.; Yurieva, T. M.; Kustova, G. N.; Itenberg, I. S.; Demeshkina, M. P.; Krieger, T. A.; Plyasova, L. M.; Chermashentseva, G. K.; Parmon, V. N. *J. Mol. Catal. A* **2001**, *168*, 193.
(76) Khassin, A. A.; Yurieva, T. M.; Kustova, G. N.; Plyasova, L. M.; Itenberg, I. S.; Demeshkina, M. P.; Chermashentseva, G. K.; Anufrienko, V. F.; Zaikovskii, V. I.; Larina, T. V.; Molina, I. Y.; Parmon, V. N. *J. Mol. Catal. A* **2001**, *168*, 209.
(77) Chen, J. G.; Sun, Y. H. *Stud. Surf. Sci. Catal*. **2004**, *147*, 277.
(78) Pakhomov, N. A.; Buyanov, R. A. *Kinet. Catal*. **2005**, *46*, 669.
(79) Burattin, P.; Che, M.; Louis, C. *J. Phys. Chem. B* **1999**, *103*, 6171.
(80) Burattin, P.; Che, M.; Louis, C. *J. Phys. Chem. B* **2000**, *104* (45), 10482.
(81) Geus, J. W. *Stud. Surf. Sci. Catal.* **1983**, *16*, 1.
(82) Geus, J. W.; van Dillen, J. In *Handbook of Heterogeneous Catalysis*; Ertl, G., Knozinger, H., Weitkamp, J., Eds.; Wiley-VCH: New York, 1997; Vol. 1, p 240.
(83) Burattin, P.; Che, M.; Louis, C. *J. Phys. Chem. B* **1998**, *102*, 2722.
(84) Burattin, P.; Che, M.; Louis, C. *J. Phys. Chem. B* **1997**, *101*, 7060.
(85) de Jong, K. P. *Stud. Surf. Sci. Catal.* **1991**, *63*, 19.
(86) van Der Grift, C. J. G.; Elberse, P. A.; Mulder, A.; Geus, J. W. *Appl. Catal.* **1990**, *59*, 275.
(87) Wielers, A. F. H.; Zwolsman, G. J.; van der Grift, C. J. G.; Geus, J. W. *Appl. Catal.* **1985**, *19* (1), 187.
(88) van Stiphout, P. C. M.; Stobbe, D. E.; Scheur, V. D.; Geus, J. W. *Appl. Catal*. **1988**, *40*, 219.
(89) Nares, R.; Ramírez, J.; Gutiérrez-Alejandre, A.; Louis, C.; Klimova, T. *J. Phys. Chem. B* **2002**, *106*, 13287.
(90) Nares, R.; Ramirez, J.; Gutiérrez-Alejandre, A.; Cuevas, R.; Louis, C.; Klimova, T. *Stud. Surf. Sci. Catal.* **2002**, *143*, 537.
(91) Gómez-Reynoso, R.; Ramírez, J.; Nares, R.; Luna, R.; Murrieta, F. *Catal. Today* **2005**, *926*, *107−108*.
(92) Ochoa-Fernández, E.; Chen, D.; Yu, Z.; Tøtdal, B.; Rønning, M.; Holmen, A. *Catal. Today* **2005**, *45*, *102−103*.
(93) Bitter, J. H.; van Der Lee, M. K.; Slotboom, A. G. T.; van Dillen, A. J.; De Jong, K. P. *Catal. Lett.* **2003**, *89*, 139.
(94) Keane, M. A.; Park, C.; Menini, C. *Catal. Lett.* **2003**, *88* (1−2), 89.
(95) van Der Lee, M. K.; van Jos Dillen, A.; Bitter, J. H.; De Jong, K. P. *J. Am. Chem. Soc*. **2005**, *127*, 13573.
(96) Bezemer, G. L.; Radstake, P. B.; Koot, V.; van Dillen, A. J.; Geus, J. W.; De Jong, K. P. *J. Catal.* **2006**, *237* (2), 291.
(97) Lok, C. M. *Stud. Surf. Sci. Catal.* **2004**, *147*, 283.
(98) Lok, M. C.; Kelly, G. J.; Gray, G. U.S. Patent 6,927,190 B2.
(99) Lok, C. M.; Bailey, S. Gray, G. U.S. Patent 6,534,436 B2.
(100) Okabe, K.; Li, X.; Wei, M.; Arakawa, H. *Catal. Today* **2004**, *89*, 431.
(101) Dunn, B. C.; Covington, D. J.; Cole, P.; Pugmire, R. J.; Meuzelaar, H. L. C.; Ernst, R. D.; Heider, E. C.; Dutta, P. *Energy Fuels* **2004**, *18* (5), 1519.
(102) Zhang, Y.; Yoneyama, Y.; Fujimoto, K.; Tsubaki, N. *Top. Catal*. **2004**, *26*, 129.
(103) Bianchi, C. L.; Martini, F.; Moggi, P. *Catal. Lett.* **2004**, *76* (1−2), 65.
(104) Hench, I. L.; West, J. K. *Chem. Res*. **1990**, *90*, 33.
(105) Ro, J. C.; Chung, I. J. *J. Non-Cryst. Solids* **1991**, *130*, 8.

(106) Okabe, K.; Sayama, K.; Matsubayashi, M.; Shimomura, K.; Arakawa, H. *Bull. Chem. Soc. Jpn.* **1992**, *65*, 2520.
(107) Moggi, P.; Predieri, G.; Di Silvestri, F.; Ferretti, A. *Appl. Catal. A* **1999**, *182*, 257.
(108) Ernst, B.; Bensaddik, A.; Hilaire, L.; Chaumette, P.; Kiennemann, A. *Catal. Today* **1998**, *39* (4), 329.
(109) Dunn, B. C.; Cole, P.; Covington, D.; Webster, M. C.; Pugmire, R. J.; Ernst, R. D.; Eyring, E. M.; Shah, N.; Huffman, G. P. *Appl. Catal. A* **2005**, *278*, 233.
(110) Baratti, R.; Feckova, V.; Morbidelli, M.; Varma, A. *Ind. Eng. Chem. Res.* **1997**, *36*, 3416.
(111) Melis, S.; Varma, A.; Pereira, C. J. *Chem. Eng. Sci*. **1997**, *52*, 165.
(112) L.; Aravind, R.; Zawada, R. J. X.; Szegner, J.; Cao, G.; Varma, A. *Chem. Eng. Sci.* **1994**, *49*, 4823.
(113) Wu, H.; Brunovska, A.; Morbidelli, M.; Varma, A. *Chem. Eng. Sci*. **1990**, *45*, 1855.
(114) Gavriilidis, A.; Varma, A.; Morbidelli, M. *Catal. Rev.-Sci. Eng*. **1993**, *35*, 399.
(115) Post, M. F. M.; Hoog, A. C.; Minderhoud, J. K.; Sie, S. T. *AIChE J.l* **1989**, *35*, 1107.
(116) Neimark, A. V.; Kheifez, L. I.; Fenelonov, V. B. *Ind. Eng. Chem.: Prod. Res. Dev.* **1981**, *20*, 439.
(117) Lee, S.-Y.; Aris, R. *Catal. Rev.-Sci Eng.* **1985**, *27*, 207.
(118) Hollewand, M. P.; Gladden, L. F. *Magn. Reson. Imaging* **1994**, *12*, 291.
(119) Kowalski, S. J. *Chem. Eng. Sci.* **2000**, *55*, 1289.
(120) Koptyug, I. V.; Kabanikhin, S. I.; Iskakov, K. T.; Fenelonov, V. B.; Khitrina, L. Yu.; Sagdeev, R. Z.; Parmon, V. N. *Chem. Eng. Sci*. **2000**, *55*, 1559.
(121) Kotter, N.; Riekert, L. *Stud. Surf. Sci. Catal*. **1978**, *3*, 51.
(122) van Dillen, A. J.; Terörde, R. J. A. M.; Lensveld, D. J.; Geus, J. W.; De Jong, K. P. *J. Catal*. **2003**, *216*, 257.
(123) Ertl, G.; Knözinger, H.; Weitkamp, J. *Preparation of solid catalysts*; Wiley-VCH: Weinheim, Germany, 1999.
(124) Maatman, R. W. *Ind. Eng. Chem.* **1959**, *51*, 913.
(125) Peluso, E.; Galarraga, C.; de Lasa, H. *Chem. Eng. Sci*. **2001**, *56*, 1239.
(126) Galarraga, C.; Peluso, E.; de Lasa, H. *Stud. Surf. Sci*. *Catal*. **2000**, *130*, 395.
(127) Galarraga, C.; Peluso, E.; de Lasa, H. *Chem. Eng. J.* **2001**, *82*, 13.
(128) Zhuang, Y. Q.; Claeys, M.; van Steen, E. *Appl. Catal. A* **2006**, *301*, 138.
(129) Iglesia, E.; Soled, S. L.; Baumgartner, J. E.; Reyes, S. C. *J. Catal.* **1995**, *153*, 108.
(130) Kapteijn, F.; Nijhuis, T. A.; Heiszwolf, J. J.; Moulijn, J. A. *Catal. Today* **2001**, *66*, 133.
(131) Kapteijn, F.; Heiszwolf, J. J.; Nijhuis, T. A.; Moulijn, J. A. *Cattech* **1999**, *3*, 24.
(132) Pérez-Cadenas, A. F.; Zieverink, M. M. P.; Kapteijn, F.; Moulijn, J. A. *Catal. Today* **2005**, *105*, 623.
(133) Hilmen, A.-M.; Bergene, E.; Lindvåg, O. A.; Schanke, D.; Eri, S.; Holmen, A. *Catal. Today* **2005**, *105*, 357.
(134) De Deugd, R. M.; Kapteijn, F.; Moulijn, J. A. *Catal. Today* **2003**, *495*, 79−80.
(135) Hilmen, A.-M.; Bergene, E.; Lindvåg, O. A.; Schanke, D.; Eri, S.; Holmen, A. *Catal. Today* **2001**, *69*, 227.
(136) De Deugd, R. M.; Chougule, R.; Kreutzer, M. T.; Meeuse, F. M.; Grievink, J.; Kapteijn, F.; Moulijn, J. A. *Chem. Eng. Sci.* **2003**, *58*, 583.
(137) Nijhuis, T. A.; Beers, A. E. W.; Vergunst, Th.; Hoek, I.; Kapteijn, F.; Moulijn J. A. *Catal. Rev.-Sci. Eng.* **2001**, *43*, 345.
(138) Kapteijn, F.; De Deugd, R. M.; Moulijn, J. A. *Catal. Today* **2005**, *105*, 350.
(139) Hilmen, A. M.; Bergene, E.; Lindvag, O. A.; Schanke, D.; Eri, S.; Holmen, A. *Stud. Surf. Sci. Catal.* **2000**, *130*, 1163.
(140) Schanke, D.; Bergene, E.; Holmen, A. Patent WO/38147, 1998.
(141) Roucoux, A.; Schulz, J.; Patin, H. *Chem. Rev.* **2002**, *102*, 3757.
(142) Turkevich, J.; Kim, G. *Science* **1970**, *169*, 873.
(143) Reetz, M. T.; Quaiser, S. A. *Angew. Chem., Int. Ed. Engl*. **1995**, *34*, 2240.
(144) Xu, Z.; Xiao, F.-S.; Purnell, S. K.; Alexeev, O.; Kawi, S.; Deutsch, S. E.; Gates, B. C. *Nature* **1994**, *372*, 346.
(145) Gates, B. C. *Chem. Rev.* **1995**, *95*, 511.
(146) Yu, W.; Liu, M.; Liu, H.; An, X.; Liu, Z.; Ma, X. *J. Mol. Catal. A* **1999**, *142*, 161.
(147) Cartenuto, G.; Pasquini, L.; Milella, E.; Pentimalli, M.; Lamanna, R.; Nicolas, L. *Eur. Phys. J. B* **2003**, *31*, 545.
(148) Green, M.; O'Brien, P. *Chem. Commun*. **2001**, 1912.
(149) Gotosh, Y.; Igarashi, R.; Ohkoshi, Y.; Nagura, M.; Akamatsu, K.; Deki, S. *J. Mater. Chem*. **2000**, *10*, 2548.
(150) Rong, M. Z.; Zhang, M. Q.; Wang, H. B.; Zeng, H. M. *J. Polym. Sci. B* **2003**, *41*, 1070.
(151) Wu, N.; Fu, L.; Su, M.; Aslam, M.; Wong, K. C.; Dravid, V. P *Nano Lett.* **2004**, *4* (2), 383.
(152) Sun, S.; Murray, C. B. *J. Appl. Phys*. **1999**, *85*, 4325.
(153) Hyeon, T. *Chem. Commun.* **2003**, 927.
(154) Qiu, J.; Zhang, H.; Liang, C.; Li, J.; Zhao, Z. *Chem. Eur. J.* **2006**, *12*, 2147.
(155) Yu, W.; Liu, M.; Liu, H.; An, X.; Liu, Z.; Ma, X. *J. Mol. Catal. A: Chem.* **1999**, *142*, 201.
(156) Yu, W.; Liu, H.; An, X.; Ma, X.; Liu, Z.; Qiang, L. *J. Mol. Catal. A: Chem.* **1999**, *147*, 73.
(157) Wang, Y.; Liu, H.; Jiang, Y. Y. *J. Chem. Soc., Chem. Commun.* **1989**, 1878.
(158) Wang, Y.; Liu, H. *Polym. Bull.* **1991**, *25*, 139.
(159) Wang, Y.; Wu, H.; Zhang, Q.; Tang, Q. *Microporous Mesoporous Mater*. **2005**, *86*, 38.
(160) Tang, Q.; Zhang, Q.; Wang, P.; Wang, Y.; Wan, H. *Chem. Mater*. **2004**, *16*, 1967.
(161) Tang, Q.; Wang, Y.; Wang, P.; Zhang, Q.; Wan, H. *Stud. Surf. Sci. Catal*. **2004**, *147*, 325.
(162) Chu, W.; Khodakov, A. Y. Manuscript in preparation, 2006.
(163) Capek, I. *Adv. Colloid Interface Sci.* **2004**, *110*, 49.
(164) Eastoe, J.; Warne, B. *Curr. Opin. Colloid Interface Sci*. **1996**, *1*, 800.
(165) Pileni, M. P. *Langmuir* **2001**, *17*, 7476.
(166) Liu, W.; Zhong, W.; Wu, X.; Tang, N.; Du, Y. *J. Cryst. Growth* **2005**, *284*, 446.
(167) Sun, G.; Cao, M.; Wang, Y.; Hu, C.; Ren, L.; Huang, K. *Chem. Commun.* **2005**, 1740.
(168) Fletcher, P. D. I.; Howe, A. M.; Robinson, B. H. *J. Chem. Soc., Faraday Trans. 1* **1987**, *83* (4), 985.
(169) Chen, J. P.; Lee, K. M.; Sorensen, C. M.; Klabunde, K. J.; Hadjipanayis, G. C. *J. Appl. Phys.* **1994**, *75* (10), 5876.
(170) Ralston, D. H.; Klabunde, K. J. *Appl. Catal*. **1982**, *3*, 13.
(171) Klabunde, K. J.; Imizu, Y. *J. Am. Chem. Soc.* **1984**, *106*, 2721.
(172) Kanai, H.; Tan, B. J.; Klabunde, K. J. *Langmuir* **1986**, *2*, 760.
(173) Tan, B. J.; Klabunde, K. J.; Sherwood, P. M. A. *J. Am. Chem. Soc.* **1991**, *113*, 855.
(174) Tan, B. J.; Klabunde, K. J.; Tanaka, T.; Kanai, H.; Yoshida, S. *J Am. Chem. Soc.* **1988**, *110*, 5951.
(175) Dittmar, A.; Kosslick, H.; Muller, J.-P.; Pohl, M.-M. *Surf. Coatings Technol.* **2004**, *182*, 35.
(176) Baerns, M.; Termath, S.; Reiche, M. In *Advanced Catalysts and Nanostructured Materials*; Moser, W. R., Ed.; San Diego, 1996; Chapter 18, p 479.
(177) Kurhinen, M.; Pakkanen, T. A. *Langmuir* **2000**, *16*, 2658.
(178) Rhee, H. S.; Ahn, B. T. *J. Electrochem. Soc.* **1999**, *146*, 2720.
(179) Londergan, A. R.; Nuesca, G.; Goldberg, C.; Peterson, G.; Kaloyeros, A. E.; Arkles, B.; Sullivan, J. J. *J. Electrochem. Soc.* **2001**, *148*, C21.
(180) Gross, M. E.; Kranz, K. S.; Brasen, D.; Luftman, H. *J. Vac. Sci. Technol*. **1998**, *B6*, 1548.
(181) De la Rosa, M. J.; Lu, T.-M.; Kumar, A.; Bakhru, H. In *Advanced Interconnects and Contacts*; Edelstein, D. C., Kikkawa, T., Ozturk, M., Tu, K.-N., Weitzman, E., Eds.; San Francisco, April 5−7, 1999; *Mater. Res. Soc. Symp. Proc.* **1999**, *564*, 559.
(182) Ko, Y. K.; Park, D. S.; Seo, B. S.; Yang, H. J.; Shin, H. J.; Kim, J. Y.; Lee, J. H.; Lee, W. H.; Reucroft, P. J.; Lee, J. G. *Mater. Chem. Phys*. **2003**, *80*, 560.
(183) Boyd, P.; Ketchum, D. R.; Deng, H.; Shore, S. G. *Chem. Mater*. **1997**, *9*, 1154.
(184) Dong, X. L.; Choi, C. J.; Kim, B. K. *Scr. Mater*. **2002**, *47*, 857.
(185) Backman, L. B.; Rautiainen, A.; Lindblad, M.; Krause, A. O. I. *Appl. Catal. A* **2000**, *191*, 55.
(186) Backman, L. B.; Rautiainen, A.; Lindblad, M.; Jylhä, O.; Krause, A. O. I. *Appl. Catal. A* **2001**, *208*, 223.
(187) Maruyama, T. *Jpn. J. Appl. Phys. (Part 2*) **1997**, *36*, L705.
(188) Puurunen, R. L.; Zeelie, T. A.; Krause, A. O. I. *Catal. Lett.* **2002**, *83*, 27.
(189) Maruyama, T.; Nakai, T. *Appl. Phys. Lett. 1991, 59*, 1433.
(190) Choi, H.; Park, S. *Chem. Mater*. **2003**, *15*, 3121.
(191) Suvanto, S.; Pakkanen, T. A. *J. Mol. Catal. A: Chem.* **1997**, *125*, 91.
(192) Suvanto, S.; Pakkanen, T. A.; Backman, L. *Appl. Catal.* **1999**, *177*, 25.
(193) Hukkamäki, J.; Suvanto, S.; Suvanto, M.; Pakkanen, T. T. *Langmuir* **2004**, *20*, 10288.
(194) Suvanto, S.; Hukkamäki, J.; Pakkanen, T. T.; Pakkanen, T. A. *Langmuir* **2000**, *16* (9), 4109.
(195) Backman, L. B.; Rautiainen, A.; Lindblad, M.; Jylhä, O.; Krause, A. O. I. *Appl. Catal. A* **2001**, *208*, 223.
(196) Rautiainen, A.; Lindblad, M.; Backman, L. B.; Puurunen, R. L. *Phys. Chem. Chem. Phys.* **2002**, *4*, 2466.

(197) Liu, C.-J.; Vissokov, G. P.; Jang, B. W.-L. *Catal. Today* **2002**, *72* (3−4), 173.
(198) Kizling, M. B.; Jaras, S. G. *Appl. Catal. A* **1996**, *147*, 1.
(199) Dalai, A. K.; Bakhshi, N. N.; Esmail, M. N. *Ind. Eng. Chem. Res.* **1992**, *31*, 1449.
(200) Dalai, A. K.; Bakhshi, N. N.; Esmail, M. N. *Fuel Process. Technol.* **1997**, *51*, 219.
(201) Kapoor, A.; Goyal, S. K.; Bakhshi, N. N. *Can. J. Chem. Eng*. **1986**, *64*, 792.
(202) Burch, R. *Acc. Chem. Res*. **1982**, *15*, 24.
(203) Ishihara, T.; Eguchi, K.; Arai, H. *Appl. Catal*. **1987**, *30*, 225.
(204) Zhang, Y.; Chu, W.; Cao, W.; Luo, C.; Wen, X.; Zhou, K. *Plasma Chem. Plasma Process.* **2000**, *20* (1), 137.
(205) Chen, M. H.; Chu, W.; Dai, X. Y.; Zhang, X. W. *Catal. Today* **2004**, *89* (1−2), 201.
(206) Chen, M.; Chu, W.; Zhang, X.; Cuihua, X. *Chin. J. Catal*. **2003**, *24* (10), 775.
(207) Batley, G. E.; Ekstrom, A.; Johnson, D. A. *J. Catal.* **1975**, *34*, 368.
(208) van't Blik, H. F. J.; Koningsberger, D. C.; Prins, R. *J. Catal*. **1986**, *97*, 210.
(209) Takeuchi, K.; Matsuzaki, T.; Arakawa, H.; Hanaoka, T.; Sugi, Y. *Appl. Catal.* **1989**, *48*, 149.
(210) Takeuchi, K.; Matsuzaki, T.; Arakawa, H.; Sugi, Y. *Appl. Catal.* **1985**, *18*, 325.
(211) Reinikainen, M.; Niemelä, M. K.; Kakuta, N.; Suhonen, S. *Appl. Catal. A* **1998**, *174*, 61.
(212) Girardon, J.-S.; Constant-Griboval, A.; Gengembre, L.; Chernavskii, P. A.; Khodakov, A. Y. *Catal. Today* **2005**, *106* (1−4), 161.
(213) Guczi, L.; Bazin, D.; Kovacs, I.; Borko, L.; Schay, Z.; Lynch, J.; Parent, P.; Lafon, C.; Stefler, G.; Koppany, Z.; Sajo, I. *Top. Catal.* **2002**, *20*, 129.
(214) Jacobs, G.; Das, T. K.; Patterson, P. M.; Li, J.; Sanchez, L.; Davis, B. H. *Appl. Catal. A* **2003**, *247*, 335.
(215) Kogelbauer, A.; Goodwin, J. G., Jr.; Oukaci, R. *J. Catal*. **1996**, *160*, 125.
(216) Jacobs, G.; Chaney, J. A.; Patterson, P. M.; Das, T. K.; Maillot, J. C.; Davis, B. H. *J. Synchrotron Radiat.* **2004**, *11* (5), 414.
(217) Tsubaki, N.; Sun, S.; Fujimoto, K. *J. Catal.* **2001**, *199*, 236.
(218) Qiu, X.; Tsubaki, N.; Sun, S.; Fujimoto, K. *Fuel* **2002**, *81*, 1625.
(219) Hilmen, A. M.; Schanke, D.; Holmen, A. *Catal. Lett.* **1996**, *38*, 143.
(220) Hilmen, A. M.; Schanke, D.; Hanssen, K. F.; Holmen, A. *Appl. Catal. A* **1999**, *186*, 169.
(221) Jacobs, G.; Das, T. K.; Zhang, Y.; Li, J.; Racoillet, G.; Davis, B. H. *Appl. Catal. A* **2002**, *233*, 263.
(222) Dees, M. J.; Ponec, V. *J. Catal.* **1989**, *119*, 376.
(223) Guczi, L. *Catal. Today* **2005**, *101*, 53.
(224) Bazin, D.; Borkó, L.; Koppány, Zs.; Kovács, I.; Stefler, G.; Sajó, L. I.; Schay, Z.; Guczi, L. *Catal. Lett.* **2002**, *84*, 169.
(225) Rønning, M.; Nicholson, D. G.; Holmen, A. *Catal. Lett.* **2001**, *72*, 141.
(226) Khan, N. A.; Murillo, L. E.; Shu, Y.; Chen, J. G. *Catal. Lett.* **2005**, *105*, 233.
(227) Noronha, F. B.; Schmal, M.; Fréty, R.; Bergeret, G.; Moraweck, B. *J. Catal.* **1999**, *186*, 20.
(228) Mierzwa, B.; Kaszkur, Z.; Moraweck, B.; Pielaszek, J. *J. Alloys Compd.* **1999**, *286*, 93.
(229) Schanke, D.; Vada, S.; Blekkan, E. A.; Hilmen, A. M.; Hoff, A.; Holmen, A. *J. Catal.* **1995**, *156*, 85.
(230) Iglesia, E.; Soled, S. L.; Fiato, R.; Via, G. H. *J. Catal.* **1993**, *143*, 345.
(231) Jongsomjit, B.; Panpranot, J.; Goodwin, J. G., Jr. *J. Catal.* **2001**, *204* (1), 98.
(232) ; Mizukami, F. *J. Mol. Catal. A* **1999**, *141*, 177.
(233) Bardi, U.; Beard, B. C.; Roos, P. N. *J. Catal.* **1990**, *124*, 22.
(234) Xu, D.; Li, W.; Duan, H.; Ge, Q.; Xu, H. *Catal. Lett.* **1995**, *102*, 229.
(235) Ma, W.-P.; Ding, Y.-J.; Lin, L.-W. *Ind. Eng. Chem. Res.* **2004**, *43* (10), 2391.
(236) Oukaci, R.; Sigleton, A. H.; Goodwin J. G., Jr. *Appl. Catal.* A **1999**, *186*, 129.
(237) Post, M. F. M.; Sie, S. T. B. Eur. Patent EP 0167 215 A2, 1985.
(238) Feller, A.; Claeys, M.; van Steen, E. *J. Catal.* **1999**, *185*, 120.
(239) Moradi, G. R.; Basir, M. M.; Taeb, A.; Kiennemann, A. *Catal. Commu.* **2003**, *4*, 27.
(240) Yin, D.; Li, W.; Yang, W.; Xiang, H.; Sun, Y.; Zhong, B.; Peng, S. *Microporous Mesoporous Mater.* **2001**, *47*, 15.
(241) Ali, S.; Chen, B.; Goodwin, J. G., Jr. *J. Catal*. **1995**, *157*, 35.
(242) Wei, M.; Okabe, K.; Arakawa, H.; Teraoka, Y. *Catal. Commun.* **2004**, *5*, 597.
(243) Rohr, F.; Lindvåg, O. A.; Holmen, A.; Blekkan, E. A. *Catal. Today* **2000**, *58*, 247.
(244) Jongsomjit, B.; Panpranot, J.; Goodwin, J. G., Jr. *J. Catal.* **2003**, *215*, 66.
(245) Xiong, H.; Zhang, Y.; Liew, K.; Li, J. *J. Mol. Catal. A* **2005**, *231*, 145.
(246) Wei, D.; Goodwin, J. G., Jr.; Oukaci, R.; Singleton, A. H. *Appl. Catal. A* **2001**, *210*, 137.
(247) Ledford, J. S.; Houalla, M.; Proctor, A.; Hercules, D. M.; Petrakis, L. *J. Phys. Chem.* **1989**, *93*, 6770.
(248) Adachi, M.; Yoshii, K.; Han, Y. Z.; Fujimoto, K. *Bull. Chem. Soc. Jpn.* **1996**, *69*, 1509.
(249) Haddad, G.; Chen, B.; Goodwin, J. G., Jr. *J. Catal*. **1996**, *161*, 274.
(250) Haddad, G. J.; Goodwin J. G. *J. Catal*. **1995**, *157*, 25.
(251) Haddad, G.; Chen, B.; Goodwin, J. G., Jr. *J. Catal.* **1996**, *160*, 43.
(252) Colley, S.; Copperthwaite, R. G.; Hutchings, G. J.; van der Riet, M. *Ind. Eng. Chem. Res*. **1988**, 27, 1339.
(253) Morales, F.; de Groot, F. M. F.; Glatzel, P.; Kleimenov, E.; Bluhm, H.; Havecker, M.; Knop-Gericke, A.; Weckhuysen, B. M. *J. Phys. Chem. B* **2004**, *108*, 16201.
(254) Morales, F.; de Groot, F. M. F.; Gijzeman, O. L. J.; Mens, A.; Stephan, O.; Weckhuysen, B. M. *J. Catal.* **2005**, *230*, 301.
(255) Riedel, T.; Cleys, M.; Schulz, G.; Schaub, G.; Nam, S.; Jun, K.; Choi, M.; Kishan, G.; Lee, K. *Appl. Catal. A* **1999**, *186*, 201.
(256) Keyser, M. J.; Everson, R. C.; Espinoza, R. L. *Appl. Catal. A* **1998**, *171*, 99.
(257) Zhang, J.-L.; Ren, J.; Chen, J.-G.; Sun, Y.-H. *Acta Phys.-Chim. Sin.* **2002**, *18* (3), 260.
(258) Morales Cano, F.; Gijzeman, O. L. J.; De Groot, F. M. F.; Weckhuysen, B. M. *Stud. Surf. Sci. Catal.* **2004**, *147*, 271.
(259) Morales, F.; Grandjean, D.; De Groot, F. M. F.; Stephan, O.; Weckhuysen, B. M. *Phys. Chem. Chem. Phys.* **2005**, *7*, 568.
(260) Bezemer, G. L.; Radstake, P. B.; Falke, U.; Oosterbeek, H.; Kuipers, H. P. C. E.; van Dillen, A. J.; De Jong, K. P. *J. Catal.* **2006**, *237*, 152.
(261) Bezemer, G. L.; Falke, U.; van Dillen, A. J.; De Jong, K. P. *Chem. Commun.* **2005**, 731.
(262) Martínez, A.; Lóipez, C.; Márquez, F.; Díaz, I. *J. Catal*. **2003**, *220*, 486.
(263) Duvenhage, D. J.; Coville, N. J. *Catal. Lett.* **2005**, *104*, 129.
(264) Guerrero-Ruiz, A.; Sepulveda-Escribano, A.; Rodriguez-Ramos, I. *Appl. Catal. A* **1994**, *120*, 71.
(265) Ernst, B.; Hiliare, L.; Kiennemann, A. *Catal. Today* **1999**, *50*, 413.
(266) Wang, T.; Ding, Y.; Xiong, J.; Yan, L.; Zhu, H.; Lu, Y.; Lin, L. *Catal. Lett.* **2006**, *107*, 47.
(267) Huffman, G. P.; Shah, N.; Zhao, J.; Huggins, F. E.; Hoost, T. E.; Halvrsen, S.; Goowin, J. G., Jr. *J. Catal.* **1995**, *151*, 17.
(268) Huber, G. W.; Butala, S. J. M.; Lee, M. L.; Bartholomew, C. H. *Catal. Lett.* **2001**, *74*, 45.
(269) Zhang, Y.; Nagamori, S.; Hinchiranan, S.; Vitidsant, T.; Tsubaki, N. *Energy Fuels* **2006**, *20*, 417.
(270) Khodakov, A. Y.; Girardon, J.-S.; Griboval-Constant, A.; Lermontov, A. S.; Chernavskii, P. A. *Stud. Surf. Sci. Catal.* **2004**, *147*, 295.
(271) Girardon, J.-S.; Lermontov, A. S.; Gengembre, L.; Chernavskii, P. A.; Griboval-Constant, A.; Khodakov, A. Y. *J. Catal*. **2005**, *230*, 339.
(272) van Steen, E.; Clayes, M.; Dry, M. E.; van de Loosdrecht, J.; Vilkoen, E. L.; Visagie, J. L. *J. Phys. Chem. B* **2005**, *109*, 3575.
(273) van Berge, P. J.; van de Loosdrecht, J.; Barradas, S.; van der Kraan, A. M. *Catal. Today* **2000**, *58*, 321.
(274) Li, J.; Zhan, X.; Zhang, Y.; Jacobs, G.; Das, T.; Davis, B. H. *Appl. Catal. A* **2002**, *228*, 203.
(275) Krishnamoorthy, S.; Tu, M.; Ojeda, M. P.; Pinna, D.; Iglesia, E. *J. Catal.* **2002**, *211*, 422.
(276) Li, J.; Jacobs, G.; Das, T.; Zhang, Y.; Davis, B. H. *Appl. Catal. A* **2002**, *236* (1−2), 67.
(277) Minderhoud, J. K.; Post, M. F. M.; Sie, S. T.; Sudholter, E. J. R. U.S. Patent 4,628,133, 1986.
(278) Das, T. K.; Conner, W. A.; Li, J.; Jacobs, G.; Dry, M. E; Davis, B. H. *Energy Fuels* **2005**, *19*, 1430.
(279) Chen, J.-G.; Xiang, H.-W.; Gao, H.-Y. Sun, Y.-H. *React. Kinet. Catal. Lett.* **2001**, *73*, 169.
(280) Kogelbauer, A.; Weber, J. C.; Goodwin, J. G., Jr. *Catal. Lett.* **1995**, *34*, 259.
(281) Wang, W.-J. Chen, Y. W. *Appl. Catal.* **1991**, *77*, 223.
(282) van Steen, E.; Sewell, G. S.; Makhothe, R. A.; Micklethwaite, C.; Manstein, H.; de Lange, M.; O'Connor, C. T. *J. Catal.* **1996**, *162*, 220.
(283) Huber, G. W.; Guymon, C. G.; Conrad, T. L.; Stephenson, B. C.; Bartholomew, C. H. *Stud. Surf. Sci. Catal.* **2001**, *139*, 423.
(284) Khodakov, A.; Ducreux, O.; Lynch, J.; Rebours, B.; Chaumette, P. *Oil Gas Sci. Technol.* **1999**, *54* (4), 525.
(285) Okamoto, Y.; Nagata, K.; Adachi, T.; Imanaka, T.; Inamura, K. Takyu, T. *J. Phys. Chem.* **1991**, *95*, 310.
(286) Morimoto, N.; Tokonami, M.; Watanabe, M.; Koto, K. *Am. Mineral.* **1974**, *59*, 475.

(287) Llusar, M.; Forés, A.; Badenes, J. A.; Calbo, J. M.; Tena, A.; Monrós, G. *J. Eur. Ceram. Soc.* **2001**, *21*, 1121.
(288) Jaboński, J. M.; Wocyrz, M.; Krajczyk, L. *J. Catal.* **1998**, *173*, 530.
(289) Casado, P. G.; Rasines, I. *J. Solid State Chem.* **1984**, 52, 187.
(290) Chemlal, S.; Larbot, A.; Persin, M.; Sarrazin, J.; Sghyar, M.; Rafiq, M. *Mater. Res. Bull.* **2000**, *35*, 2515.
(291) Cho, W. S.; Kakihana, M. *J. Alloys Compd.* **1999**, *287*, 87.
(292) Zayat, M.; Levy, D. *Chem. Mater.* **2000**, *12*, 2763.
(293) Garcia Casado, P.; Rasines, I. *J. Solid State Chem.* **1984**, *52*, 187.
(294) Alarcon, J.; Escribano, P.; Marín, R. M. B. *Ceram. Trans. J.* **1985**, *84*, 170.
(295) Busca, G.; Lorenzelli, V.; Bolis, V. *Mater. Chem. Phys.* **1992**, *31*, 221.
(296) Angeletti, C.; Pepe, F.; Porta, P. *J. Chem. Soc., Faraday Trans. 1* **1977**, *73*, 1972.
(297) Bolt, P. H.; Habraken, F. H. P. M.; Geus, J. W. *J. Solid State Chem.* **1998**, *135*, 59.
(298) Arnoldy, P.; Moulijn, J. A. *J. Catal.* **1985**, *93*, 38.
(299) van de Loosdrecht, J.; van der Haar, M.; van der Kraan, A. M.; van Dillen, A. J.; Geus, J. W. *Appl. Catal. A* **1997**, *150*, 365.
(300) Zayat, M.; Levy, D. *J. Sol-Gel Sci. Technol.* **2005**, *25*, 201.
(301) Niemelä, M. K.; Backman, L.; Krause, A. O. I.; Vaara, T. *Appl. Catal. A* **1997**, *156*, 319.
(302) Johnson, B. G.; Bartholomew, C. H.; Goodman, D. W. *J. Catal.* **1991**, *128*, 231.
(303) Xiong, J.; Ding, Y.; Wang, T.; Yan, L.; Chen, W.; Zhu, H.; Lu, Y. *Catal. Lett.* **2005**, *102*, 265.
(304) Ishihara, T.; Egichi, K.; Arai, H. *J. Mol. Catal.* **1992**, *72*, 253.
(305) Griboval-Constant, A.; Khodakov, A. Y.; Bechara, R.; Zholobenko, V. L. *Stud. Surf. Sci. Catal.* **2002**, *144*, 609.
(306) Bessell, S. *Appl. Catal. A* **1993**, *96* (2), 253.
(307) Reuel, C. R.; Bartholomew, C. H. *J. Catal.* **1984**, *85*, 78.
(308) Ernst, B.; Libs, S.; Chaumette, P.; Kiennemann, A. *Appl. Catal. A.* **1999**, *186*, 145.
(309) Saib, A. M.; Claeys, M.; Steen, E. V. *Catal. Today* **2002**, *71*, 395.
(310) Song, D.; Li, J. *J. Mol. Catal. A* **2006**, *247* (1−2), 206.
(311) Chin, R. L.; Hercules, D. M. *J. Phys. Chem.* **1982**, *86*, 360.
(312) Barradas, S.; Caricato, E. A.; van Berge, P. J.; van de Loosdrecht, J. *Stud. Surf. Sci. Catal.* **2002**, *143*, 55.
(313) Zhang, Y.; Xiong, H.; Liew, K.; Li, J. *J. Mol. Catal. A.* **2005**, *237*, 172.
(314) Bechara, R.; Balloy, D.; Vanhove, D. *Appl. Catal.* **2001**, *207*, 343.
(315) Xiong, H.; Zhang, Y.; Wang, S.; Li, *J. Catal. Commun.* **2005**, 6, 512.
(316) Zhao, H. X.; Chen, J. G.; Sun, Y. H. *Chin. J. Catal.* **2003**, *12* (24), 933.
(317) Ryan, K. M.; Coleman, N. R. B.; Lyons, D. M.; Hanrahan, J. P.; Spalding, T. R.; Morris, M. A.; Steytler, D. C.; Heenan, R. K.; Holmes, J. D. *Langmuir* **2002**, *18*, 4996.
(318) Corma, A. *Chem. Rev.* **1997**, *87*, 2373.
(319) *Appl Catal. A: Special Issue* **2003**, *2*, 254.
(320) Khodakov, A. Y.; Griboval-Constant, A.; Bechara, R.; Zholobenko, V. L. *J. Catal.* **2002**, *206*, 230.
(321) Biz, S.; Occeli, M. L. *Catal. Rev-Sci. Eng.* **1998**, *40*, 329.
(322) Kresge, C. T.; Leonowicz, M. E.; Roth, W. J.; Vartuli, J. C.; Beck, J. S. *Nature* **1992**, *359*, 710.
(323) Zholobenko, V. L.; Evans, A.; Plant, D.; Holmes S. M. *Microporous Mesoporous Mater.* **2001**, *793*, 44−45.
(324) Beck, J. S.; Vartuli, J. C.; Roth, W. J.; Leonowicz, M. E.; Kresge, C. T.; Schmitt, K. D.; Chu, C. T.-W.; Olson, D. H.; Sheppard, E. W.; McCullen, S. B.; Higgins, J. B.; Schlenker, J. L. *J. Am. Chem. Soc.* **1992**, *114*, 10834.
(325) Chen, C.-Y.; Li, H.-X.; Davis, M. E. *Microporous Mater.* **1993**, *2*, 17.
(326) Holmes, S.; Zholobenko, V.; Thursfield, A.; Plaisted, R. J.; Candy, S. C.; Dwyer, J. *J. Chem. Soc., Faraday Trans.* **1998**, *94*, 2025.
(327) Zhao, D.; Feng, J.; Huo, Q.; Melosh, N.; Fredrickson, G. H.; Chmelka, B. F.; Stucky, G. D. *Science* **1998**, *279*, 548.
(328) Zhao, D.; Sun, J.; Li, Q.; Stucky, G. D. *Chem. Mater.* **2000**, *12*, 275.
(329) Zhao, D.; Huo, Q.; Feng, J.; Chmelka, B. F.; Stucky, G. D. *J. Am. Chem. Soc.* **1998**, *120*, 6024.
(330) Li, H.; Wang, S.; Ling, F.; Li, J. *J. Mol. Catal A* **2006**, *244*, 33.
(331) Panpranot, J.; Kaewgun, S.; Praserthdam, P. *React. Kinet. Catal. Lett.* **2005**, *85*, 299.
(332) Khodakov, A. Y.; Zholobenko, V. L.; Bechara, R.; Durand, D. *Microporous Mesoporous Mater.* **2005**, *79*, 29.
(333) Wei, M.; Okabe, K.; Arakawa, H.; Teraoka, Y. *New J. Chem.* **2003**, *27*, 928.
(334) Panpranot, J.; Goodwin, J. G., Jr.; Sayari, A. *Catal. Today* **2002**, *77*, 269.
(335) Wei, M.; Okabe, K.; Arakawa, H.; Teraoka, Y. *React. Kinet. Catal. Lett.* **2002**, *77*, 381.
(336) Panpranot, J.; Goodwin, J. G., Jr.; Sayari, A. *J. Catal.* **2002**, *211*, 530.
(337) Ohtsuka, Y.; Arai, T.; Takasaki, S.; Tsubouchi, N. *Energy Fuels* **2003**, *17*, 804.
(338) Ohtsuka, Y.; Takahashi, Y.; Noguchi, M.; Arai, T.; Takasaki, S.; Tsubouchi, N.; Wang, Y. *Catal. Today* **2004**, *89*, 419.
(339) Kim, D. J.; Dunn, B. C.; Cole, P.; Turpin, G.; Ernst, R. D.; Pugmire, R. J.; Kang, M.; Kim, J. M.; Eyring, E. M. *Chem. Commun.* **2005**, *11*, 1462.
(340) Iwasaki, T.; Reinikainen, M.; Onodera, Y.; Hayashi, H.; Ebina, T.; Nagase, T.; Torii, K.; Kataja, K.; Chatterjee, A. *Appl. Surf. Sci.* **1998**, 130−132, 845.
(341) Khodakov, A. Y.; Griboval-Constant, A.; Bechara, R.; Villain, F. *J. Phys. Chem B* **2001**, *105*, 9805.
(342) Khodakov, A. Y.; Bechara, R.; Griboval-Constant, A. *Stud. Surf. Sci. Catal.* **2002**, 142 B, 1133.
(343) Khodakov, A. Y.; Bechara, R.; Griboval-Constant, A. *Appl. Catal. A* **2003**, *254*, 273.
(344) Moreno-Castilla, C.; Carrasco-Marin, F. *J. Chem. Soc., Faraday Trans.* **1995**, *91*, 3519.
(345) Chen, A. A.; Kaminsky, M.; Geffroy, G. L.; Vannice, M. A. *J. Phys. Chem.* **1986**, *90*, 4810.
(346) Wang, T.; Ding, Y.-J.; Xiong, J.-M.; Chen, W.-M.; Pan, Z.-D.; Lu, Y.; Lin, L.-W. *Stud. Surf. Sci. Catal.* **2004**, *147*, 349.
(347) Shinoda, M.; Zhang, Y.; Yoneyama, Y.; Hasegawa, K.; Tsubaki, N. *Fuel Process. Technol.* **2004**, *86*, 73.
(348) Zhang, Y.; Koike, M.; Yang, R.; Hinchiranan, S.; Vitidsant, T.; Tsubaki, N. *Appl. Catal. A* **2005**, *292*, 252.
(349) Takahashi, R.; Sato, S.; Sodesawa, T.; Yabuki, M. *J. Catal.* **2001**, *200*, 197.
(350) Sun, S.; Fujimoto, K.; Zhang, Y.; Tsubaki, N. *Catal. Commun.* **2003**, *4* (8), 361.
(351) Zhang, Y.; Shinoda, M.; Tsubaki, N. *Catal. Today* **2004**, 93−95, 55.
(352) *AIChE J.* **2005**, *51*, 2068.
(353) Zhang, Y.; Koike, M.; Tsubaki, N. *Catal. Lett.* **2005**, *91*, 193.
(354) Zhang, Y.; Yoneyama, Y.; Fujimoto, K.; Tsubaki, N. *J. Chem. Eng. Jpn.* **2003**, *36*, 874.
(355) Cotton, A. L.; Wilkinson, G. *Advanced Inorganic Chemistry*, 2nd ed.; Interscience: New York, 1966; p 869.
(356) Grennwood, N. N.; Earnshaw, A. *Chemistry of the Elements*; Pergamon Press: Oxford, 1984; p 1313.
(357) Xu, R.; Zeng, H. C. *Langmuir* **2004**, *20*, 9780.
(358) He, T.; Chen, D.; Jiao, X.; Wang, Y.; Duan, Y. *Chem. Mater.* **2005**, *17*, 4023.
(359) Cheng, C.-S.; Serizawa, M.; Sakata, H.; Hirayama, T. *Mater. Chem. Phys.* **1998**, *53*, 225.
(360) Barreca, D.; Massignan, C.; Daolio, S.; Fabrizio, M.; Piccirillo, C.; Armelao, L.; Tondello, E. *Chem. Mater* **2001**, *13*, 588.
(361) Wood, D. L.; Remeika, J. P. *J. Chem. Phys.* **1967**, *46*, 3595.
(362) Noronha, F. B.; Perez, C. A.; Schmal, M.; Fréty, R. *Phys. Chem. Chem. Phys.* **1999**, *1*, 2861.
(363) Khodakov, A.; Lynch, J.; Bazin, D.; Rebours, B.; Zanier, N.; Moisson, B.; Chaumette, P. *J. Catal.* **1997**, *168*, 16.
(364) Lefez, B.; Nkeng, P.; Lopitaux, J.; Poillerat, G. *Mater. Res. Bull.* **1996**, *31*, 1263.
(365) Lin, H.-K.; Chiu, H.-C.; Tsai, H.-C.; Chien, S.-H.; Wang, C.-B. *Catal. Lett.* **2003**, 88 (3−4), 169.
(366) Spencer, C.; Schroeder, D. *Phys. Rev. B: Condens. Matter*, **1974**, *9*, 3658.
(367) Christoskova, St. G.; Stayonava, M.; Georgieva, M.; Mehandjiev, D. *Mater. Chem. Phys.* **1999**, *60*, 39.
(368) Shaheen, W. M.; Selim, M.; M. *Int. J. Inorg. Mater.* **2001**, *3*, 417.
(369) Zhao, H. X.; Chen, J. G.; Sun, Y.-H. *Stud. Surf. Sci Catal.* **2004**, *147*, 355.
(370) Heal, M. J.; Leisegang, E. C.; Torrington, R. G. *J. Catal.* **1978**, *51*, 314.
(371) Lapidus, A.; Krylova, A.; Kazanskii, V.; Borokov, V.; Zaitsev, A.; Rathousky, J.; Zukal, A.; Jancalkova, M. *Appl. Catal.* **1991**, *73*, 65.
(372) Rygh, L. E. S.; Ellestad, O. H.; Klæboe, P.; Nielsen, C. J. *Phys. Chem. Chem. Phys.* **2000**, *2*, 1835.
(373) Kazanskii, V. B.; Zaitsev, A. V.; Borokov Yu, V.; Lapidus, A. L. *Appl. Catal.* **1988**, *40*, 17.
(374) Kuznetsov, V. L.; Aleksandrov, M. N.; Bulgakova, L. N. *J. Mol. Catal.* **1989**, *55*, 146.
(375) Choi, J.-G.; Rhee, H.-K.; Moon, S. H. *Appl. Catal.* **1985**, *13*, 269.
(376) Davydov, A. A. *IR-spectroscopy in the Chemistry of Oxide Surfaces*: Nauka: Novosibirsk, 1984.
(377) Blyholder, G. *J. Phys. Chem.* **1964**, *68*, 2772.
(378) Kadinov, G.; Bonev, C.; Todorova, S.; Palazov, A. *J. Chem. Soc., Faraday Trans.* **1998**, *94*, 3027.
(379) Persson, B. N. J.; Ryberg, R. *Phys. Rev. B* **1981**, *24*, 6954.

(380) Mojet, B. L.; Miller, J. T.; Koningsberger, D. C. *J. Phys. Chem. B* **1999**, *103*, 2724.
(381) Fredriksen, G. R. Ph.D. Thesis, Univerisity of Trondheim, Norway 1993.
(382) Sato, K.; Inoue, Y.; Kojima, I.; Miyazaki, E.; Yasumori, I. *J. Chem. Soc., Faraday, Trans. I* **1984**, 80, 841.
(383) Jiang, M.; Koizumi, N.; Ozaki, T.; Yamada, M. *Appl. Catal. A* **2001**, *209*, 59.
(384) Fredriksen, G. R.; Blekkan, E. A.; Schanke, D.; Holmen, A. *Chem. Eng. Technol.* **1995**, *18*, 125.
(385) Fredriksen, G. R.; Blekkan, E. A.; Schanke, D.; Holmen, A. *Ber. Bunsen-Ges. Phys. Chem. Chem. Phys.* **1993**, *97*, 308.
(386) Jongsomjit, B.; Wongsalee, T.; Praserthdam, P. *Mater. Chem. Phys.* **2006**, *97*, 343.
(387) Madikizela, N. N.; Coville, N. J. *J. Mol. Catal. A* **2002**, *181*, 129.
(388) Shull, C. G. *Phys. Rev.* **1946**, *70*, 679.
(389) Paterson, A. L. *Phys. Rev.* **1939**, *56*, 972.
(390) Waren, B. E.; Avrebach, B. L. *J. Appl. Phys.* **1952**, *23*, 497.
(391) Wiliamson, G. K.; Hall, W. H. *Acta. Metal.* **1953**, *1*, 22.
(392) van Berkum, J. G. M.; Delhez, R.; de Keuser, T. H.; Mittemeijer, E. J. *Acta. Crystallogr.* **1996**, *A52*, 730.
(393) Ungár, T.; Borbély, A. *Appl. Phys. Lett.* **1996**, *69* (21), 3173.
(394) Scardi, P.; Leoni, M. *J. Appl. Crystallogr.* **2006**, *39*, 24.
(395) Sun, S.; Tsubaki, N.; Fujimoto, K. *Appl. Catal. A* **2000**, *202*, 121.
(396) Castner, D. G.; Watson, P. R.; Chan, I. Y. *J. Phys. Chem.* **1990**, *94*, 819.
(397) Bechara, R.; Balloy, D.; Dauphin, J.-Y.; Grimblot, J. *Chem. Mater.* **1999**, *11*, 1703.
(398) Wang, Y.; Noguchi, M.; Takahashi, Y.; Ohtsuka, Y. *Catal. Today* **2001**, 68, 3.
(399) Concepción, P.; López, C.; Martínez, A.; Puntes, V. F. *J. Catal.* **2004**, *228*, 321.
(400) Bechara, R.; Balloy, D.; Vanhove, D. *Appl. Catal. A* **2001**, *207*, 343.
(401) Saib, A. M.; Borgna, A.; van de Loosdrecht, J.; van Berge, P. J.; Geus, J. W.; Niemantsverdriet, J. W. *J. Catal.* **2006**, *239*, 326.
(402) Srinivasan, R.; De Angelis, R. J.; Reucroft, P. J.; Dhere, A. G.; Bentley, J. *J. Catal.* **1989**, *116*, 144.
(403) Colley, S. E.; Copperthwaite, R. G. *Catal. Today* **1989**, *9*, 203.
(404) Ducreux, O. Ph.D. thesis, Univeristé Paris VI, 1999.
(405) Madikizela-Mnqanqeni, N. N.; Coville, N. J. *J. Mol. Catal. A* **2005**, *225*, 137.
(406) Borgna, A.; Anderson, B. G.; Saib, A. M.; Bluhm, H.; Hävecker, M.; Knop-Gericke, A.; Kuiper, A. E. T.; Tamminga, Y.; Niemantsverdriet, J. W. H. *J. Phys. Chem. B* **2004**, *108*, 17905.
(407) Carlsson, A. F.; Naschitzki, M.; Bäumer, M.; Freund, H.-J. *J. Phys. Chem. B* **2003**, *107*, 778.
(408) Gopinath, C. S.; Mathew, T.; Shiju, N. R.; Sreekumar; K.; Rao, B. S. *J. Catal.* **2002**, *210*, 405.
(409) Fierro, G.; Lo Jacono, M.; Inversi, M.; Dragone, R.; Porta, P. *Top. Catal.* **2000**, *10*, 39.
(410) Tihay, F.; Pourroy, G.; Richard-Plouet, M.; Roger, A. C.; Kiennemann, A. *Appl. Catal. A* **2001**, *206*, 29.
(411) Ye, D.-X.; Pimanpang, S.; Jezewski, C.; Tang, F.; Senkevich, J. J.; Wang, G.-C.; Lu, T.-M. *Thin Solid Films* **2005**, *485*, 95.
(412) Hagelin-Weaver, H. A. E.; Hoflund, G. B.; Minahan, D. M.; Salaita, G. N. *Appl. Surf. Sci.* **2004**, *235* (4), 420.
(413) Joyner, R. W.; Roberts, M. W. *Chem. Phys. Lett.* **1979**, *60*, 459.
(414) Ruppender, H.-J.; Grunze, M.; Kong, C. W.; Wilmers, M. *Surf. Interface Anal.* **1990**, *15*, 245.
(415) Kaichev, V. V.; Prosvirin, I. P.; Bukhtiyarov, V. L.; Unterhalt, H.; Rupprechter, G.; Freund, H.-J. *J. Phys. Chem. B* **2003**, *107*, 3522.
(416) Teschner, D.; Pestryakov, A.; Kleimenov, E.; Hävecker, M.; Bluhm, H.; Sauer, H.; Knop-Gericke, A.; Schlögl, R. *J. Catal.* **2005**, *230*, 195.
(417) Teschner, D.; Pestryakov, A.; Kleimenov, E.; Hävecker, M.; Bluhm, H.; Sauer, H.; Knop-Gericke, A.; Schlögl, R. *J. Catal.* **2005**, *230*, 186.
(418) Bluhm, H.; Hävecker, M.; Knop-Gericke, A.; Kleimenov, E.; Schlögl, R.; Teschner, D.; Bukhtiyarov, V. I.; Ogletree, D. F.; Salmeron, M. *J. Phys. Chem. B* **2004**, *108*, 14340.
(419) Mekki, A.; Holland, D.; Ziq, Kh.; McConville, C. F. *J. Non-Cryst. Solids* **1997**, *220*, 267.
(420) Chaung, T. J.; Brundle, C. R.; Rice, D. W. *Surf. Sci.* **1976**, *59*, 413.
(421) Haber, J.; Stoch, J.; Ungier, L. *J. Electron Spectrosc. Relat. Phenom.* **1976**, *9*, 459.
(422) Ho, S. W.; Horialla, M.; Hercules, D. M. *J. Phys. Chem.* **1990**, *94*, 6396.
(423) Jiménez, V. M.; Espinós, J. P.; González-Elipe, A. R. *Surf. Interface Anal.* **1998**, *26*, 62.
(424) Jacobs, G.; Chaney, J. A.; Patterson, P. M.; Das, T. K.; Davis, B. H. *Appl. Catal. A* **2004**, *264*, 203.
(425) Brundle, C. R.; Chuang, T. J.; Rice, D. W. *Surf. Sci.* **1976**, *60*, 286.
(426) Shirley, D. A. *Phys. Rev.* **1972**, *B5*, 4709.
(427) Kerkhof, F. P. J.; Moulijn, J. A. *J. Phys. Chem.* **1979**, *83*, 1612.
(428) Kuipers, H. P. C. E. *Solid State Ion.* **1985**, *16*, 15.
(429) Kuipers, H. P. C. E.; van Leuven, H. C. E.; Visser, W. M. *Surf. Interface Anal.* **1986**, *8*, 235.
(430) Castner, D. G.; Watson, P. R.; Chan, I. Y. *J. Phys. Chem.* **1989**, *93* (8), 3188.
(431) Pichon, C.; Lynch, J. *Oil Gas Sci. Technol.* **2005**, *60*, 735.
(432) Lynch, J. *Oil Gas Sci. Technol.* **2002**, *57*, 281.
(433) Lynch, J. *J. Phys. III* **1994**, *4*, C9-253−C9-259.
(434) *X-ray Absorption: Principles, Applications, Techniques of EXAFS, SEXAFS, XANES*; Koningsberger, D. C., Prins, R., Eds.; Wiley: New York 1988.
(435) *Handbook on Synchrotron Radiation*; Koch, E. E., Eds.; North-Holland: New York, 1983; Vol. 1.
(436) Cheng, G.; Carter, J. D.; Guo, T. *Chem. Phys. Lett.* **2004**, *400*, 122.
(437) Tohji, K.; Udagawa, Y.; Tanabe, S.; Ida, T.; Ueno, A. *J. Am. Chem. Soc.* **1984**, *106*, 5172.
(438) Bazin, D.; Kovács, I.; Guczi, L.; Parent, P.; Laffon, C.; De Groot, F.; Ducreux, O.; Lynch, J. *J. Catal.* **2000**, *189*, 456.
(439) Dinega, D. P.; Bawendi, M. G. *Angew. Chem., Int Ed.* **1999**, *38*, 1788.
(440) Bazin, D.; Dexpert H.; Lynch, J. In situ XAFS Measurement of Catalysts. In *X-Ray Absorption Fine Structure for Catalysts and Surfaces*; Iwasawa, Y., Ed.; World Scientific: Singapore, 1996; pp 113−129.
(441) Matsuzaki, T.; Hanaoka, T.-A.; Takeuchi, K.; Arakawa, H.; Sugi, Y.; Wei, K.; Dong, T.; Reinikainen, M. *Catal. Today* **1997**, *36*, 311.
(442) Mierzwa, B. J. *Alloys Compd.* **2004**, *362*, 178.
(443) Mierzwa, B. J. *Alloys Compd.* **2005**, *401*, 127.
(444) Bazin, D.; Kovács, I.; Lynch, J.; Guczi, L. *Appl. Catal. A* **2003**, *242*, 179.
(445) Jacobs, G.; Patterson, P. M.; Zhang, Y.; Das, T.; Li, J.; Davis, B. H. *Appl. Catal. A* **2002**, *233*, 215.
(446) Das, T. K.; Jacobs, G.; Patterson, P. M.; Conner, W. A.; Li, J.; Davis, B. H. *Fuel* **2003**, *82*, 805.
(447) Jacobs, G.; Patterson, P. M.; Das, T. K.; Luo, M.; Davis, B. H. *Appl. Catal. A* **2004**, *270*, 65.
(448) Benfield, R. *J. Chem. Soc., Faraday Trans.* **1992**, *88* (8), 1107.
(449) Barbier, A.; Tuel, A.; Arcon, I.; Kodre, A.; Martin, G. A. *J. Catal.* **2001**, *200*, 106.
(450) Kanervo, J. Ph.D. thesis, Helsinki University of Technology, 2003.
(451) Robertson, S. D.; McNicol, B. D.; De Baas, J. H.; Kloet, S. C.; Jenkins, J. W. *J. Catal.* **1975**, *37*, 424.
(452) Jones, A.; McNicol, B. *Temperature-Programmed Reduction for Solid MaterialsCharacterization*; Marcel Dekker Inc.: New York, 1986.
(453) Bhatia, S.; Beltramini, I.; Do, D. D. *Catal. Today* **1990**, *7*, 309.
(454) Hurst, N. W.; Gentry, S. J.; Jones, A. *Catal. Rev.-Sci. Eng.* **1982**, *24*, 233.
(455) Lemaitre, J. L. Temperature-programmed methods. In *Characterization of Heterogeneous Catalysts*; Delannay, F.. Ed.; Marcel Dekker, Inc.: New York, 1984; pp 29−70.
(456) Brown, R.; Cooper, M.; Whan, D. *Appl. Catal.* **1982**, *3*, 177.
(457) van't Blik, H.; Prins, R. *J. Catal.* **1986**, *97*, 188.
(458) Sexton, B.; Hughes, A.; Turney, T. *J. Catal.* **1986**, *97*, 390.
(459) Viswanathan, B.; Gopalkrishnan, R. *J. Catal.* **1986**, *99*, 342.
(460) Chernavskii, P. A.; Khodakov, A. Y. Unpublished results.
(461) Milt, V. G.; Ulla, M. A.; Lombardo, E. A. *J. Catal.* **2001**, *200*, 241.
(462) van Berge, P. J.; van De Loosdrecht, J.; Visagie; J. L. U.S. Patent 6,806,226, 2004.
(463) Storsæter, S.; Borg, Ø.; Blekkan, E. A.; Holmen, A. *J. Catal.* **2005**, *231*, 405.
(464) Enache, D. I.; Roy-Auberger, M.; Revel, R. *Appl. Catal. A* **2004**, *268* (1−2), 51.
(465) Li, Y.; Fan, Y.; Yang, H.; Xu, B.; Feng, L.; Yang, M. Chen, Y. *Chem. Phys. Lett.* **2003**, 372, 160.
(466) Haller, G. L.; Resasco, D. E. *Adv. Catal.* **1989**, *36*, 173.
(467) Jongsomjit, B.; Sakdamnuson, C.; Praserthdam, P. *Mater. Chem. Phys.* **2004**, *89*, 395.
(468) Jongsomjit, B.; Sakdamnuson, C.; Goodwin, J. G., Jr.; Praserthdam, P. *Catal. Lett.* **2004**, *94*, 209.
(469) Chernavskii, P. A.; Lermontov, A. S.; Pankina, G. V.; Torbin, S. N.; Lunin, V. V. *Kinet. Catal.* **2002**, *43*, 268.
(470) Ciuparu, D.; Ensuque, A.; Shafeev, G.; Bozon-Verduraz, F. *J. Mater. Sci. Lett.* **2000**, *19*, 931.
(471) Panpranot, J.; Taochaiyaphum, N.; Praserthdam, P. *Mater. Chem. Phys.* **2005**, *94*, 207.
(472) Ichiyanagi, Y.; Yamada, S. *Polyhedron* **2005**, *24*, 2813.
(473) Romero, J.; Jiménez, J.; Del Cerro, J. *J. Magn. Magn. Mater.* **2004**, *280*, 257.
(474) Dutta, P.; Elbashir, N. O.; Manivannan, A.; Seehra, M. S.; Roberts, C. B. *Catal. Lett.* **2004**, *98*, 203.
(475) Chernavskii, P. A. *Kinet. Catal.* **2005**, *46*, 634.
(476) Néel, L. *C. R. Acad. Sci* **1949**, *228*, 664.

(477) Weil, L. *J. Chem. Phys*. **1954**, 17, 263.
(478) Wolhlfarth, E. P. *J. Phys. F: Met. Phys.* **1980**, *10*, L241.
(479) Leslie-Pelecky, D. L.; Rieke, R. D. *Chem. Mater* **1996**, *8*, 1770.
(480) Petrov, Y. I. *Physics of Small Particles*: Nauka: Moscow, 1982.
(481) Kittel, C. *Introduction to Solid State Physics*; Wiley: New York, 1996.
(482) Bedel, L.; Roger, A. C.; Estournes, C.; Kiennemann, A. *Catal. Today* **2003**, *85*, 207.
(483) Bedel, L.; Roger, A.-C.; Rehspringer, J.-L.; Zimmermann, Y.; Kiennemann, A. *J. Catal*. **2005**, *235*, 279.
(484) Jabłoński, J. M.; Okal, J.; Potoczna-Petru, D.; Krajczyk, L. *J. Catal*. **2003**, *220*, 146.
(485) Chernavskii, P. A.; Khodakov, A. Y.; Pankina, G. V.; Girardon, J.-S.; Quinet, E. *Appl. Catal. A* **2006**, *306*, 108.
(486) Pankina, G. V.; Chernavskii, P. A.; Lunin, V. V. *Kinet. Catal*. **2005**, *46* (5), 719.
(487) Rana, R. K.; Xu, X. N.; Yeshurun, Y.; Gedanken, A. *J. Phys. Chem. B* **2002**, *106*, 4079.
(488) Cabrera, N.; Mott. N. F. *Rep. Prog. Phys*. **1948/1949**, *12*, 163.
(489) Gruyters, M. M.; Riegel, D. *Phys. Rev. B* **2000**, *63*, 52401.
(490) Elbashir, N. O.; Dutta, P.; Manivannan, A.; Seehra, M. S.; Roberts, C. B. *Appl. Catal. A* **2005**, *285*, 169.
(491) Barbier, A.; Hanif, A.; Dalmon, J.-A.; Martin, G. A. *Appl. Catal. A* **1998**, *168*, 333.
(492) Llorca, J.; De la Piscina, R. P.; Dalmon, J.-A.; Sales, J.; Homs, N. *Appl. Catal. B* **2003**, *43*, 355.
(493) Helveg, S.; Hansen, P. L. *Catal. Today*, **2006**, *111*, 68.
(494) Datye, A. K. *J. Catal.* **2003**, *216*, 144.
(495) Thomas, J. M.; Tersaki, O.; Gai, P. L.; Zhou, W.; Gonzales-Calbet, J. *Acc. Chem. Res*. **2001**, *34*, 583.
(496) Boyes, E. D. *Adv. Mater*. **1998**, *10*, 1277.
(497) Boyes, E. D.; Gai, P. L. *Ultramicroscopy* **1997**, *67*, 219.
(498) Gai, P. L. *Top. Catal*. **2002**, *21*, 161.
(499) McIntyre, B. J.; Salmeron, M.; Somorjai, G. A. *Catal. Lett*. **1992**, 1*4*, 263.
(500) McIntyre, B. J.; Salmeron, M.; Somorjai, G. A. *Rev. Sci. Instrum*. **1993**, *64*, 687.
(501) Lauritsen, J. V.; Vang, R. T.; Besenbacher, F. *Catal. Today* **2006**, 111 (1−2), 34.
(502) Hendriksen, B. L. M.; Bobaru, S. C.; Frenken, J. W. M. *Top. Catal*. **2005**, *36*, 43.
(503) Okabe, K.; Li, X.; Matsuzaki, T.; Arakawa, H.; Fujimoto, K. *J. Sol-Gel Sci. Technol*. **2000**, *19*, 519.
(504) Riva, R.; Miessner, H.; Vitali, R.; Del Piero, G. *Appl. Catal. A* **2000**, *196*, 111.
(505) Panpranot, J.; Kaewkun, S.; Praserthdam, P.; Goodwin, J. G., Jr. *Catal. Lett.* **2003**, *91*, 95.
(506) De La Pena O'Shea, V. A.; Alvarez-Galvan, M. C.; Campos-Martin, J. M.; Fierro, J. L. G. *Catal. Lett.* **2005**, *100*, 105.
(507) Dutta, P.; Dunn, B. C.; Eyring, E. M.; Shah, N.; Huffman, G. P.; Manivannan, A.; Seehra, M. S. *Chem. Mater.* **2005**, *17*, 5183.
(508) Ravishankar, R.; Li, M. M.; Borgna, A. *Catal. Today* **2005**, *106*, 149.
(509) Storsæter, S.; Tøtdal, B.; Walmsley, J. C.; Tanem, B. S.; Holmen, A. *J. Catal.* 236, **2005**, 139.
(510) Morales, F.; Grandjean, D.; Mens, A.; De Groot, F. M. F.; Weckhuysen, B. M. *J. Phys. Chem. B* **2006**, *110* (17), 8626.
(511) Wilson, J.; de Groot, C. *J. Phys. Chem*. **1995**, *99*, 7860.
(512) Ponec, V.; van Barneveld, W. A. *Ind. Eng. Chem. Prod. Res. Dev*. **1979**, *18*, 268.
(513) Ernst, K. H.; Schwarz, E.; Christmann, K. *J. Chem. Phys*. **1994**, *101* (6), 5388.
(514) Reuel, R. C.; Bartholomew, C. H. *J. Catal.* **1984**, *85*, 63.
(515) Bartholomew, C. H. *Catal. Lett.* **1990**, *7*, 27.
(516) Zowtiak, J. M.; Bartholomew, C. H. *J. Catal.* **1983**, *83*, 107.
(517) Zowtiak, J. M.; Weatherbee, G. D.; Bartholomew, C. H. *J. Catal.* **1983**, *82*, 230.
(518) Bartholomew, C. H.; Reuel, R. C. *Ind. Eng. Prod. Res. Dev.* **1985**, *24*, 56.
(519) Khodakov, A. Y.; Peregryn, B.; Lermontov, A. S.; Girardon, J.-S.; Pietrzyk, S. *Catal. Today* **2005**, *106*, 132.
(520) Belambe, A. R.; Oukaci, R.; Goodwin, J. G., Jr. *J. Catal*. **1997**, *166*, 8.
(521) Jones, R. D.; Bartholomew, C. H. *Appl. Catal*. **1988**, *39*, 77.
(522) Hanssen, K. F.; Blekkan, E. A.; Schanke, D.; Holmen, A. *Stud. Surf. Sci. Catal*. **1997**, *109*, 193.
(523) Vada, S.; Hoff, A.; Ådnanes, E.; Schanke, D.; Holmen, A. *Top. Catal*. **1995**, *2*, 155.
(524) Spadaro, L.; Arena, F.; Granados, M. L.; Ojeda, M.; Fierro, J. L. G.; Frusteri, F. *J. Catal*. **2005**, *234*, 451.
(525) Wang, W.-J.; Lin, H.-Y.; Chen, Y.-W. *J. Porous Mater*. **2005**, *12*, 5.
(526) Riedel, T.; Schaub, G. *Top. Catal*. **2003**, *26*, 145.
(527) Aaserud, C.; Hilmen, A.-M.; Bergene, E.; Eric, S.; Schanke, D.; Holmen, A. *Catal. Lett*, **2004**, *94*, 171.
(528) Schanke, D.; Eri, S.; Rytter, E.; Aaserud, C.; Himen, A.-M.; Lindvag, O. A.; Bergene, E.; Holmen, A. *Stud. Surf. Sci. Catal.* **2004**, *147*, 301.
(529) Lermontov, A. S.; Girardon, J.-S.; Griboval-Constant, A.; Pietrzyk, S.; Khodakov, A. Y. *Catal. Lett*, **2005**, *101* (1−2), 117.
(530) Girardon, J.-S.; Constant-Griboval, A.; Gengembre, L.; Chernavskii, P. A.; Khodakov, A. Y. *Catal. Today* **2005**, *106*, 161.
(531) Happel, J. J. *Chem. Eng. Sci*. **1978**, *33*, 1567.
(532) Bennett, C. O. In *ACS Symposium Series* ; Bell, A. T., Hegedus, L. L., Eds.; American Chemical Society: Washington, DC, 1982; Vol. 178, p 1.
(533) Biloen, P. *J. Mol. Catal*. **1983**, *21*, 17.
(534) Bennett, C. O. *Catal. Rev.-Sci. Eng.* **1976**, *13*, 121.
(535) Schannon, S. L.; Goodwin, J. G., Jr. *Chem. Rev*. **1995**, *95*, 677.
(536) Rothaemel, M.; Hanssen, K. F.; Blekkan, E. A.; Schanke, D.; Holmen, A. *Catal. Today* **1998**, *40* (2−3), 171.
(537) van Dijk, H. A. J. Ph.D. Thesis, Technical University of Eindhoven, 2001.
(538) Mims, C. A.; McCandlish, L. E. *J. Phys. Chem*. **1987**, *91*, 929.
(539) van Dijk, H. A. J.; Hoebink, J. H. B. J.; Schouten, J. C. *Chem. Eng. Sci.* **2001**, *56* (4), 1211.
(540) van Dijk, H. A. J.; Hoebink, J. H. B. J.; Schouten, J. C. *Stud. Surf. Sci. Catal.* **2000**, *130* A, 383.
(541) Frøseth, V.; Storsæter, S.; Borg, O.; Blekkan, E. A.; Rønning, M.; Holmen, A. *Appl. Catal. A* **2005**, *289* (1), 10.
(542) Rothaemel, M.; Hanssen, K. F.; Blekkan, E. A.; Schanke, D.; Holmen, A. *Catal. Today* **1997**, *38* (1), 79.
(543) Efremenko, I.; Sheintuch, M. *J. Catal*. **2003**, *214*, 53.
(544) Suvanto, S.; Hirva, P.; Pakkanen, T. A. *Surf. Sci*. **2000**, *465*, 277.
(545) Hernández Cruz, N.; Márquez, A.; Sanz, J. F.; Gomes, J. R. B.; Illas, F. *J. Phys. Chem. B* **2004**, *108*, 15671.
(546) Ma, Q.; Klier, K.; Cheng, H.; Mitchell, J. W.; Hayes, K. S. *J. Phys. Chem. B* **2001**, *105*, 2212.
(547) Ma, Q.; Klier, K.; Cheng, H.; Mitchell, J. W.; Hayes, K. S. *J. Phys. Chem. B* **2000**, *104*, 10618.
(548) Ma, Q.; Klier, K.; Cheng, H.; Mitchell, J. W.; Hayes, K. S. *J. Phys. Chem. B* **2001**, *105*, 9230.
(549) Gong, X.-Q.; Raval, R.; Hu, P. *J. Chem. Phys.* **2005**, *122* (2), 1.
(550) Mikhailov, M. N.; Zhidomirov, G. M.; Krylova, A. Yu. *Russ. Chem. Bull., Int. Ed*. **2005**, *54*, 2264.
(551) Klinke, D. J.; Broadbelt, L. J. *Surf. Sci*. **1999**, *429*, 169.
(552) Forsythe, W. L., Jr.; Hertwig, W. R. *Ind. Eng. Chem.* **1949**, *41*, 1200.
(553) Werther, J.; Reppenhagen, J. Attrition in Fluidized Beds and Pneumatic Conveying Lines. In *Fluidization Solids Handling and Processing*; Yang. W.-C., Ed.; Noyes Publications: West Wood, NJ, 1999.
(554) Pham, H. N.; Reardon, J.; Datye, A. K. *Powder Technol*. **1999**, *103* (2), 95.
(555) Pham, H. N.; Viergutz, A.; Gormley, R. J.; Datye, A. K. *Powder Technol.* **2000**, *110*, 196.
(556) ASTM D5757-95, Standard Test Method for Determination of Attrition and Abrasion of Powdered Catalysts by Air Jets.
(557) Jothimurugesan, K.; Goodwin, J. G., Jr.; Gangwal, S. K.; Spivey, J. J. *Catal. Today* **2000**, *58* (4), 335.
(558) Slimane, R. B.; Abbasian, J. *Adv. Environ. Res.* **2000**, *4*, 147.
(559) Zhao, R.; Goodwin, J. G., Jr.; Oukaci, R. *Appl. Catal. A* **1999**, *189*, 99.
(560) Moulijn, J. A.; Tarfaoui, A.; Kapteijn, F. *Catal. Today* **1991**, *11*, 1.
(561) Moulijn, J. A.; Pérez-Ramýrez, J.; Berger, R. J.; Hamminga, G.; Mul, G.; Kapteijn, F. *Catal. Today* **2003**, 81, 457.
(562) Bremaud, M.; Fongarland, P; Anfray, J.; Jallais; S.; Schweich, D.; Khodakov, A. Y. *Catal. Today* **2005**, 106, 137.
(563) Beitel, G. A.; Laskov, A.; Oosterbeek, H.; Kuipers, E. W. *J. Phys. Chem.* **1996**, *100*, 1249.
(564) Beitel, G. A.; de Groot, C. P. M.; Oosterbeek, H.; Wilson, J. H. *J. Phys. Chem. B* **1997**, *101*, 4035.
(565) Danckwerts, P. V. *Chem. Eng. Sci.* **1953**, *2*, 1.
(566) Nauman, E. B. *Chem. Eng. Commun.* **1981**, *8*, 53.
(567) Villermaux, J. *Génie de la Réaction Chimique*; Tec. and Doc.: Lavoisier, 1982.
(568) Winterbottom, J. M.; Khan, Z.; Raymahasay, S.; Knight, G.; Roukounakis, N. *J. Chem. Technol. Biotechnol.* **2000**, *75*, 1015.
(569) Yates, I. C.; Satterfield, C. N. *Energy Fuels* **1991**, *5*, 168.
(570) van Steen, E.; Schulz, H. *Appl. Catal. A* **1999**, *186*, 309.
(571) Wang, Y.-N; Xu, Y.-Y; Xiang, H.-W; Li, Y.-W.; Zhang, B-J. *Ind. Eng. Chem. Res.* **2001**, *40*, 4324.
(572) Berger, R. J.; Perez-Ramirez, J.; Kapteijn, F.; Moulijn, J. A. *Chem. Eng. Sci.* **2002**, *57*, 4921.
(573) Perez-Ramírez, J.; Berger, Rob J.; Mul, G.; Kapteijn, F.; Moulijn, J. A. *Catal. Today* **2000**, *60*, 93.

(574) Krishna, R.; Sie, S. T. *Chem. Eng. Sci.* **1994**, *49*, 4029.
(575) Sie, S. T. *Am. Inst. Chem. Eng. J.* **1996**, *42*, 3498.
(576) Ouyang, X.; Besser, R. S. *Catal. Today* **2003**, *84*, 33.
(577) Kubo, R. J. *Phys. Soc. Jpn.* **1962**, *71*, 975.
(578) Bond, G. C. *Surf. Sci.* **1985**, *156* (2), 966.
(579) Lei, Y.; Liang, C. H.; Wu, Y. C.; Zhang, L. D.; Mao, Y. Q. *J. Vac. Sci Technol. B: Microelectr. Nanomet. Struct.* **2001**, *19* (4), 1109.
(580) Alivisatos, A. P. *Science* **1996**, *271*, 933.

CR050972V